Physics – Uspekhi **51** (12) 1229 – 1260 (2008)

REVIEWS OF TOPICAL PROBLEMS

PACS numbers: **74.10.+v**, **74.20.–z**, **74.25.–q**, 74.70.Dd

New high-temperature superconductors based on rare-earth and transition metal oxyarsenides and related phases: synthesis, properties, and simulations

A L Ivanovskii

DOI: 10.1070/PU2008v051n12ABEH006703

Contents

Abstract. The discovery in February 2008 of superconductivity with the transition temperature about 26 K in fluorine-doped oxyarsenide $LaO_{1-x}F_xFeAs$ stimulated numerous studies of superconducting and other physical properties of this and related materials, resulting in a new family of high-temperature ($T_c \sim 26-55$ K) superconductors. The experimental and theoretical state of the art is reviewed concerning the synthesis, properties, and simulation of the new family and related systems.

1. Introduction

In February 2008, the authors of [1] announced the discovery of a $T_c \sim 26$ K superconducting transition in a fluorine-doped iron and lanthanum oxyarsenide $LaO_{1-x}F_xFeAs$, which is a representative of the large group of layered quaternary phases, the so-called oxypnictides of rare-earth (Ln) and transition (M) metals $LnOMPn$, where Pn is pnictogen (p is an element of the nitrogen subgroup).

A L Ivanovskii Institute of Solid State Chemistry,
Ural Branch of the Russian Academy of Sciences,
ul. Pervomaiskaya 91, 620041 Ekaterinburg, Russian Federation
Tel. (343) 374 53 31. Fax (343) 374 44 95,
E-mail: ivanovskii@ihim.uran.ru

Received 15 July 2008
Uspekhi Fizicheskikh Nauk **178** (12) 1273 – 1306 (2008)
DOI: 10.3367/UFNr.0178.200812c.1273
Translated by M B Tsaplina; edited by A M Semikhatov

Because the new superconductor belonged to none of the known classes of high-temperature superconductors (HTSCs) such as HTSC cuprates [2], fullerides [3] or MgB_2 [4], this discovery immediately attracted rapt attention [5 – 82]. A distinctive feature of the new superconductor is its layered structure (Fig. 1) formed by alternate LaO and FeAs molecular layers, and a considerable amount of iron (a typical magnetic metal) in its composition. Furthermore, the $LaO_{1-x}F_xFeAs$ superconductivity occurs at the boundary of the magnetic phase instability under variation of the carrier concentration as a result of fluorine doping of LaO layers, the so-called charge reservoirs, which are spatially separated from the conducting FeAs layers, the T_c value being rather sensitive to the concentration and to the type of doping elements.

The discovery in [1] initiated numerous studies (see [5 – 35]) of the origin of superconductivity and other physical properties of $LaO_{1-x}F_xFeAs$ and an intense search for new superconducting materials among related systems. Discovered in these studies were two related families of new superconducting materials, which are sometimes denoted as type-1111 and 122 FeAs superconductors in the literature.

The first family, 1111 superconductors, involves materials based on the above-mentioned rare-earth and transition metal LnOMPn oxypnictides (Table 1). They include superconducting materials obtained by the electron doping of quaternary oxypnictides via introduction of doping elements (fluorine) into the oxygen sublattice. In addition to $LaO_{1-x}F_xFeAs$ ($T_c \sim 26$ K), the group of these superconductors includes LnOFeAs oxyarsenides of the majority of light rare-earth metals Ln = Ce, Pr, Nd, Sm, Gd, Tb, and Dy. The

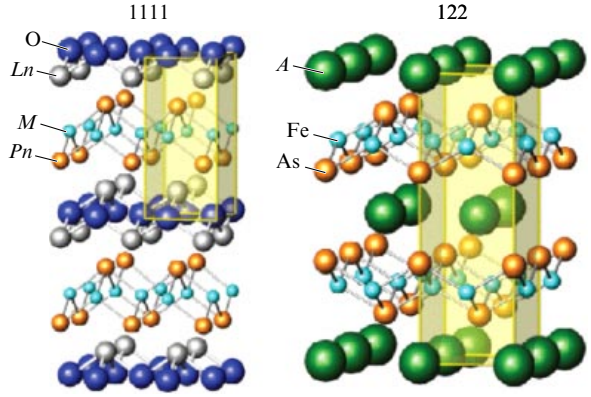

Figure 1. Crystal structures [39] of tetragonal quaternary *Ln*O*Pn* oxypnictides (type 1111 phases) and ternary AFe_2As_2 arsenides (type 122 phases), i.e., basic phases of the new $T_c = 26-55$ K superconductors.

critical temperature $T_c \sim 56$ K detected for a number of fluorine-doped samarium oxyarsenide $SmO_{1-x}F_xFeAs$ samples [26] belonging to this group of compounds is now the maximum shown for the available superconducting systems of this class. The other group of oxyarsenide superconductors was obtained by means of *Ln*OFeAs hole doping, which can, in particular, be attained by forming vacancies in the oxygen sublattice (nonstoichiometric $LnO_{1-x}FeAs$ compositions with the maximum $T_c \sim 51$ K for $NdO_{1-x}FeAs$ and $T_c \sim 55$ K for $SmO_{1-x}FeAs$ [36]) or substituting a bivalent, e.g., Ln^{3+} ion for a trivalent Sr^{2+} ion [17]. Thus, the oxyarsenide 1111 superconductors form a new HTSC group with critical temperatures rather close to the 'nitrogen level' $T = 77$ K that had previously been reached only for HTSC cuprates.

The second family of related superconductors, the so-called 122 superconductors, contains materials based on ternary arsenides AFe_2As_2, where *A* stands for the alkali-earth metals (Ca, Cr, and Ba) (see [37–45]). As with the

Table 1. Synthesis of rare-earth and transition metal oxypnictides (1111 phase) and superconducting materials based on them.

Phase	T_c^{max}, K *	Method (conditions of synthesis), ** sample ***	References
		Oxyarsenides	
LaOFeAs	—	SPS: LaAs + FeAs + L_2O_3 ($T = 1250$ °C, $t = 40$ h), PC	[1]
$LaO_{1-x}F_xFeAs$, $x = 0.05-0.12$	26	SPS: LaAs + FeAs + L_2O_3 + LaF_3 + La ($T = 1250$ °C, $t = 40$ h), PC	[1]
$La_{1-x}Ca_xOFeAs$	—	SPS: LaAs + FeAs + L_2O_3 + CaO ($T = 1250$ °C, $t = 40$ h), PC	[1]
$La_{1-x}Sr_xOFeAs$, $x = 0.13$	25	SPS: (Fe + As) + $SrCO_3$ + La_2O_3 + La ($T = 1200$ °C, $t = 48$ h), PC	[17]
$La_{0.85}Sr_{0.15}O_{1-x}FeAs$, $x = 0.13$	4.2–8	SPS: (Fe + As) + $SrCO_3$ + Fe_2O_3 + LaAs ($T = 1160$ °C, $t = 40$ h), PC	[63]
$LaO_{0.89}F_{0.11}FeAs$ ($P \sim 4$ GPa)	43	SPS: La_2O_3 + LaAs + Fe_2As + FeAs ($T = 1250$ °C, $t = 40$ h), PC	[6]
$LaO_{0.9}F_{0.1}FeAs_{1-x}$, $x = 0.05-0.1$	26–28	SPS: Fe + As + La + La_2O_3 + LaF_3 (2 stages: $T = 940$ °C, $t = 8$ h, $T = 1150$ °C, $t = 48$ h), PC	[57]
$LaO_{1-x}FeAs$, $x = 0-0.15$	—	SPS: Fe + As + La + La_2O_3 ($T = 500-1100$ °C, $t = 12-33$ h), PC	[58]
$LaO_{0.85}FeAs$	28.3	PC	[36]
$LaO_{1-x}F_xNiAs$, $x = 0-0.15$	3.8	SPS: NiO + Ni + As + La + LaF_3 ($T = 1150$ °C, $t = 50$ h), PC	[60]
$La_{1-x}K_xO_{1-x}F_xFeAs$, $x = 0.15, 0.20$	26.2	SPS: La_2O_3 + FeAs + La + KF ($T = 1180$ °C, $t = 48$ h), PC	[70]
LaOCoAs	—	SPS: LaAs + CoO ($T = 1100$ °C, $t = 20$ h), PC	[61]
$CeO_{1-x}F_xFeAs$, $x = 0-0.20$	41	SPS: CeAs + Fe + CeO_2 + CeF_3 + Fe_2As ($T = 1150$ °C, $t = 50$ h), PC	[51]
$CeO_{0.85}FeAs$	42.6	PC	[36]
$PrO_{0.89}F_{0.11}FeAs$	52	SPS: PrAs + Fe + Fe_2O_3 + FeF_3 ($T = 1250$ °C; $t = 2$ h, $P = 6$ GPa), PC	[56]
$PrO_{0.85}FeAs$	48.2	PC	[36]
$NdO_{0.89}F_{0.11}FeAs$	51	SPS: Nd + As + Fe + Fe_2O_3 + FeF_3 ($T = 1300$ °C, $t = 2$ h, $P = 6$ GPa), PC	[19]
$NdO_{0.9}F_{0.1}FeAs$	51	SPS: $NdFe_3As_3$ + Nd_2O_3 + NdF_3 + Nd ($T = 1350$ °C, $t = 4$ h, $P = 3.3$ GPa), PC	[54]
$NdO_{0.82}F_{0.18}FeAs$	50	Crystallization in NaCl melt Nd + As + NdF_3 + Fe_2O_3 + Fe ($T = 1050$ °C, $t = 10$ days in NaCl melt), SC	[55]
$NdO_{0.75}FeAs$	—	SPS: NdAs + Fe + Fe_2O_3 ($T = 900$ °C, $t = 36$ h), PC	[49]
$NdO_{0.85}FeAs$	51	PC	[36]
$NdO_{0.90}F_{0.10}FeAs$	53	SPS: $NdFe_3As_3$ + Nd_2O_3 + NdF_3 + Nd ($T = 1400$ °C, $t = 8$ h, $P = 3.3$ GPa), SC	[65]
$SmO_{0.90}F_{0.10}FeAs$	55	SPS: SmAs + As + Fe + Fe_2O_3 + FeF_2 ($T = 1250$ °C, $t = 2$ h, $P = 6$ GPa), PC	[26]
$SmO_{0.90}F_{0.10}FeAs$	43	SPS: SmAs + SmF_3 + Fe + Fe_2O_3 ($T = 1200$ °C), PC	[9]
$SmO_{0.85}FeAs$	55	PC	[36]
SmOFeAs	—	SPS: SmAs + Fe + Fe_2O_3 + FeF_2 ($T = 1200$ °C, $t = 24$ h), PC	[64]
$SmO_{0.93}F_{0.07}FeAs$	36		
$GdO_{1-x}F_xFeAs$, $x = 0.12-0.17$	36.6	SPS: Gd_2O_3 + CdF_3 + Fe + As + Gd, PC	[22]
$Gd_{1-x}Th_xOFeAs$, $x = 0-0.2$	55	SPS: GdAs + Gd_2O_3 + ThO_2 + Fe + FeAs ($T = 1423$ °C, $t = 48$ h), PC	[53]
$GdO_{0.85}FeAs$	53.5	SPS: Gd + As + Fe + Fe_2O_3 ($T = 1350$ °C, $t = 2$ h, $P = 6$ GPa), PC	[27]

Table 1 (continued)

Phase	T_c^{max}, K *	Method (conditions of synthesis) **, sample ***	References
$TbO_{1-x}F_xFeAs$, $x = 0-0.2$	45.9	SPS: TbAs + Fe_2O_3 + FeF_2 + Fe ($T = 1110-1150$ °C, $t = 20$ min, $P = 10$ GPa), PC	[59]
$Tb_{1-x}Th_xOFeAs$, $x = 0-0.2$	52	SPS: TbAs + Tb_4O_7 + ThO_2 + Fe + FeAs ($T = 1453$ °C, $t = 48$ h), PC	[62]
$DyO_{1-x}F_xFeAs$, $x = 0-0.2$	45.4	SPS: DyAs + Fe_2O_3 + FeF_2 + Fe ($T = 1110-1150$ °C, $t = 20$ min, $P = 12$ GPa), PC	[59]
LaOZnAs	—	Synthesis of reagents La + As + ZnO (in NaCl/KCl melt (1:1) at $T = 500$ °C, $t = 1$ day and $T = 800$ °C, $t = 7$ day), SC	[72]
LaOZnAs	Sc ****	Epitaxial film on a (001)MgO surface	[73]
		Oxyphosphides	
*Ln*FePO (*Ln* = La–Nd), *Ln*RuPO (*Ln* = La–Nd, Sm, Gd), *Ln*CoPO (*Ln* = La–Nd, Sm)	—	SPS of simple reagents (*Ln* + (Fe, Co, Ru) + red phosphorus) or oxides Ln_2O_3, Fe_2O_3, Co_3O_4, RuO_2, PC	[71]
LaOFeP	~ 5	SPS: LaP + FeP + Fe_2P + La + LaF_3 + La_2O_3 ($T = 1200$ °C, $t = 40$ h), PC	[74]
LaOFeP	< 0.35	SPS: LaP + Fe + Fe_3O_4 ($T = 1200$ °C, $t = 48$ h), PC	[76]
LaOFeP	6.6	Synthesis of La + Fe_2O_3 + P reagents in tin melt ($T = 1135$ °C, $t = 96$ H), SC	[77]
LaONiP	~ 3	SPS: La + P + NiO ($T = 1000$ °C, $t = 24$ h), PC	[75]
LaOCoP	—	SPS: LaP + CoO ($T = 1250$ °C, $t = 20$ h), PC	[61]
LaZnOP	Sc	Synthesis of reagents La + red phosphorus + ZnO (in NaCl/KCl (1:1) melt at $T = 500$ °C, $t = 1$ day and $T = 800$ °C, $t = 7$ days), SC	[72]
LaZnOP	Sc	Epitaxial film on a (001)MgO surface	[73]
		Oxybismuthides	
$LaO_{1-x}FeBi$	—	SPS: LaBi + Fe + Fe_3O_4 ($T = 800$ °C, $t = 10$ h), PC	[28]
$LaO_{1-x}NiBi$	4.4	SPS: LaBi + Ni + NiO ($T = 800$ °C, $t = 10$ h), PC	[28]

* Maximum superconducting transition temperature (for a series of samples with variable composition).
** SPS is solid-phase synthesis.
*** PC and SC are polycrystal and single crystal samples.
**** Sc is semiconductor

quaternary oxypnictide 1111 materials, the 122-phase AFe_2As_2 have layered structures (see Fig. 1) composed of alternating FeAs layers and flat atomic nets of alkali metals *A*. As in *Ln*OFeAs crystals, molecular FeAs layers in AFe_2As_2 consist of conjugate $FeAs_4$ tetrahedrons. But in contrast to oxyarsenides, 122 superconductors are oxygen-free and contain no rare-earth metals, and the superconducting transition of the original AFe_2As_2 phases can only be achieved through their hole doping, i.e., the introduction of univalent ions of alkali-earth metals (K, Na, Cs) into *A* nets. The maximum T_c values currently registered for AFe_2As_2-based 122 superconductors are nearly 37–38 K for $Ba_{1-x}K_xFe_2As_2$ [38] and $Sr_{1-x}Cs_xFe_2As_2$ [41] systems (Table 2).

We also note the recently synthesized LiFeAs superconductor [46] (with the maximum $T_c \sim 18$ K for the $Li_{0.6}FeAs$ composition), which may perhaps open a third group of the so-called 111-superconductors. The LiFeAs structure is similar to 122-AFe_2As_2, but the number of atoms of the alkali metal Li in the flat nets separating FeAs layers is twice as large as the number of atoms of alkali-earth metals in 122-phase nets.

In this review, we attempt to summarize the state of the art in experimental and theoretical studies in the fields of the synthesis, analysis of the properties, and simulation of new HTSCs based on layered oxypnictides of transition and rare-earth metals and the above-mentioned related systems.

Before proceeding to the main material, we briefly comment on the chemical formulas of the new 1111-superconductors. Two ways of writing them can be found in the literature. For example, the pure iron–lanthanum oxyarsenide can be written as either LaOFeAs or LaFeAsO and the fluoride-doped one as $LaO_{1-x}F_xFeAs$ or $LaFeAsO_{1-x}F_x$. Strictly speaking [47], according to the adopted IUPAC (International Union of Pure and Applied Chemistry) nomenclature [48], elements in the formulas of inorganic substances should appear in the increasing order of their electronegativeness. To meet this principle and allow electronegativeness values, La(1.1) < Fe(1.83) < As(2.18) < O(3.44), the chemical formulas of the indicated phases should be represented as LaFeAsO and $LaFeAsO_{1-x}F_x$.

Nevertheless, in view of the sharply anisotropic layered structure of oxypnictides formed by molecular layers (rare-earth element oxygen)/(transition metal pnictogen), an alternative notation for these phases is very frequently used in which the chemical formula directly refers to the composition and interchange of separated structural blocks (layers), for example, LaOFeAs or $LaO_{1-x}F_xFeAs$. This second way of writing is most widespread in the original papers and is therefore used in what follows.

The first part of this review (Sections 2–4) presents data on the synthesis, investigation of the properties, and simulation of new oxypnictide superconductors (of the 1111 phase) and the second part (Section 5) gives data on

Table 2. Synthesis of ternary arsenides of alkali-earth and transition metals (122 phase) and superconducting materials based on them.

Phase	T_c^{max}, K *	Method (conditions of synthesis), ** sample ***	References
$SrFe_2As_2$	—	SPS: Sr + Fe + As ($T = 1100\,^\circ$C, $t = 10$ h), PC	[37]
$Ba_{0.6}K_{0.4}Fe_2As_2$	38	SPS: Ba + K + Fe + As, PC	[38]
$Sr_{0.6}K_{0.4}Fe_2As_2$	38	SPS: SrAs + KAs + Fe_2As ($T = 750-900\,^\circ$C, $t = 24$ h), PC	[40]
KFe_2As_2	3.8		
$CsFe_2As_2$	2,7	SPS: K/Sr/Cs + FeAs ($T = 700-1000\,^\circ$C, $t = 20-24$ h), PC	[41]
$Sr_{1-x}K_xFe_2As_2$, $0 \leqslant x \leqslant 0/9$	37		
$Sr_{1-x}Cs_xFe_2As_2$, $0 \leqslant x \leqslant 0.6$	37		
$Ba_{1-x}K_xFe_2As_2$, $x = 0.4$, 0.5	38	SPS: BaAs + FeAs + Fe + (LaAs + K) ($T = 1273\,^\circ$C, $t = 12$ h), PC	[42]
$Ba_{0.85}La_{0.15}Fe_2As_2$	—		
$EuFe_2As_2$	—	SPS: Eu + Fe + As ($T = 1073\,^\circ$C, $t = 12$ h), PC	[78]
$Ca_{0.5}Na_{0.5}Fe_2As_2$	~ 20	SPS: CaAs + NaAs + Fe_2As ($T = 930\,^\circ$C, $t = 15$ h), PC	[81]
$EuFe_2As_2$	—	Bridgman method (of pure substances: Eu + Fe + As), SC	[78]
$BaFe_2As_2$	—	Spontaneous crystallization in FeAs melt, SC	[44]
$SrFe_2As_2$	—	Crystallization in Sn melt, SC	[45]
Sr, $Ba_{0.6}K_{0.4}Fe_2As_2$	> 30		
$BaFe_2As_2$	—	Crystallization in Sn melt, SC	[79]
$Ba_{0.55}K_{0.45}Fe_2As_2$	~ 30		
$CaFe_2As_2$	—	Crystallization in Sn melt, SC	[80, 82]
$CaFe_2As_2$	—	Spontaneous crystallization in FeAs melt, SC	[81]

* Maximum superconducting transition temperature (for a series of variable-composition samples).
** SPS is solid-phase synthesis; reagents, temperature T and time t of thermal treatment are given.
*** PC and SC are polycrystalline and single crystal samples.

the related 122 phases, whose systematic studies are only now beginning.

2. Synthesis and crystal structure of transition and rare-earth metal oxypnictides (phase 1111) and superconductors based on them

2.1 Methods of synthesis

Rather many ways of obtaining *Ln*O*M*P*n* 1111-oxypnictides and superconducting materials based on them have been proposed. These methods differ significantly by the choice of the initial reagents and the conditions of synthesis. Because the superconducting transition has now been reached only for materials based on iron-containing oxyarsenides *Ln*OFeAs, we here mention the methods by which these systems can be obtained and which can be conditionally divided into several main groups (see Table 1).

All *polycrystalline* (PC) oxyarsenides are obtained using solid-phase synthesis (SPS). Either simple substances are used as reagents or precursors (binary or, more seldom, ternary phases) are first synthesized. Such precursors are most often binary arsenides or (and) metal oxides. The methods proposed differ in the number of stages, the temperature T and time t of annealing, and the composition of the atmosphere in which the experiment is carried out. The intermediate and final products are sometimes treated under pressure. As an illustration, we briefly present possible ways of obtaining neodymium-containing oxyarsenide $NdO_{1-x}F_xFeAs$, whose samples exhibit the critical temperature $T_c \sim 50-51$ K [19, 54] close to the highest record for this class of materials.

To obtain a PC $NdO_{1-x}F_xFeAs$ sample, the authors of [19] used Nd + As + Fe + Fe_2O_3 + FeF_3 reagents, whose powders were mixed to prepare the working mass of nominal stoichiometry $NdO_{0.89}F_{0.11}FeAs$, which was then pressure-pelleted and annealed at $T = 1300\,^\circ$C in a container with boron nitride at the pressure $P = 6$ GPa for two hours. Along with Nd – Fe oxyarsenide as the main superconducting phase, the final products contained nonsuperconducting impurity oxide, fluoride, and arsenide phases. To obtain $NdO_{0.9}F_{0.1}FeAs$ samples, the authors of [54] used another set of reagents: $NdFe_3As_3 + Nd_2O_3 + NdF_3 + Nd$. The pellets made of the mixture of these reagents were heated for an hour to 1350 – 1400 °C, kept at this temperature for 4 to 8 h, and then cooled in air. The synthesis was carried out at the pressure 3.3 GPa. The polycrystalline samples obtained included small (nearly 300 mm) single-crystal plates.

A similar method was used to obtain samples of a more involved chemical composition [70], namely, $La_{1-x}K_x(O_{1-x}F_x)FeAs$ ($x = 0.15$, 0.20) oxyarsenides with a potassium-doped lanthanum sublattice and a fluorine-doped oxygen sublattice. A mixture of La_2O_3+FeAs+La+KF powders was used, which was first annealed for 48 h at $T = 1000\,^\circ$C and then pelleted under pressure. The pellets were wrapped in Ta foil, placed into a vacuumized SiO_2 cell, and again annealed for 48 h at $T = 1180\,^\circ$C. Such a procedure allows [70] using the set of reagents La_2O_3 + FeAs+ La +LaF_3 to obtain superconducting samples of conventional fluorine-doped $LaO_{1-x}F_xFeAs$ oxyarsenide in which LaOF (10%) and Fe_2As ($\sim 5\%$) have been identified as impurity phases. It is noted in [70] that when $LaO_{1-x}F_xFeAs$ is obtained by other methods (see Table 1), the set of secondary phases is much richer and can include LaOF, FeAs, Fe_2As, $La_{4.67}(SiO_4)_3O$, and La_2O_3.

The so-called low-temperature method for obtaining oxyarsenide $NdO_{0.85}FeAs$, which is nonstoichiometric in

oxygen, was proposed in [49], where the synthesis is carried out at $T \sim 900\,^{\circ}C$, as distinct from other methods, in which thermal treatment proceeds at $T > 1150\,^{\circ}C$ (see Table 1). The authors used the standard scheme of solid-phase synthesis from a pelleted $NdAs + Fe + Fe_2O_3$ mixture that was annealed in a quartz tube for 36 h at $T \sim 900\,^{\circ}C$. At the second stage, the obtained polycrystalline samples were additionally annealed at $T = 1300\,^{\circ}C$ for two hours at the pressure 6 GPa. The analysis has shown that sufficiently high-quality $NdO_{0.85}FeAs$ samples can be obtained without additional thermal and pressure treatment. As a preliminary stage, the methods in [19, 49, 54] included obtaining binary (ternary) phase-reagents NdAs, $NdFe_3As_3$, Nd_2O_3, NdF_3, etc.

The authors of [66] developed the so-called single-stage method, which was applied successfully to obtain superconducting 54.6-K $SmO_{0.7}F_{0.3}FeAs$ samples. The method allowed avoiding some intermediate procedures such as grinding, repeated pelleting, and annealing, which is very important in handling toxic substances such as arsenic. The $Sm + As + SmF_3 + Fe + Fe_2O_3$ mixture was immersed in a tantalum tube sealed on one end. When filled, the Ta tube was closed on the other end by squeezing and was placed in an iron tube. The procedures were performed in an inert atmosphere and then annealing was applied in a furnace at $T = 1160\,^{\circ}C$ (in an Ar flow to minimize possible product oxidation) for 40 hours. The samples (which were a conglomerate of nearly 10 μm plates) (Fig. 2a) were taken off after breaking the tantalum tube.

The above technique (known in the technology of obtaining HTSC materials as 'powder in tube') is not only used to synthesize samples of superconducting materials but is also regarded as a method allowing fabrication of long wires of superconducting materials for further use. The first attempts were made to use this method to obtain wires of superconducting oxypnictides $NdO_{0.82}F_{0.18}FeAs$ [67] and $LaO_{1-x}F_xFeAs$ [68]. For example, an iron tube (8 mm in diameter with the wall thickness 1.5 mm) was used that was covered inside with a very thin titanium buffer layer. The tube was filled with $La + As + LaF_3 + Fe + Fe_2O_3$ powder and was then wiredrawn to obtain wire 2 mm in diameter. After this, it was annealed at the temperature 1150 °C for 40 h. These wires are shown in Fig. 2b. Measurement of the electric resistance of the material thus synthesized gave the critical transition temperature close to 24 K.

Several methods have been proposed (see Table 1) for obtaining single-crystal superconducting oxyarsenide samples, which is exceedingly important for detailed studies of anisotropy of the physical properties of these layered compounds.

The most frequently used method is crystallization in a melt. For example, the authors of [55] obtained $NdO_{0.82}F_{0.18}FeAs$ single crystals in an NaCl melt. The synthesis went on in two stages. First, an Nd + As (1:1) pelleted mixture was used to prepare neodymium arsenide. The pellets were put into a vacuumized quartz ampule and annealed at $T = 800\,^{\circ}C$ for ten hours. Then the pellets were ground and mixed with NdF_3, Fe_2O_3, and Fe powders in the ratio corresponding to the $NdO_{0.82}F_{0.18}FeAs$ stoichiometry. The mixture obtained was pressed into tablets and mixed with NaCl (in the ratio 1:10) and was again placed into a vacuumized quartz ampule. The thermal treatment proceeded at $T = 1050\,^{\circ}C$ for ten days. The sample was first cooled with a step of 3 °C an hour to $T = 850\,^{\circ}C$ and was then rapidly cooled to room temperature. The resulting product (with an NdClO impurity phase) contained scaly crystallites 5 to 30 μm long and 1 to 5 μm thick (Fig. 2c).

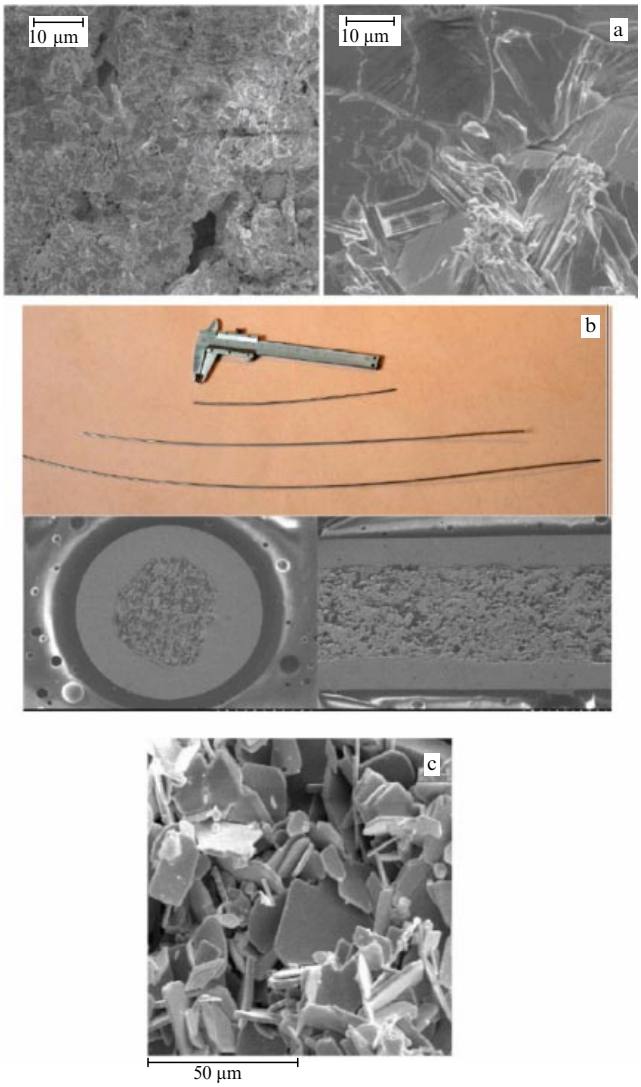

Figure 2. (a) Microphotograph of a superconducting ($T_c = 54.6$ K) $SmO_{0.7}F_{0.3}FeAs$ sample synthesized by the single-stage method [66]. (b) The general view of the wires: the superconducting $LaO_{1-x}F_xFeAs$ in an iron tube (at the top of the figure) and the microphotographs of the longitudinal and transverse wire cross sections [68]. (c) Microphotograph of single-crystal $NdO_{0.82}F_{0.18}FeAs$ plates, taken using scanning electron microscopy [55].

Another approach suggests obtaining single crystals under pressure. For example, $PrO_{1-x}FeAs$ crystal samples nonstoichiometric in oxygen were obtained in [69] from a mixture of $PrAs + Fe + Fe_2O_3$ powders placed in a cell of boron nitride for two hours at $T = 1300\,^{\circ}C$ to obtain scaly crystallites with characteristic sizes 150 × 150 μm.

Along with the above-mentioned oxyarsenides, a fairly representative set of related phases oxyphosphides, as well as the first oxybismuthides of transition and rare-earth metals (see Table 1), were obtained, which can be regarded as the initial phases in the search for new superconducting materials.

On the whole, we note that a number of effective methods for obtaining sufficiently high-quality single-crystal and polycrystalline samples of superconducting 1111-materials based on oxyarsenides of transition and rare-earth metals

have been worked out. These methods allow obtaining samples for numerous physical experiments on the study of their physical properties and underlie the further progress in the science of materials of new superconductors.

2.2 Crystal structure of oxypnictides and superconductors based on them

As has already been mentioned, the discussed superconducting oxyarsenides belong to the large family of rare-earth and transition metal *Ln*O*MPn* oxypnictides, which comprise more than a hundred known representatives [71, 83–86].

Under ordinary conditions, zero-defect stoichiometric *Ln*O*MPn* phases have a layered tetragonal structure (ZrCuSiAs type, space group $P4/nmm$, $Z = 2$) [71] formed by stacking oppositely charged molecular layers $(LnO)^{\delta+}/(MPn)^{\delta-}$ along the *c*-axis (Figs 1, 3a). It is immediately noted that for superconductors ($T_c > 26$ C) obtained on the basis of matrix 111-phase *Ln*OFeAs, the electron concentration in FeAs layers changes considerably as a result of the so-called modulation doping. For instance, the donor electrons in FeAs layers can be due to a partial replacement of bivalent O^{2-} anions by univalent F^{1-} in neighboring *Ln*O layers, which results in an increase in the difference between the charge states of *Ln*O and FeAs layers.

Each *MPn* layer consists of a square net of *M* atoms, above and below which are the pnictogen *Pn* atoms. The transition metal atoms have coordination numbers (CNs) equal to four, and their coordination polyhedrons (CPs) are MPn_4 tetrahedrons compressed along the *c*-axis. In other words, the *MPn* molecular layer can be represented as consisting of conjugate MPn_4 tetrahedrons. In turn, for the atoms of rare-earth elements *Ln* with CN = 8, the CPs are distorted square LnO_4Pn_4 antiprisms; for oxygen atoms, CN = 4 and the CPs are OLn_4 tetrahedrons.

The crystal structure of tetragonal *Ln*O*MPn* is characterized by the lattice parameters *a* ($b = a$) and *c* and by two so-called internal parameters z_{Ln} and z_{Pn} respectively determining the *Ln*–O and *M*–*Pn* interlayer spacings (see [71]). In the cell, the atoms occupy the following positions: *Ln*, $2c(0.25, 0.25, z_{Ln})$; O, $2a(0.75, 0.25, 0)$; *M*, $2b(0.75, 0.25, 0.5)$; and *Pn*, $2c(0.25, 0.25, z_{Pn})$.

The lattice parameters for several four-component *Ln*OFeAs oxyarsenides and new superconducting materials based on them are presented in Table 3.

The authors of [36] noticed a correlation between the critical temperature and the *Ln*OFeAs lattice parameters: the T_c value decreases considerably with increasing the parameter *a* (Fig. 3b). This dependence is sometimes interpreted in terms of the internal or chemical pressure created by rare-earth metal (REM) atoms in the lattice, but the origin of such a correlation actually remains unclear. Another interesting correlation was found between T_c and the angles α of As–Fe–As bonds in $FeAs_4$ tetrahedrons that form FeAs layers in the oxyarsenide structure [88]. Figure 3c shows that the critical temperature increases greatly as α approaches 109.47°, i.e., when $FeAs_4$ groups assume a shape close to regular tetrahedrons. It was noted that such a structural transformation of $FeAs_4$ groups, for instance, in the structure of NdOFeAs was favored by oxygen vacancies in the composition of NdO layers [88].

In the low-temperature range, according to the results of neutron diffraction experiments [20] and X-ray diffraction on $LaO_{1-x}F_xFeAs$ powders [89], in nonsuperconducting compositions of 1111 oxyarsenides, the tetragonal (space group

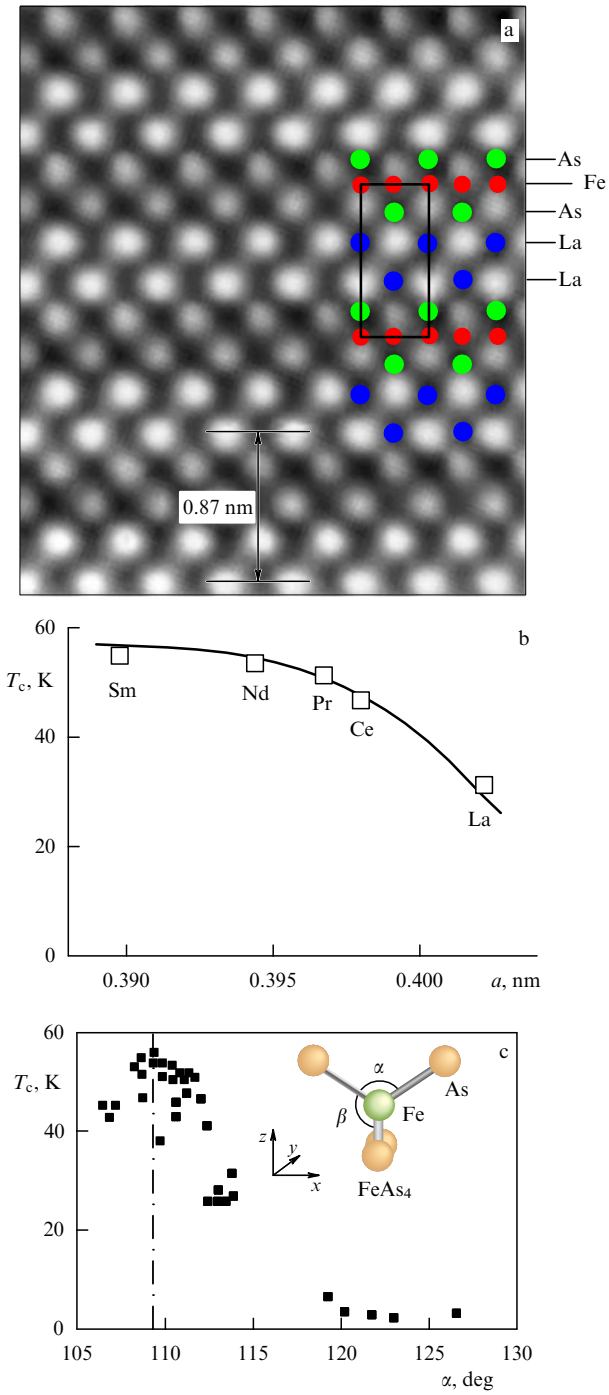

Figure 3. Atomic structure of LaOFeAs (in the [100] direction) (according to the data of high-resolution transmission microscopy) [87]). (b) Correlations between the critical transition temperature and the lattice parameter *a* for superconducting oxyarsenides $LnO_{1-x}FeAs$, *Ln* = La, Ce, Pr, Nd, and Sm [36]. (c) Correlations between the critical transition temperature T_c and the As–Fe–As bond angle α in $FeAs_4$ tetrahedrons constituting the FeAs molecular layers for a number of superconducting oxyarsenides [88].

$P4/nmm$) structure is distorted and a phase transition occurs to the orthorhombic (or monoclinic) structure (space group *Cmma*). Similar conclusions were drawn by the authors of [29], who revealed distortions of the NdOFeAs tetragonal cells at $T = 145$ K, which is 20 K lower than for LaOFeAs; the phase transition to the monoclinic structure can be stimulated by the application of external pressure.

Table 3. Lattice parameters of tetragonal (ZrCuSiAs structural type, space group $P4/nmm$) oxyarsenides of rare-earth and transition metals and superconducting phases based on them.

Phase	T_c^{max}	Lattice parameters			References
		$a(=b)$, nm	c, nm	c/a	
LaOFeAs	—	0.403552	0.87393	2.16559	[1]
$LaO_{1-x}F_xFeAs$, $x = 0.05-0.12$	26	0.40320	0.87263	2.16426	[1]
$LaO_{0.9}F_{0.1}FeAs_{1-x}$, $x = 0.05-0.1$	26–28	0.402819	0.872397	2.16573	[57]
$La_{0.87}Sr_{0.13}OFeAs$	25	0.40350	0.87710	2.17373	[17]
$LaO_{0.9}FeAs$	—	0.403421	0.873545	2.16534	[58]
$LaO_{0.85}FeAs$	28.3	0.4022	0.8707	2.16484	[36]
$La_{1-x}K_xO_{1-x}F_xFeAs$, $x = 0.15$	26.2	0.40293	0.8718	2.16365	[70]
LaONiAs	2.75	0.4119	0.8180	1.98591	[60]
$LaO_{0.9}F_{0.1}NiAs$	3.8	0.4115	0.8169	1.98518	[60]
LaOCoAs	—	0.40526	0.84620	2.0880	[61]
CeOFeAs	—	0.3996	0.8648	2.16416	[51]
$CeO_{0.84}F_{0.16}FeAs$	41	0.3989	0.8631	2.16370	[51]
$CeO_{0.85}FeAs$	42.6	0.3979	0.8605	2.16260	[36]
PrOFeAs	—	0.39853	0.8595	2.15668	[56]
$PrO_{0.89}F_{0.11}FeAs$	52	0.3967	0.8561	2.15805	[56]
$PrO_{0.85}FeAs$	48.2	0.3968	0.8566	2.15877	[36]
$NdO_{0.85}FeAs$	51	0.3943	0.8521	2.16104	[36]
SmOFeAs	—	0.3933	0.8495	2.15993	[26]
SmOFeAs	—	0.39391	0.84970	2.15709	[64]
$SmO_{0.93}F_{0.07}FeAs$	—	0.39344	0.84817	2.15578	[64]
$SmO_{0.90}F_{0.10}FeAs$	55	0.3915	0.8428	2.15275	[26]
$SmO_{0.90}F_{0.10}FeAs$	43	0.3940	0.8496	2.15634	[9]
$SmO_{0.85}FeAs$	55	0.3897	0.8407	2.15730	[36]
$GdO_{0.83}F_{0.17}FeAs$	36.6	0.4001	0.8650	2.16196	[22]
$Gd_{0.8}Th_{0.2}OFeAs$	55	0.3917	0.8440	2.15471	[53]
$GdO_{0.85}FeAs$	53.5	0.3890	0.8383	2.15501	[27]
TbOFeAs	—	0.38632	0.8322	2.15596	[59]
$TbO_{0.8}F_{0.2}FeAs$	45.9	0.3860	0.8332	2.15855	[59]
$Tb_{0.8}Th_{0.2}OFeAs$	52	0.3902	0.84115	2.15569	[62]
$DyO_{0.9}F_{0.1}FeAs$	45.4	0.3843	0.82837	2.15552	[59]

An clear picture of phase transitions for nonsuperconducting ($x \leqslant 0.07$) and superconducting ($x > 0.07$) $SmO_{1-x}F_xFeAsO$ was obtained in [90] using high-resolution synchrotron X-ray diffraction. Figure 4 shows that the phase transition is gradually suppressed under doping and vanishes completely for the fluorine content $x \sim 0.15$. This is also confirmed by the results of other physical experiments, for example, in [35], on measurements of the thermal capacity $C(T)$ of the compound $SmO_{1-x}F_xFeAs$ (Fig. 5a). It is important [90] that for a number of superconducting compositions with the degree of doping below optimum ($x = 0.20$), a low-temperature transition to the monoclinic structure is preserved, but the degree of tetragonal structure distortion notably decreases (see Fig. 4).

On the other hand, it was shown in [91] that primitive cells of these structures become identical if z coordinates of O and Fe atoms are assumed to be respectively equal to 0 and 0.5. In the experiments in [20], the corresponding z values were -0.0057 and 0.5006.

A more involved picture of the interrelation of structural and phase transitions was observed in [92] in a complex study of undoped LaOFeAs with the use of a number of complementary methods. According to the data in [92], a phase transition occurs at $T < 200$ K from the tetragonal

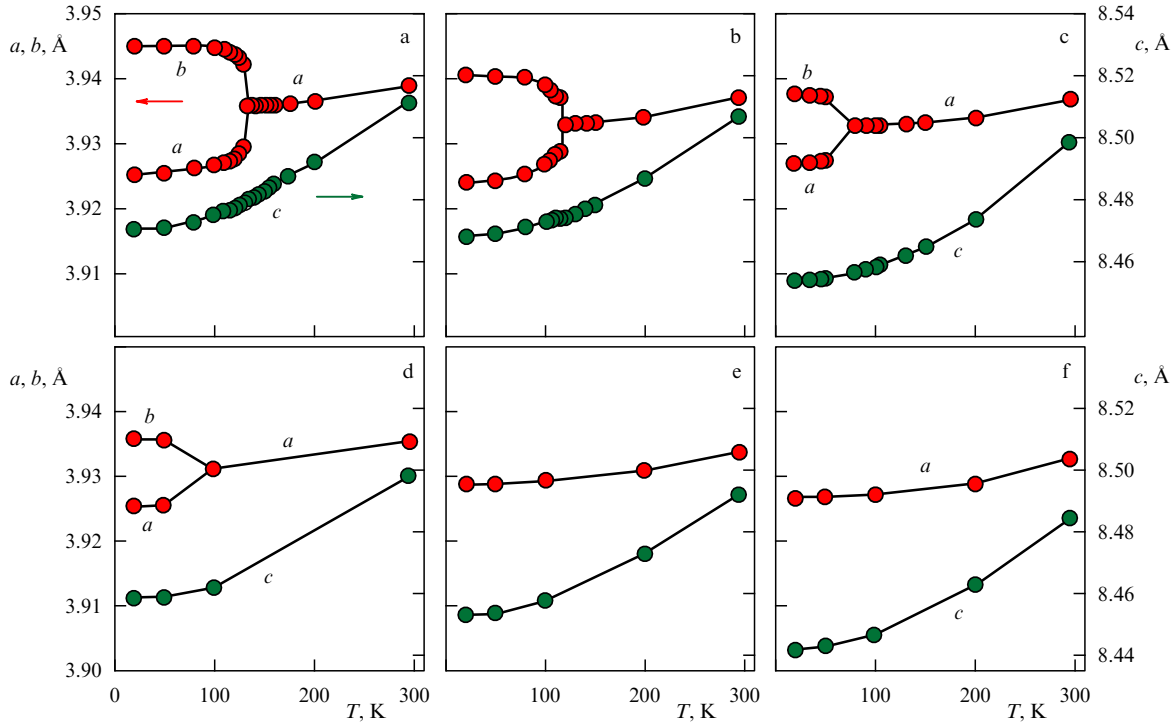

Figure 4. Temperature dependences of the lattice constants a, b, and c for $SmO_{1-x}F_xFeAs$ for $x = 0$ (a), $x = 0.05$ (b), $x = 0.10$ (c), $x = 0.12$ (d), $x = 0.15$ (e), and $x = 0.20$ (f) [90]. The distortion of the tetrahedral structure ($a \neq b$) is seen to decrease with increasing the fluorine content and to vanish at $x \sim 0.15$.

structure (space group $P4/nmm$) with the parameters $a = b = 0.403463(5)$ nm and $c = 0.874382(15)$ nm to the orthorhombic structure (space group $Cmma$) with the parameters $a = 0.568100(14)$ nm, $b = 0.571000(14)$ nm, and $c = 0.87144(2)$ nm ($T = 85$ K). The transition could be induced [92] by the Jahn–Teller effect accompanied by a significant decrease in the density of states $N(E_F)$ at the Fermi level upon lattice distortion. After the end of the structural transition at $T = 145$ K, a magnetic phase transition occurs due to the formation of a long-range order for Fe magnetic moments. It is noteworthy that the electron or hole doping of oxyarsenides suppresses these phase transitions.

The situation described is vividly illustrated by the diagram in Fig. 5b based on the results of experiments with fluorine-doped oxyarsenide $LaO_{1-x}F_xFeAs$ using muon (muon spin rotation, μSR) nuclear gamma-resonant (NGR) (on ^{57}Fe nuclei) spectroscopy [93]. It follows that in the region of low fluorine concentrations ($x < 0.04$) when the temperature decreases at the first stage (at $T \sim 155$ K), a phase transition occurs from the tetragonal structure to the orthorhombic one and then (at $T \sim 140$ K) a long-range magnetic order [i.e., the region of spin density waves (SDWs)] is formed. On the contrary, for $x > 0.045$, $LaO_{1-x}F_xFeAs$ oxyarsenides preserve their tetragonal structure and pass into the superconducting state at low temperatures. The features of the structure of the transition region — between the magnetic and superconducting states of $LaO_{1-x}F_xFeAs$ ($x \sim 0.04-0.06$) — are discussed in more detail in [94] based on the data of μSR spectroscopy.

Because all superconducting 1111 materials are nonideal (doped or nonstoichiometric) *Ln*OFeAs compositions, certain attention is paid to the study of the sublattice doping effect (or the presence of atomic vacancies) on their crystallographic parameters. Generalizing the results (see Table 3), we can state that changes in the lattice parameters of doped phases normally obey the Vegard rule, i.e., the parameters increase (decrease) monotonically with increasing the concentration of a dopant with a larger (smaller) ion radius than that of the replaced element.

For nonstoichiometric oxyarsenides, no systematic data are available on the interrelation between the type and concentration of vacancies (in the oxygen [27, 36, 49, 58] or arsenic [57] sublattices). It was noted in [36] that when 15% of oxygen vacancies are introduced in $LnO_{0.85}FeAs$ phases (*Ln* = La–Sm), the FeAs layers are compressed (by about 3.1%) along the *a*-axis. For all superconducting phases based on *Ln*OFeAs, the basic tetragonal structure is preserved. Detailed information on local structure deformations (atomic relaxation effects) near impurities and (or) vacancies in oxyarsenides is absent. Neither do systematic data exist on the concentration changes in the structure parameters of *Ln*OFeAs upon a simultaneous introduction into a crystal of different types of defects, for instance, substitutional impurities (Sr → La) and oxygen sublattice vacancies ($La_{0.85}Sr_{0.15}O_{1-x}FeAs$ [63]) or As-vacancies and fluorine impurities in the oxygen sublattice ($(La(O_{0.9}F_{0.1})FeAs_{1-x}$ [57]).

Studies [87] of the structure features of *Ln*OFe*Pn* (*Ln* = La, Nd, *Pn* = As, P) phases by electron diffraction and high-resolution transmission electron microscopy (TEM) have in particular allowed visualizing their atomic structure (Fig. 3a) and discussing some structural defects in these crystals. For example, defects in layer stacks (stack faults) and extensive planar defects (along *ab*-planes) have been noted to appear near the grain boundaries in polycrystalline samples. The structural stresses and distortions in the vicinity of such defects (within the radius of 5 nm) can be seen in Fig. 5c. The origin of such defects is

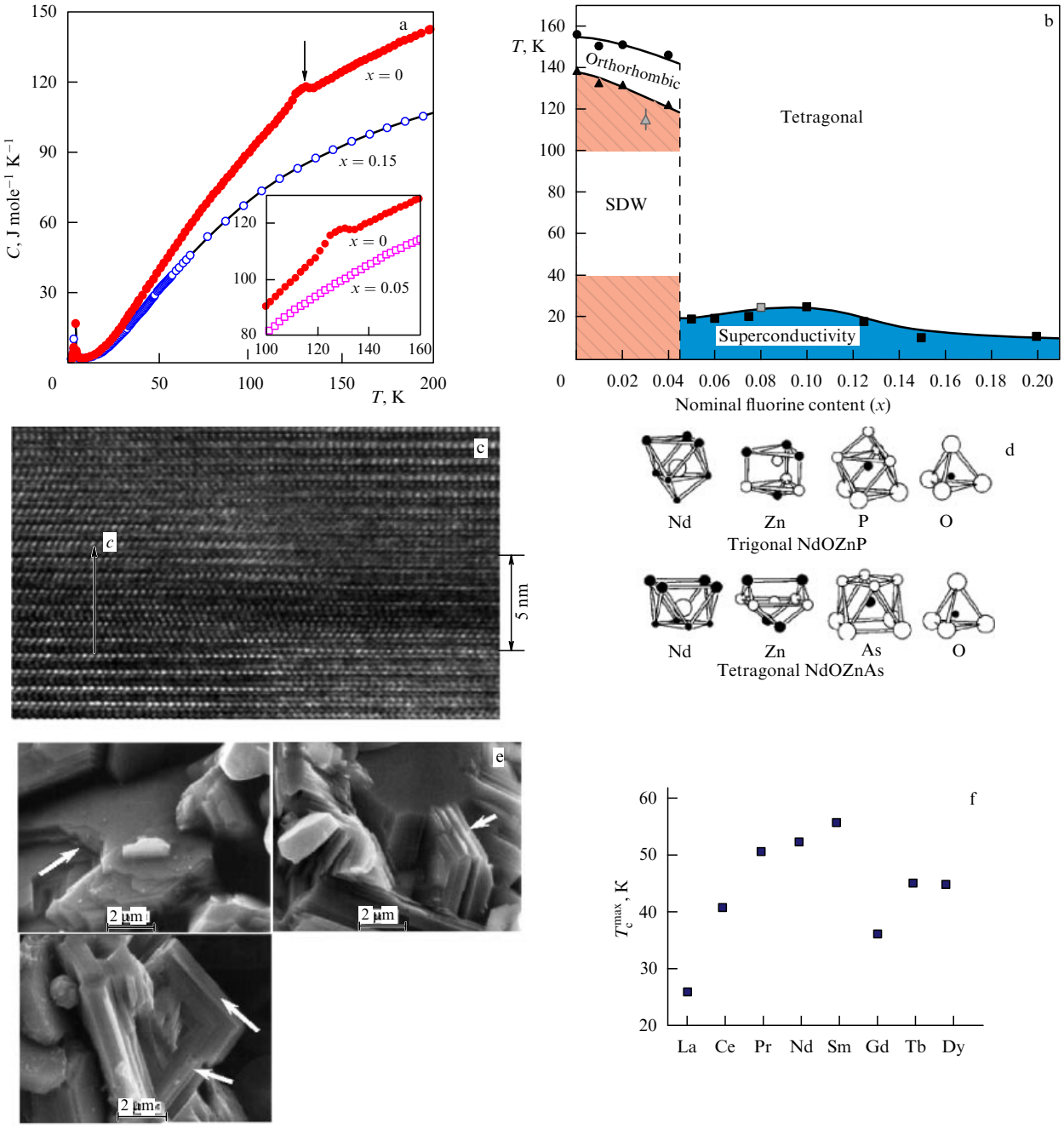

Figure 5. (a) Temperature dependence of the thermal capacity of $SmO_{1-x}F_xFeAs$ with a variable composition (x) [35]. The arrow shows a C jump at $T = 130$ K corresponding to the phase (magnetic) transition. (b) Generalized phase diagram of fluorine-doped $LaO_{1-x}F_xFeAs$ [93]. (c) Region of distortion (in the [100] direction) of an LaOFeP atomic structure in the presence of layer stack faults according to the data of high-resolution transmission microscopy [87]. (d) Coordination polyhedrons of the component atoms for the tetragonal and trigonal structures of the *Ln*OZn (P, As) oxypnictide family [72]. (e) Microphotographs of the structure of $LaO_{1-x}F_xFeAs$ samples [95]. The arrows indicate lamellar microcrystallites. (f) Maximum critical transition temperatures for fluorine-doped $LnO_{1-x}F_xFeAs$ oxyarsenides.

associated with the characteristics of the synthesis of these oxypnictides [87].

The crystallographic parameters of 17 quaternary oxyphosphide phases — *Ln*OFeP (*Ln* = La–Nd), *Ln*ORuP (*Ln* = La–Nd, Sm, Gd), and *Ln*OCoP (*Ln* = La–Nd–Sm) — are given in [71]. The authors of [72] present crystallographic data on the structure of 12 zinc-containing *Ln*OZnAs oxyphosphides (*Ln* = Y, La–Nd, Sm, Gd–Tm) and nine *Ln*OZnAs oxyarsenides (*Ln* = Y, La–Nd, Sm, Gd–Dy), which are crystallized in the form of either a tetragonal ZrCuSiAs-type or a trigonal NdOZnP-type (space group *R*3*m*) structure. Both structures are composed of *Ln*O and Zn(P, As) layers, but differ in the atom coordination types (Fig. 5d).

To conclude this section, we mention papers [95–97], where the oxypnictide microstructure was studied. Attention is typically given to the lamellar form of microcrystallites in the composition of the obtained products; these microcrystallites can form different conglomerates (Fig. 5e). The microstructure of $NdO_{1-x}F_xFeAs$ samples was recently studied with the help of scanning SQUID (superconducting quantum interference device) microscopy [96]. The depen-

dence of magnetization of polycrystalline $LaO_{0.89}F_{0.11}FeAs$ and the occurrence of percolation currents on the grain size were considered in [97].

3. Physical properties of superconducting oxyarsenides

In this section, we present the results of physical experiments on the study of properties of new oxyarsenide 1111 materials, the greatest attention being naturally attracted by their superconducting and magnetic parameters.

3.1 Superconductivity of oxyarsenides

As has already been noted, the majority of known ideal undoped tetragonal ZrCuSiAs-type *Ln*O*MPn* oxypnictides are not superconductors, and only some phases (e.g., LaOFeP or LaONiP [see Table 1]) exhibit a low-temperature ($T_c < 6$ K) transition to the superconducting state [74–76]. This effect is well described [98–101] within the standard concepts of the electron–phonon mechanism in the Bardeen–Cooper–Schrieffer (BCS) model and is of no special interest for science.

We note that based on measurements of the temperature dependences of the LaOFeP and $LaO_{0.94}F_{0.06}FeP$ thermal capacity, the authors of [102] assume the presence in these phases of strong electron correlations and spin fluctuations, which may be indicative of a nontraditional type of pairing due to the above-mentioned spin fluctuations. On the other hand, detailed studies [76] of highly certified LaOFeP samples have not revealed any superconducting transition (at temperatures up to $T \sim 0.35$ K), and reports on the superconductivity of this oxyphluoride were explained in [76] either by the nonstoichiometry of the investigated samples in oxygen or by the presence in them of impurity phases such as $LaFe_4P_{12}$ ($T_c = 4.1$ K [103]) or metallic lanthanum ($T_c = 6.9$ K), whereas the stoichiometric LaOFeP is an ordinary paramagnetic metal.

According to the available data (see [1, 5–27]), high-temperature ($T_c > 26$ K) superconductivity occurs exclusively in oxyarsenide phases under the obligatory condition of their doping by electrons or holes (see Table 1).

As was shown in the pioneering work [1], the critical temperature $T_c \sim 26$ K for LaOFeAs could be obtained when the oxygen sublattice was doped with fluorine, $LaO_{1-x}F_xFeAs$ ($x = 0.12-0.15$), $T_c \sim 26$ K. This technique was immediately used for a number of related *Ln*OFeAs phases (*Ln* = Ce, Pr, Nd, Sm, Gd), with the result that a family of new HTSCs was discovered with the critical temperatures $T_c \sim 41$ K ($CeO_{1-x}F_xFeAs$) [51], $T_c \sim 52$ K ($PrO_{1-x}F_xFeAs$) [56], $T_c \sim 51$ K ($NdO_{1-x}F_xFeAs$) [19], $T_c \sim 56$ K ($SmO_{1-x}F_xFeAs$) [26], and $T_c \sim 37$ K ($GdO_{1-x}F_xFeAs$) [53]. Furthermore, fluorine-doped terbium and dysprosium oxyarsenides $TbO_{1-x}F_xFeAs$ ($T_c \sim 46$ K) and $DyO_{1-x}F_xFeAs$ ($T_c \sim 45$ K) with unstable stoichiometric (TbDy)OFeAs phases have been synthesized for the first time [59]. We note that the critical temperature $T_c \sim 56$ K attained for a number of fluorine-doped samarium oxyarsenide samples [26] is presently the maximum for the given class of materials (Fig. 5f).

It has been found that the HTSC state in 1111 oxypnictides through electron doping can also be reached by replacing the trivalent ion Ln^{3+} by tetravalent thorium in the *Ln*O layer. As a result, the superconductors $Gd_{1-x}Th_xOFeAs$ ($T_c \sim 55$ K) [22] and $Tb_{1-x}Th_xOFeAs$ ($T_c \sim 52$ K) [62] were successfully synthesized [62]. We note that T_c of these materials was by $\sim 10-15$ K higher than that for HTSC systems based on the same oxyarsenides (GdOFeAs and TbOFeAs), in which a close doping level was reached by the introduction of fluorine into the oxygen sublattice. The cause of this effect is yet unknown. Attempts to reach an HTSC state by fluorine doping of oxyarsenides containing transition metals (Ni, Ru [60, 104]) other than iron have failed, the same as doping of oxyphosphides [76].

The hole doping, which turned out to be an effective way of obtaining HTSC oxyarsenides along with the electron doping, was realized in two ways (see Table 1). The first way is by creating a certain concentration of atomic vacancies in the oxygen sublattice; for a series of nonstoichiometric $LnO_{0.85}FeAs$ phases (*Ln* = La, Ce, Pr, Nd, Sm), the achieved effect [36] is illustrated in Fig. 6a, b. Interestingly, the introduction of oxygen vacancies into some *Ln*OFeAs oxyarsenides allowed obtaining HTSC materials with the maximum T_c exceeding the T_c values of the corresponding fluorine-doped systems, whereas for other *Ln*OFeAs, the situation was the opposite (see Table 1).

The second way of hole doping consists in replacing the trivalent ion Ln^{3+} in the *Ln*O layer by a bivalent dopant, e.g., Sr^{2+} [17]. At the same time, an attempted double hole doping (i.e., a simultaneous creation of oxygen vacancies and a partial substitution of strontium for lanthanum atoms in LaOFeAs) has led to a dramatic decrease in T_c: for an $La_{0.85}Sr_{0.15}O_{0.87}FeAs$ sample, the temperature $T_c \sim 8$ K was obtained [63]. On the other hand, double doping La → K and O → F (the compositions $La_{1-x}K_x(O_{1-x}F_x)FeAs$ with $x = 0.15, 0.20$) practically unaffected the value $T_c \sim 26$ K [70] achieved for $LaO_{1-x}F_xFeAs$ samples with $x = 0.05-0.12$ [1]. Finally, a third way of hole doping was considered in [57]. The investigated samples contained vacancies in the arsenic sublattice: $LaO_{0.9}F_{0.1}FeAs_{1-x}$, $x = 0.05-0.1$. Compared to $T_c \sim 26$ K of the oxyarsenide $LaO_{1-x}F_xFeAs$, the critical temperature of $LaO_{0.9}F_{0.1}FeAs_{1-x}$ changes little ($T_c \sim 26-28$ K) [57].

The accumulated experimental material suggests a number of factors affecting the critical transition temperature for superconducting 1111 materials based on oxyarsenides.

Some of them have already been mentioned. These are structural factors: lattice parameters (Fig. 3b) and the As–Fe–As bond angles in $FeAs_4$ tetrahedrons (Fig. 3c), and also chemical factors directly related to them: the composition (Fig. 5f) and the degree of completeness of crystal sublattices (deviation from stoichiometry). In studying the correlation relations between T_c and the angles ($\alpha_{1,2}$) of Fe–As–Fe bonds and between T_c and the lengths (d) of Fe–Fe and Fe–As bonds, the authors of [105] revealed the absence of any correlations between T_c and d and, on the contrary, a clear dependence of T_c on the angles $\alpha_{1,2}$ (Fig. 6c). This dependence is explained by the existence of correlation relations between these angles, the exchange parameters $J_{1,2}$, and the valence band width [106, 107]. Then the quantity T_c must be directly related to the parameter U/W [105], where U is the Coulomb correlation parameter.

Analyzing the data on the concentration dependence of T_c for the electron (F → O) and hole (Sr → La) doping of LaOFeAs, the authors of [108] found that the change in T_c of 1111 superconducting materials relative to T_c of the basis (nonsuperconducting) phase is symmetric (Fig. 6d). However, no correlation exists between the lattice parameters (a and c) and T_c in the region of either electron (I) or hole (II)

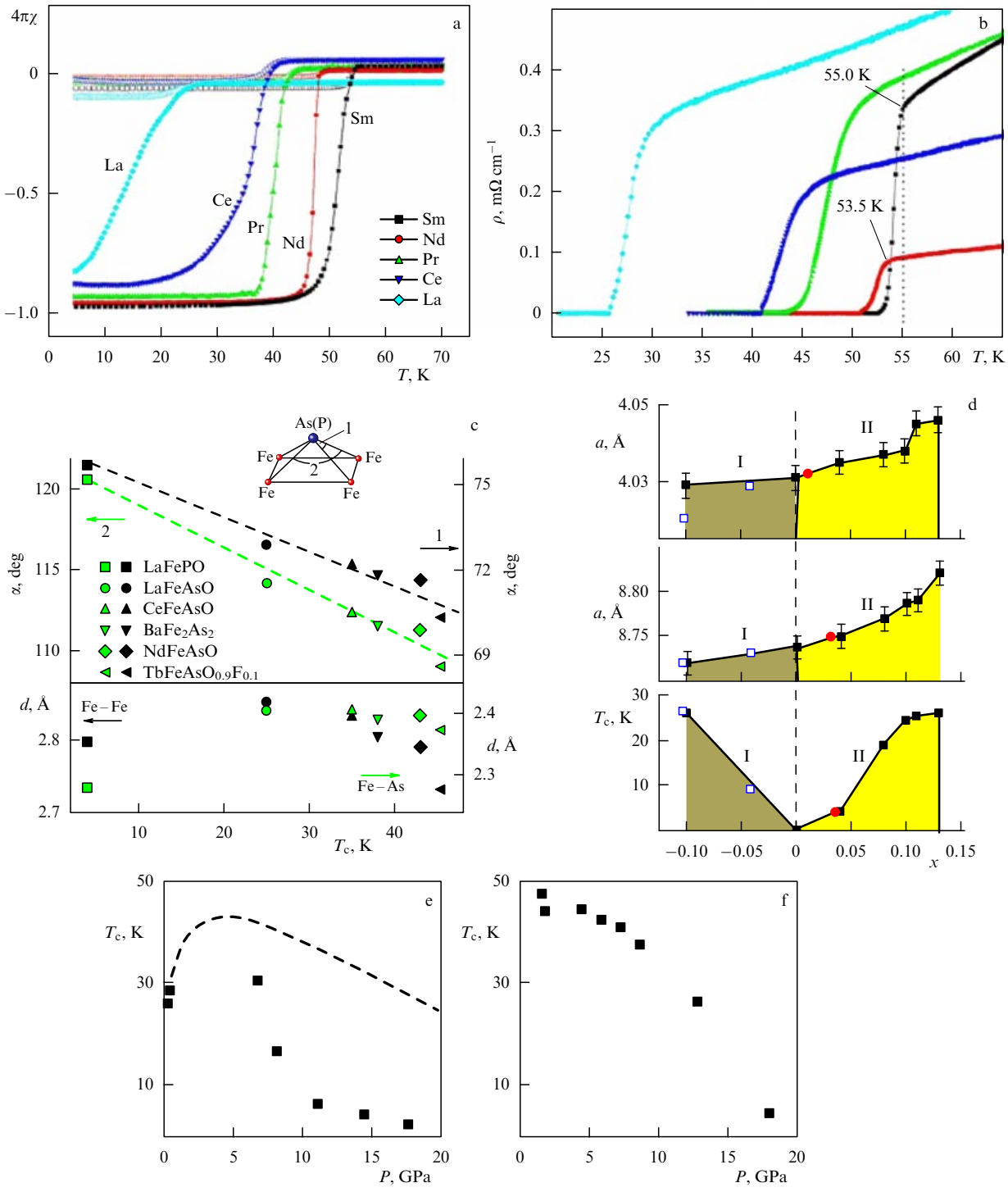

Figure 6. Temperature dependences of the magnetic susceptibility χ (a) and the electric resistance ρ (b) for nonstoichiometric $LnO_{0.85}FeAs$ oxyarsenides (Ln = La, Ce, Pr, Nd, Sm) [36]. (c) Correlation relations between T_c and the bond angles $\alpha_{1,2}$ and between T_c and the interatomic distances d for some superconducting arsenides [105]. (d) Concentration dependences of T_c and the lattice parameters a and c on the electron (region I: F $\rightarrow$ O) and hole (region II: Sr $\rightarrow$ La) doping of LaOFeAs [108]. Dependences of the critical temperature of $La_{0.89}F_{0.11}FeAs$ (e) (dashed curve is the data in [6]) and $CeO_{0.88}F_{0.12}FeAs$ (f) on the external pressure P [111].

doping: with increasing T_c, both parameters (a and c) decrease in region I and increase in region II.

One of the important factors that significantly affects the critical transition temperature in oxyarsenides is the external pressure P. This fact was repeatedly noticed in those papers (see [49, 109, 110]) where synthesis under pressure was used.

Special studies of the effect of pressure for samples of the nominal composition $La_{0.89}F_{0.11}FeAs$ [6, 50] revealed a nonmonotonic increase in T_c from 26 K at $P = 0$ to the maximum value $T_c \sim 43$ K at $P = 4$ GPa. A further increase in P leads to a rapid decrease in T_c. According to the estimates in [50], T_c increases in the pressure range from atmospheric to $P = 1.93$ GPa: $dT_c/dP \sim 1.2$ K GPa^{-1}.

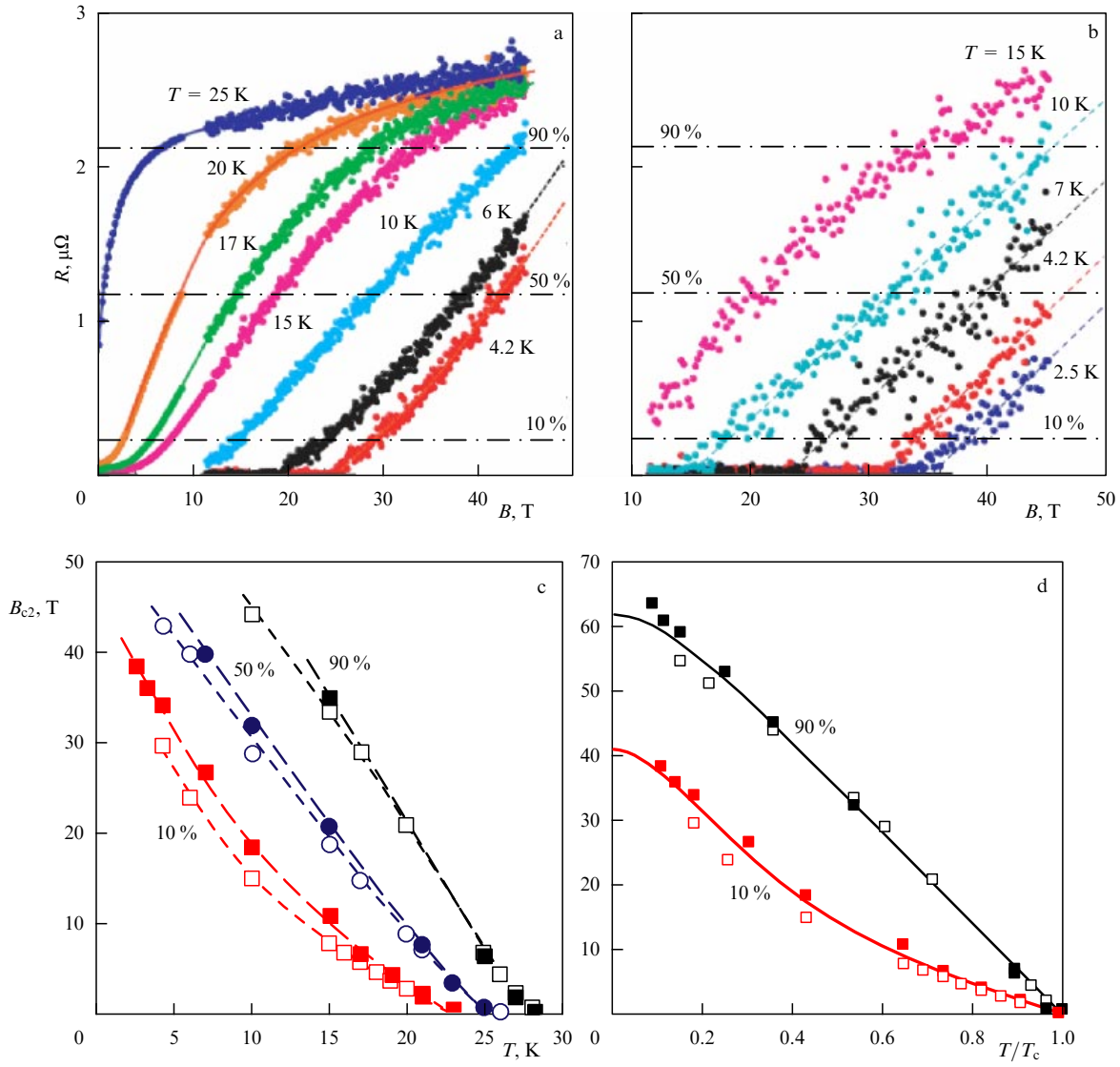

Figure 7. (a, b) Dependence of the resistance R of superconducting oxyarsenide $LaO_{0.89}F_{0.11}FeAs$ on the external magnetic field B perpendicular (a) and parallel (b) to the sample plane in the temperature range $T = 4.2-25$ K. The horizontal dash-dotted lines show the ratio of the sample resistance to its normal-state resistance $R^T/R^{273\,K}$ [10]. (c) Temperature dependence of the critical magnetic field B_{c2}. (d) Comparison of the experimental and theoretical dependences $B_{c2}(T)$ (calculated in the Ginzburg–Landau theory for different resistive states) for an $LaO_{0.89}F_{0.11}FeAs$ sample (the ratio $R^T/R^{273\,K}$ is given in percent). The symbols □, ○ and ■, ● respectively correspond to parallel and perpendicular sample plane orientation relative to the external field.

Comparative studies [111] of the dependence T_c/P for oxyarsenides with different REMs, $La_{0.89}F_{0.11}FeAs$ and $CeO_{0.88}F_{0.12}FeAs$, showed (Fig. 6e, f) that T_c reaches its maximum in the pressure range 1–6.8 GPa for $La_{0.89}F_{0.11}FeAs$, but when pressure is applied to a $CeO_{0.88}F_{0.12}FeAs$ sample, T_c decreases monotonically (from 47 K) to 4.5 K at $P = 19$ GPa. A possible simple explanation of this result is as follows [111]. The application of external pressure promotes an increase in the carrier concentration in the FeAs layer. But each superconducting oxyarsenide has its own optimum doping level corresponding to the maximum T_c. Therefore, the initial T_c increase with increasing the pressure can be explained for $La_{0.89}F_{0.11}FeAs$ by the fact that the doping level of this sample is below ideal, whereas the $CeO_{0.88}F_{0.12}FeAs$ doping level is close to the ideal and its compression leads to a decrease in T_c.

The character (positive or negative) of the applied pressure effect on the T_c value of a particular oxypnictide is directly determined by the level of its doping [112]. An analysis of the experimental results for a series of $SmO_{1-x}F_xFeAs$ samples, both nonsuperconducting ($x = 0$ and 0.05) and superconducting ($x = 0.15$ and 0.30), revealed that T_c increases for $SmO_{0.85}F_{0.15}FeAs$ at the rate ~ 0.9 K GPa^{-1} in the interval $0 < P < 1$ GPa^{-1} and remains practically unchanged (25.6 K) with a further increase in pressure. For $SmO_{0.70}F_{0.30}FeAs$, however, T_c decreases monotonically: $dT_c/dP \sim -2.3$ K GPa^{-1}. We note that the magnetic structure of nonsuperconducting compositions $SmO_{1-x}F_xFeAs$ is also very sensitive to the external pressure (see [112]). This fact was also reported in [29].

3.2 Magnetic characteristics

In a study of the magnetic properties of oxyarsenide phases, attention was largely concentrated on two problems: the establishment of the magnetic state (structure) of the initial (undoped) *Ln*OFeAs crystals and the study of critical fields for superconductors based on these crystals.

The magnetic structure of *Ln*OFeAs crystals was analyzed using several experimental and theoretical approaches, whose results are presented in Sections 3.3 and 4. Here, we only mention some interesting data on the discovery of unexpectedly high upper critical fields B_{c2} for certain 1111 oxyarsenide superconductors, which can be of considerable applied importance for the generation of strong magnetic fields.

The authors of [10] measured the resistance R of superconducting ($T_c = 26$ K) $LaO_{0.89}F_{0.11}FeAs$ depending on the strength of the applied external field B (parallel and perpendicular to the lamellar sample surface) generated by a hybrid magnet at different temperatures (Fig. 7a, b). These data were used to construct the temperature dependences of B_{c2}. Figure 7c, d shows that B_{c2} changes with temperature as $B_{c2}/T = -2$ T K^{-1}, and the maximum B_{c2}^{max} value ($T = 0$) is very high and may reach 60 T. Such investigations were carried out for $NdO_{0.82}F_{0.18}FeAs$ ($B_{c2}^{max} \sim 300$ T) [113], $LaO_{0.9}F_{0.1}FeAs_{1-x}$ ($B_{c2}/T = -5.4$ T K^{-1}, $B_{c2}^{max} \sim 63$ T) [57], $LaO_{0.9}F_{0.1}FeAs$ ($B_{c2}/T = -2.5$ T K^{-1}, $B_{c2}^{max} \sim 56$ T) [114], $SmO_{0.85}F_{0.15}FeAs$ ($B_{c2}/T = -5$ T K^{-1}, $B_{c2}^{max} \sim$ ~ 150 T) [115], $La_{0.9}K_{0.2}O_{0.8}F_{0.8}FeAs$ ($B_{c2}^{max} \sim 122$ T) [70], and $SmO_{0.9}F_{0.1}FeAs$ ($B_{c2}/T = -0.69$ T K^{-1}, $B_{c2}^{max} \sim$ ~ 312 T) [116]. The linear dependence of the lower critical field B_{c1} on T revealed for $LaO_{1-x}F_xFeAs$ samples is discussed in [117].

The authors of [118–122] experimentally measured the magnetic anisotropy parameter $\gamma = \lambda_c/\lambda_{ab}$ (λ is the London penetration depth of the magnetic field into a superconductor) to obtain $\gamma \sim 30$ ($SmO_{0.82}F_{0.18}FeAs$ [119]), $\gamma \sim 5$ ($NdO_{0.82}F_{0.18}FeAs$ [120]), and $\gamma \sim 10$ ($LaO_{0.9}F_{0.1}FeAs$ [121, 122]). For a single-crystal $SmO_{0.8}F_{0.2}FeAs$ sample, a significant temperature dependence of γ was found in [118]: this parameter changed from $\gamma \sim 8$ (at $T \sim T_c$) to $\gamma \sim 23$ at $T \sim 0.4T_c$, which was regarded in [118] as evidence of a multiband type of the superconductor.

Special experiments on a $SmO_{0.8}F_{0.2}FeAs$ single crystal revealed an exponential type of the dependence λ_{ab}/T. According to the estimates in [118], λ_{ab} nearly equals 210 ± 30 nm, and the μRS spectroscopy data [124] give $\lambda(T = 0) \sim 190$ nm.

3.3 Spectroscopic studies of oxyarsenide properties

In this section, we present information on the physical properties of oxyarsenide superconductors obtained using various spectroscopic methods.

X-ray emission spectroscopy (XES) and X-ray absorption spectroscopy (XAS) methods were applied to study lanthanum oxyarsenide $LaO_{1-x}F_xFeAs$ samples for $x = 0, 0.13$ and samarium $SmO_{1-x}F_xFeAs$ for $x = 0.05, 0.15$ [125]. The lines Fe L_3 — XES, (O, F) K_α — XES, and (O,F) 1s — XAS were obtained, which are known to respectively reflect the energy distributions of occupied (Fe) 3d states and occupied and vacant (O,F) 2p states. For undoped LnOFeAs (Fig. 8), it was found that occupied O2p states are practically absent near the Fermi energy E_F and form an intense peak (Fig. 8b) lying approximately 5 eV below E_F. The absorption O1s spectrum contains pronounced peaks at the energies 0.7, 2.6, and 5.9 eV above the Fermi level. The maximum of the emission Fe L_3 spectrum lies 0.9 eV below E_F, while the spectral line also contains burls at energies approximately 3.0 eV below E_F. Such an energy distribution of 3d states of Fe corresponds well to the results of computations in the local density approximation (LDA) and in the LDA + U method (LDA with Coulomb correlations) [14, 15, 30, 126–133], testifying to weak correlation effects in the La–Fe oxyarsenide [125]. Similar conclusions were drawn in [134], where OK spectra (XAS) of $LaO_{1-x}F_xFeAs$ with $x = 0$ and 0.15 were studied.

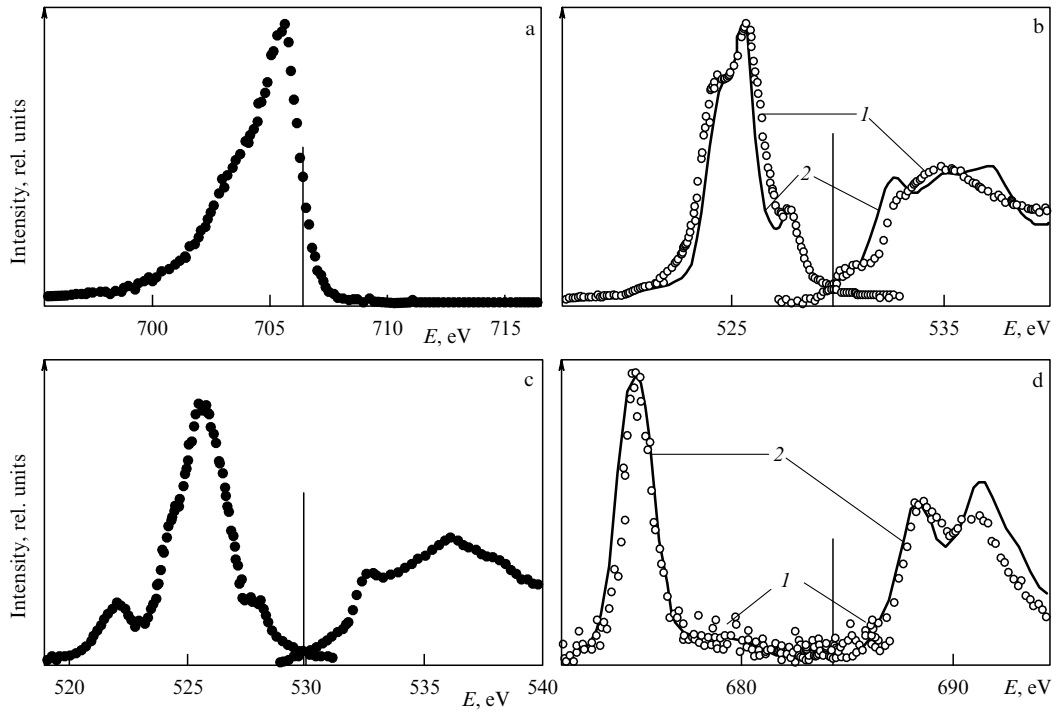

Figure 8. X-ray emission and absorption spectra of La–Fe and Sm–Fe oxyarsenides [125]: (a) FeL_3 — XES and (b) O K_α — XES, O 1s — XAS of undoped LaOFeAs, (c) O K_α — XES, O 1s — XAS and (d) F L_α — XES, F 1s XAS of $SmO_{1-x}F_xFeAs$; (*1*) $x = 0.05$, (*2*) $x = 0.15$. Vertical lines indicate the Fermi level.

With an increase in the doping element (fluorine) in the composition of (La, Sm)$O_{1-x}F_xFeAs$ samples, the main effect was narrowing of the O K_α-bands (XES) and O ls(XAS) (see Fig. 8) [125], whereas the form of the emission Fe L_3-band was virtually unchanged. The emission F K_α-band with maxima lying 7.5 and 9.0 eV below the Fermi level hardly overlaps with the Fe L_3- and O K_α-bands, and therefore the role of fluorine is mainly reduced to a change in the degree of occupation of pre-Fermi states of FeAs layers [125].

***Electron spectroscopy* (*ES*)** was used to study the distribution of valence and core states of 1111 superconductors $SmO_{1-x}F_xFeAs$ ($x = 0.15$ [33], $x = 0.12$, 0.15 [135] and $x = 0$, 0.12, 0.15, 0.2 [136]), $LaO_{1-x}F_xFeAs$ and $LaO_{1-x}F_xFeP$ [137, 138], $LaO_{1-x}F_xFeAs$ ($x = 0$, 0.1, 0.2 [139], and $x = 0.07$ [140]), $NdO_{1-x}F_xFeAs$ ($x = 0$, 0.10) [65], and the isostructural magnets LaOCoAs and LaOCoP [141].

The valence region of a polycrystalline $SmO_{0.85}F_{0.15}FeAs$ sample [33] shows up as a peak in the spectral density of states (SDOS) with the energy lower than E_F by approximately 0.25 eV. This peak is assumed to be due to the pre-Fermi Fe 3d band. No substantial temperature-dependent changes in the form of ES lines (in the range $T = 31-170$ K) testifying to the occurrence of a pseudogap in the superconducting sample were observed. One of the possible explanations can be a very wide superconducting transition region in the investigated polycrystalline ceramics.

However, in subsequent, more detailed experiments [135, 136] (in particular, with the use of angle-resolved ES [136]), a considerable decrease in the spectral density near E_F with decreasing temperature was observed for $SmO_{1-x}F_xFeAs$ samples (Fig. 9), which is indirect evidence of the occurrence of a superconducting pseudogap. No definite dependence of the SDOS variation on the degree of oxyarsenide doping with fluoride was revealed.

A series of ES experiments was performed for oxyarsenides $LaO_{1-x}F_xFeAs$ [137–140]. The core La 4d- and As 3d-lines were found to shift toward the region of high binding energies with an increase in the degree of electron doping (the F/O ratio) [139], and the shift of the 3d line of As, whose atomic surrounding remains unchanged under doping, turned out to be smaller than that for lanthanum. The

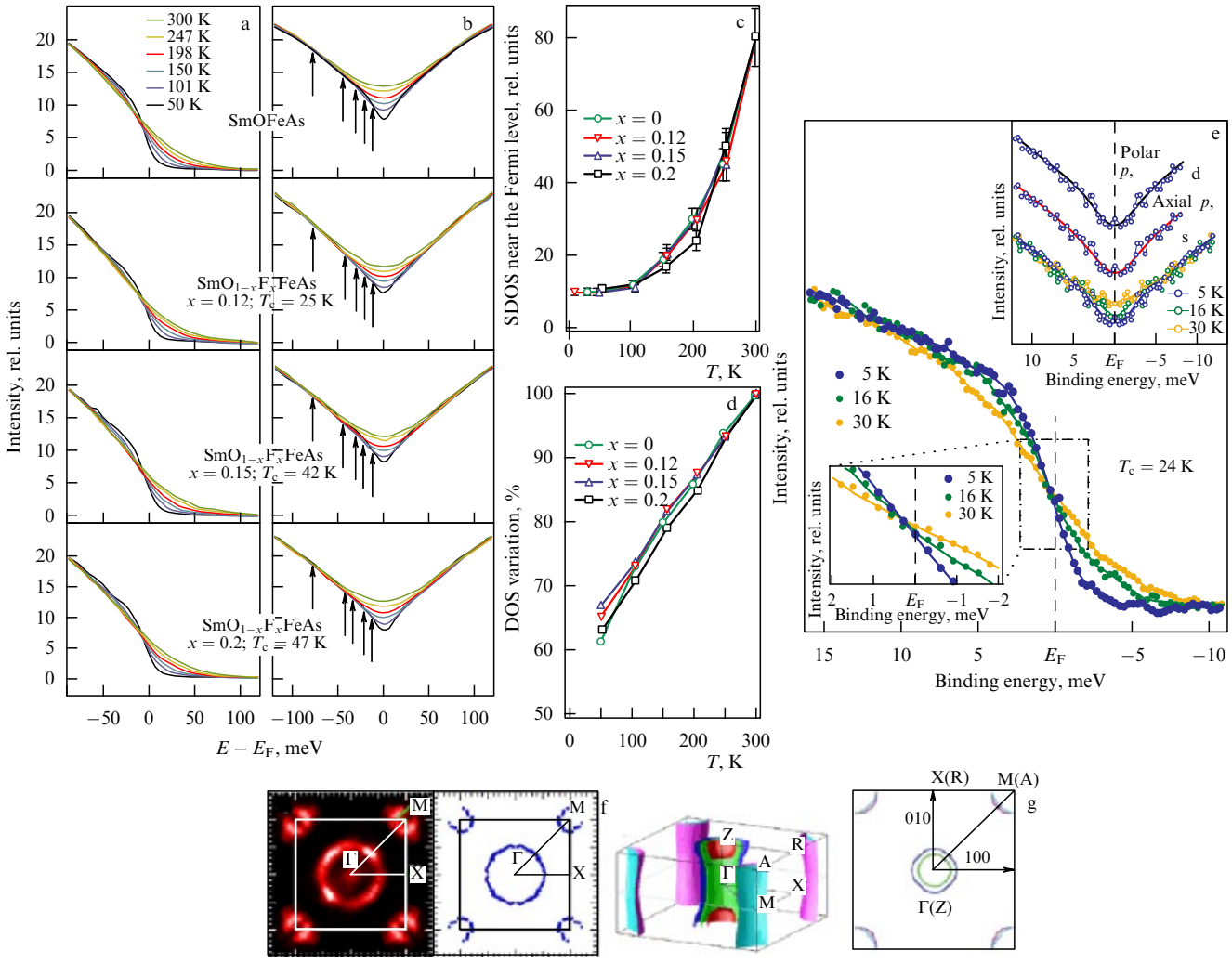

Figure 9. (a) Temperature-dependent electron spectrum variation (excitation energy $h = 22.7$ eV) for $SmO_{1-x}F_xFeAs$ in the pre-Fermi region. (b) Symmetrized forms of spectral lines (the arrows indicate suppression of the spectral density of states (SDOS) with lowering temperature). (c) SDOS near the Fermi level. (d) Temperature-dependent variation of the density of states for different $SmO_{1-x}F_xFeAs$ compositions [136]. (e) Temperature dependences of high-resolution ES spectra in the pre-Fermi region of $LaO_{0.94}F_{0.07}FeAs$ [140]; inset: symmetrized (about E_F) ES spectra and the results of their fitting (at $T = 5$ K) with the use of s-, p- (polar and axial), and d-wave functions. (f, g) Fermi surface of $NdO_{1-x}F_xFeAs$ according to angle-resolved ES data (f) and FLAPW calculations [65] (g).

temperature-dependent behavior of the ES spectra of $LaO_{1-x}F_xFeAs$ (Fig. 9e) testifies to a decrease in the SDOS near E_F with decreasing T. Nevertheless, at low temperatures ($T \approx 5$ K), much lower than $T_c = 24$ K, the DOS is nonzero, which can be due to: 1) a multiband superconductivity type and a gapless state of a part of the Fermi surface (FS) sheets, 2) the presence of an impurity of metal-like nonsuperconducting phases in the sample, or 3) the presence of p- or d-type sites. Numerical approximation of the form of symmetrized (about E_F) spectra (Fig. 9e) in the model of s-, p-, or d-type gaps for the cylindrical topology of the FS has allowed estimating the gap: $\Delta E \sim 3.6 \pm 0.3$ MeV (s-type and axial p-type) and $\Delta E \sim 4.1 \pm 0.3$ MeV (polar p and d-types). Interestingly, the presence of a pseudogap ($\Delta E \sim 15-20$ MeV) was revealed at $T > T_c = 24$ K, which is analogous to the situation with cuprate HTSCs [142].

Similar ES experiments [137] for $LaO_{0.89}F_{0.11}FeAs$ and $LaO_{0.94}F_{0.06}FeP$ samples allowed estimating the pseudogap for $LaO_{0.89}F_{0.11}FeAs$ as $\Delta E \sim 0.1$ eV; at the same time, the pseudogap was found to be absent from the low-temperature ($T_c = 5$ K) superconductor $LaO_{0.94}F_{0.06}FeP$. The angle-resolved electron spectra for the series $LnO_{1-x}F_xFeAs$ (Ln = La, Ce and Pr) were analyzed in [143].

The ES method with high angular resolution in energy and angles (30 MeV and 0.5°, respectively) was used in the experiments in [65] to study the FS on a single-crystal $NdO_{0.90}F_{0.10}FeAs$ sample. Figure 9f, g gives an experimental picture of the FS constructed by integration of an ES series (in the interval of 20 MeV near E_F) in comparison with the FS taken from calculations by the zone method of a full-potential linearized augmented plane wave, FLAPW). It can be seen that the experiment agrees well with the theory, distinguishing the FS hole stackings around the center (Γ point) of the Brillouin zone (BZ) and the smaller-diameter electron stackings centered at the BZ edges (along the symmetric A–M direction). The experimental pseudogap estimate for $NdO_{0.90}F_{0.10}FeAs$ is $\Delta E \sim 20$ MeV.

Mössbauer (nuclear gamma-resonance, NGR) spectroscopy on ^{57}Fe nuclei was used to investigate the magnetic, electron, and structural characteristics of LaOFeAs [144, 145] and 1111 superconductors: $LaO_{0.89}F_{0.11}FeAs$ [144], $LaO_{0.9}FeAs$ [146], $SmO_{0.85}FeAs$ [147], and superconducting LaOFeP ($T_c = 7$ K) [148].

The NGR ^{57}Fe spectra of LaOFeAs were investigated in the temperature range from 298 K to 4.2 K [144]. These spectra have a singlet form at $T > 130$ K with their consequent multiplet splitting reflecting the occurrence of an ultra-thin magnetic field ($B_{hf} \sim 5$ T [145]) on resonating ^{57}F nuclei. The effect is associated with a magnetic phase transition in the region $T \sim 160$ K. The local magnetic moments of the Fe atom estimated from NGR experiments were 0.36 μ_B [144] and 0.26 μ_B [145]. The small quadrupole splitting value (QS ~ 0.03 mm s^{-1} [144] and 0.3 mm s^{-1} [145]) may be indicative [144] of the density distribution of 3d electrons close to isotropic.

Doping of the oxygen sublattice with fluorine radically changes the temperature dependence of NRG-^{57}Fe spectra of LaOFeAs, which preserve their singlet form (Fig. 10) in the entire temperature range both above and below $T_c = 26$ K, unambiguously showing the suppression of the magnetic

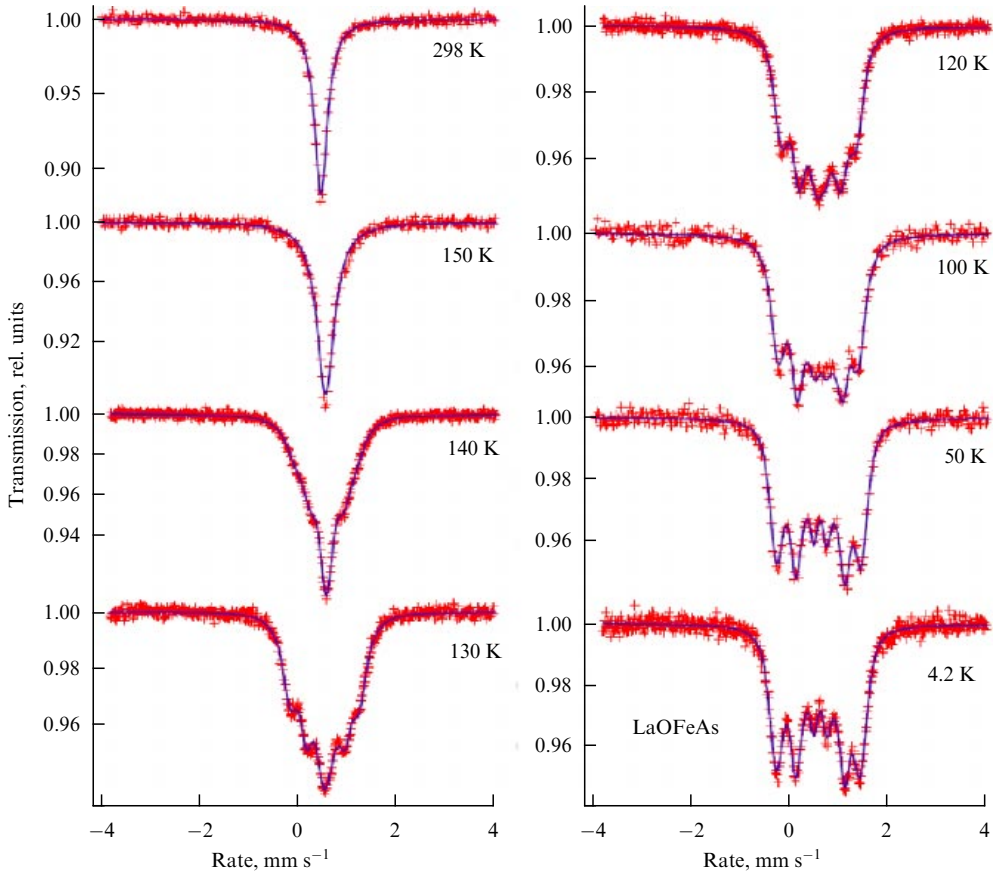

Figure 10. NGR ^{57}Fe spectra of LaOFeAs in the temperature range 4.2–298 K [144].

phase transition and the absence of a magnetic order in the $LaO_{0.89}F_{0.11}FeAs$ phase. The isomeric shift (IS) (relative to α-Fe) for both oxyarsenide samples [144–146] varies in the range 0.44–0.58 mm s^{-1}, increasing when the temperature decreases.

When oxygen vacancies are introduced into the LaOFeAs composition [146], the NgR ^{57}Fe spectra exhibit two absorption bands with the intensities proportional to the degree of nonstoichiometry of the $LaO_{0.9}FeAs$ sample, and this form of the spectra is preserved in the entire investigated temperature range (200–95 K). The most intense singlet corresponds to ^{57}Fe nuclei completely surrounded by oxygen atoms, while the second one corresponds to ^{57}Fe nuclei containing one O vacancy in its nearest surrounding. No other peaks that could be identified as manifestations of the states of Fe atoms surrounded by two O vacancies were discovered, which shows the absence of a noticeable vacancy clusterization. The IS values 0.31–0.51 mm s^{-1} for both nonequivalent positions of Fe atoms are close to those typical of the bivalent low-spin state of Fe atoms. At $T = 95$ K, both types of Fe atoms are magnetically ordered [146]. Similar results were obtained for an $SmO_{0.85}FeAs$ sample with an oxygen deficit [147], for which the changes in the NGR ^{57}Fe spectra in the superconducting region ($T < T_c = 52.4$ K) were considered to be due to the occurrence of magnetic ordering in FeAs layers.

In contrast to the LaOFeAs case, the NGR ^{57}Fe spectra for the low-temperature superconductor LaOFeP have a singlet form in the entire investigated temperature range (4–298 K) [148], and only exhibit some broadening at $T < T_c =$ 7 K. The IS value approximately equal to 0.30 mm s^{-1} is close to the corresponding values for oxyarsenides.

The authors of [149] proposed using the NGR method for phase analysis of superconducting oxyarsenides via comparison of the spectra of synthesized samples with the spectra of the most typical impurity phases, binary iron arsenides Fe_2As, FeAs, and $FeAs_2$. Applying this method to the $La_{0.9}FeAs$ sample obtained by the method in [1], the authors of [149] found that the product includes about 11% of the $FeAs_2$ phase as impurity.

NMR spectroscopy on ^{75}As and ^{139}La nuclei for $LaO_{1-x}F_xFeAs$ ($x = 0$, 0.04 and 0.11) [150], on ^{75}As nuclei for $LaO_{0.9}F_{0.1}FeAs$ [151], $PrO_{0.89}F_{0.11}FeAs$ [152], $LaO_{1-x}FeAsO$ ($x = 0$, 0.25, 0.4) and $NdFeAsO_{0.6}$ [153], and on ^{19}F nuclei for $LaO_{0.89}F_{0.11}FeAs$ [146] was used to study a number of local electron, magnetic, and superconducting parameters of these systems. In particular, measurements of the Knight shift K and the inverse spin–lattice relaxation time T_1^{-1} for $LaO_{1-x}F_xFeAs$ demonstrate that the local magnetic susceptibility and spin fluctuations decrease as the temperature approaches T_c, the same as they do in cuprate HTSCs [154]. The small K value (~ 100 MD) points to an insignificant spin transfer between FeAs and LaO layers, thus confirming the quasi-two-dimensional type of the oxyarsenide electronic structure.

One of the interesting results [154] concerns the estimate of the London penetration depth λ of the magnetic field. According to the data obtained, λ^{-2} increases monotonically without saturation in the range from T_c to 2 K ($0.1\,T_c$), whereas in BCS superconductors, λ^2 remains practically unchanged in the range from T_c to $0.3\,T_c$. Extrapolation of the data obtained to $T = 0$ gave the value $\lambda \sim 215$ nm, which agrees well with the results in [118, 124] (see Section 3.2). At the same time, because oxyarsenide is an essentially anisotropic system, we should assume that $\lambda_{ab} \ll \lambda_c$. According to the theory in [155], $\lambda_{ab} \sim \lambda/1.23$ for anisotropic media, and hence $\lambda_{ab} \sim 175$ nm for $LaO_{0.89}F_{0.11}FeAs$, which is sufficiently close to the value $\lambda_{ab} \sim 250$ nm for the HTSC cuprate $La_{1.85}Sr_{0.15}CuO_4$ with the comparable value $T_c = 38$ K [156]. Using the value of the coherence length $\xi = 4$ nm [10], we can then calculate the Ginzburg–Landau parameter $\kappa = \lambda/\xi \sim 44$ [154].

The analysis of ^{75}As-NGR lines for $LaO_{0.9}F_{0.1}FeAs$ in [151] has demonstrated that the T_1^{-1} value changes as T^3 in the interval from T_c to $0.1\,T_c$, which is characteristic of d-type superconductors. For the normal oxyarsenide state, both T_1^{-1} and K decrease with decreasing the temperature. The temperature-dependent spin dynamics (an antiferromagnet–superconductor transition) for $LaO_{1-x}F_xFeAs$ ($x = 0$, 0.04 and 0.11) was discussed in [150] using the data of NGR spectra on ^{75}As and ^{139}La nuclei.

As a result of NMR experiments on ^{75}As nuclei for nonstoichiometric $LaO_{1-x}FeAs$ compositions ($x = 0$, 0.25, 0.4), a correlation between the quadrupole frequency $^{75}\nu_Q$ and T_c was revealed [153]. The oxyarsenide critical temperature was assumed to depend directly on the local electron configuration of iron and arsenic atoms, which affect the crystal band structure as a result of the hybridization of 4p orbitals of As and 3d orbitals of Fe.

Vibrational characteristics of oxyarsenides. Measurements of Raman polarization spectra [31] for undoped LaOFeAs and SmOFeAs single crystals allowed determining the frequencies ω and the symmetry of Raman phonons due to interplane shifts (Fig. 11); their values compared to the theoretically calculated ones [14, 107, 129] are presented in Table 4. Comparing the vibrational frequencies of atoms for LaOFeAs and SmOFeAs, we notice that $\omega_{Sm} > \omega_{La}$, which

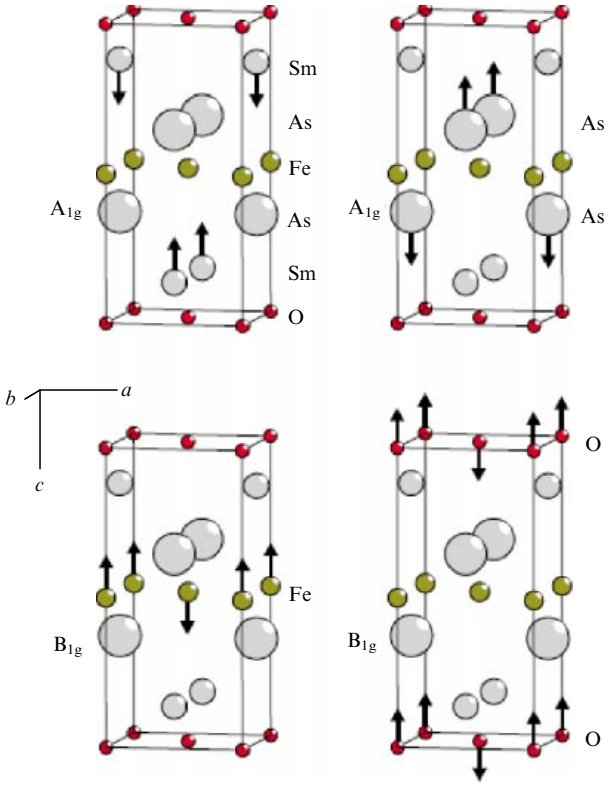

Figure 11. Eigenvectors of all nondegenerate phonons for interplane atomic vibrations in SmOFeAs [31].

Table 4. Experimental [31] and theoretical [14, 107, 129] values of the frequency [cm^{-1}] at the Γ point of Raman phonons for SmOFeAs and LaOFeAs.

Mode (symmetry)	SmOFeAs [31]	LaOFeAs [31]	LaOFeAs [14]	LaOFeAs [129]	LaOFeAs [107]
A_{1g} (Sm, La)	170	162	180	183	178
A_{1g} (As)	201	208	200	208	201
B_{1g} (Fe)	208	201	217	216	221
B_{1g} (O)	345	316	311	294	284

can readily be explained by the standard dependence [157] of phonon frequencies on the atomic masses m and the nearest interatomic distances d, which in this case has the form $\omega_{Sm}/\omega_{La} \sim (m_{Sm}/m_{La})^{1/2}(d_{Sm}/d_{La})^{2/3}$. Using the values of atomic masses and interatomic distances, we obtain $\omega_{Sm} \sim 1.026\omega_{La}$, which agrees well with the experimental data ($\omega_{Sm} \sim 1.049\omega_{La}$). The changes in the vibrational frequencies of other atoms undergoing transition from LaOFeAs to SmOFeAs can be explained similarly [31].

In [158], room-temperature Raman spectra were investigated and the observed modes were classified using group-theory analysis and ab initio calculations for the doped oxyarsenides $LaO_{1-x}F_xFeAs$ and $CeO_{1-x}F_xFeAs$ with a variable composition of O/F. Consideration of not only interplane but also intraplane atomic shifts allowed determining eight active modes. It was established that the vibrational modes F_g and A_{1g} of lanthanum atoms are substantially suppressed by fluorine atoms doped into the oxyarsenide lattice, whereas the E_g and A_{1g} modes of arsenic and iron are only affected a little by the dopant. In the case of $CeO_{1-x}F_xFeAs$, the E_g and A_{1g} modes corresponding to lanthanum vibrations are absent, and the oxygen E_g mode is shifted to the frequency about 450 cm^{-1}. The three spectral singularities in the frequency range about 500 cm^{-1} can be associated with multiphonon processes [158], although their relation to magnetic fluctuations or interband transitions of d states is not excluded.

The vibrational spectra of $LaO_{1-x}F_xFeAs$ in the temperature range 8–300 K are given in [159]. The authors report a spectral intensity suppression in the frequency range $\omega < 400$ cm^{-1} with decreasing the temperature, which may indicate opening a gap in the spectrum of the DOS.

Concluding this section, we briefly mention the other methods for studying the properties of superconducting oxyarsenides. Among them are muon spectroscopy [160–163]; Andreev (microcontact) [164–168], optical [169, 170], and scanning tunnel [171] spectroscopy; and infrared ellipsometry [172]. The Nernst [173] and Hall [174, 175] effects were investigated. Finally, the high (negative) Seebeck coefficients of some low-temperature *Ln*OFeAs point out that these compounds with high electron conductivity may become promising materials for thermoelectric modules working in the nitrogen temperature range [176].

4. Simulation of the band structure and properties of superconducting oxypnictides

Band theory methods have found wide application in studying the features of the electronic structure, the nature of interatomic interactions, and the magnetic and some other properties of new oxyarsenide 1111 superconductors, and have also been actively used in the construction of theoretical microscopic models of these materials. The basic results of these studies are described in Sections 4.1–4.3.

4.1 Band calculations

4.1.1 Energy bands and the Fermi surface. Interesting information on the features of the electronic structure of basis phases of the new superconducting materials — oxyarsenide (LaOFeAs [14, 15, 30, 127–129, 177–183], LaO*M*As (M = V, Cr, ..., Ni, Cu) [177], *Ln*OFeAs (Ln = Y, Ce, Pr, Nd, Sm) [30], and *Ln*OFeAs (Ln = Ce, Pr, Nd) [184]), oxyphosphide (LaOFeP [99, 185, 186], LaONiP [100]), and oxybismuthide (LaO*M*Bi (M = V, Cr, ..., Ni, Cu) [28, 187, 188]) — were obtained using the computational band theory of condensed state.

We describe the main features of the energy spectrum of these compounds with the example of LaOFeAs (Fig. 12a) [129], whose total and partial DOS [14] are presented in

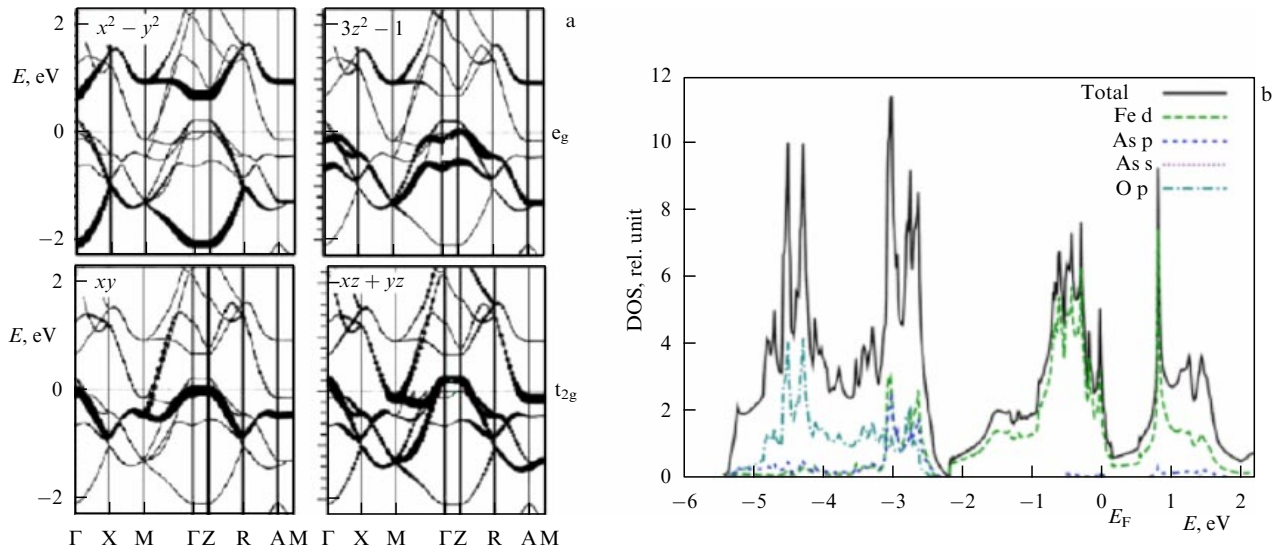

Figure 12. (a) LaOFeAs energy bands (contributions of 3d states of Fe with different symmetries are marked) [129]. (b) Total and partial densities of LaOFeAs states [14].

Fig. 12b. The oxyarsenide valence band in the energy range from −5.6 eV to the Fermi level ($E_F = 0$) is seen to be largely composed of Fe 3d and As 4p states. Its lower edge (in the range from −5.6 eV to −2.3 eV) includes overlapping (hybrid) Fe 3d and As 4p states. The pre-Fermi region (from −2.3 eV to E_F) consists mainly of Fe 3d states, which make the leading contribution to the total DOS at the Fermi level $N^{tot}(E_F)$, i.e., are responsible for the conducting properties of the system. It is important that the contributions of states of the LaO layer to this region of the valence band are very small, i.e., the covalent interaction between LaO and FeAs states is weak. The La band of 4f-states lies approximately 2 eV above E_F.

The quasi-plane Fe 3d-like bands crossing E_F constitute a system of electron and hole pockets (Fig. 12a) forming a characteristic topology of the FS (Fig. 9f, g) consisting of two hole cylinders in the center of the BZ and two electron sheets lying along the BZ edges.

The Fermi level for complete LaOFeAs lies on the steep slope of the peak of the density of Fe 3d states (the DOS at the Fermi level $N(E_F) \sim 4.2$ states per eV [129]) near the spectral pseudogap (Fig. 12b). In the framework of the rigid band model, the electron doping can be assumed to promote a sharp decrease in $N(E_F)$. The inverse effect should accompany the hole doping, which favors a sharp $N(E_F)$ increase and the magnetic instability of the system.

The results of calculations of the electronic structure of oxypnictides [14, 15, 30, 127–129, 177–188] suggested an explanation for the main features of the interatomic interactions (chemical bond) in these phases. It follows from the LaOFeAs DOS distribution (Fig. 12b) that in the valence band region (in the range from −5 eV to E_F), the maximum contributions belong to Fe 3d- and As 3p-states, whose hybridization determines the covalent component of Fe–As bonds in FeAs layers. The oxygen (arsenic) and lanthanum atomic orbitals overlap to a much lesser degree. A pictorial idea of the role of interlayer interactions in oxypnictides is suggested (using the example of LaOFeP) [99] by the so-called construction block concept [189–191]. This concept implies calculation of the construction blocks of the phase (LaO and FeP layers for LaOFeP) with their geometry in the composition of oxyphosphide and a comparison of their DOS with that for LaOFeP. It can be seen (Fig. 13) that as a result of the interaction of these layers, the states of the metal-like LaO layers shift the energy scale down by ∼ 2 eV. Furthermore, due to the electron transfer from the LaO layer to the FeP layer, a notable filling of Fe 3d states is observed in the FeP layer, whereas a forbidden gap occurs in the LaO layer spectrum in the LaOFeP crystal. At the same time, the effective atomic charges (as is shown by their numerical estimates in Table 5 in accordance with the Bader scheme [192]) differ from the formal ionic charges, testifying to a mixed covalent-ion bond type in oxypnictides. The picture of charge distributions [193] in these phases is demonstrated in Fig. 13d.

Additional information on the covalent bond component (the character the Fe–As-orbital hybridization) and its effect on the oxypnictide band structure was obtained in [194], where the bonds were analyzing using the formalism of Wannier functions.

Therefore, the discussed oxypnictides can be defined as anisotropic ionic metals in which conductivity is realized exclusively due to the states of transition metal–pnictogen

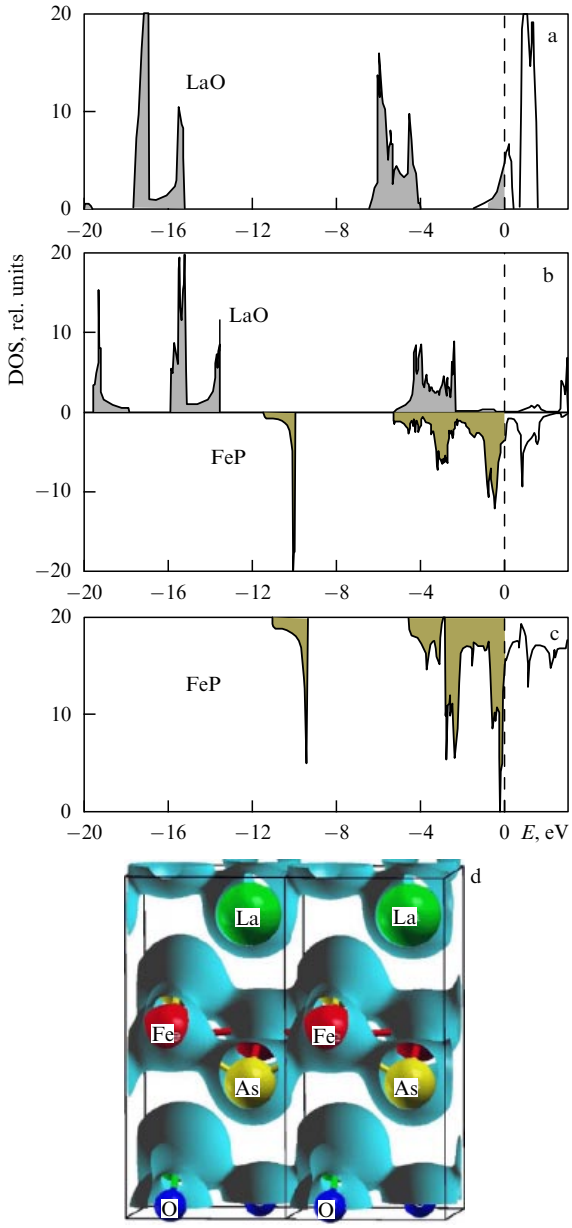

Figure 13. DOS of isolated construction blocks of oxyfluoride Fe–La: (a) LaO layer, (c) FeP layer, and (b) these layers in the composition of the LaOFeP phase (the dashed lines indicate the Fermi level) [99]. (d) Isoelectronic ($\rho = 3.6\,e$ per 1 Å^3) surface of LaOFeAs [193].

Table 5. Atomic charges (e) for LaOFeP calculated in accordance with the Bader scheme compared to formally ionic charges [99].

Atom (layer)	La	O	Fe	P	LaO	FeP
Bader scheme	9.05	7.31	7.59	6.05	16.36	13.64
Ionic charges	8 (La^{3+})	8 (O^{2-})	6 (Fe^{2+})	8 (P^{3-})	16 $(LaO)^{1+}$	14 $(FeP)^{1-}$

layers and the bond between neighboring layers in the crystal is primarily of ionic character [195].

In [14, 107, 129], the electron–phonon interaction is considered in the example of LnOFeAs using computational methods; the phonon spectrum parameters of this crystal are

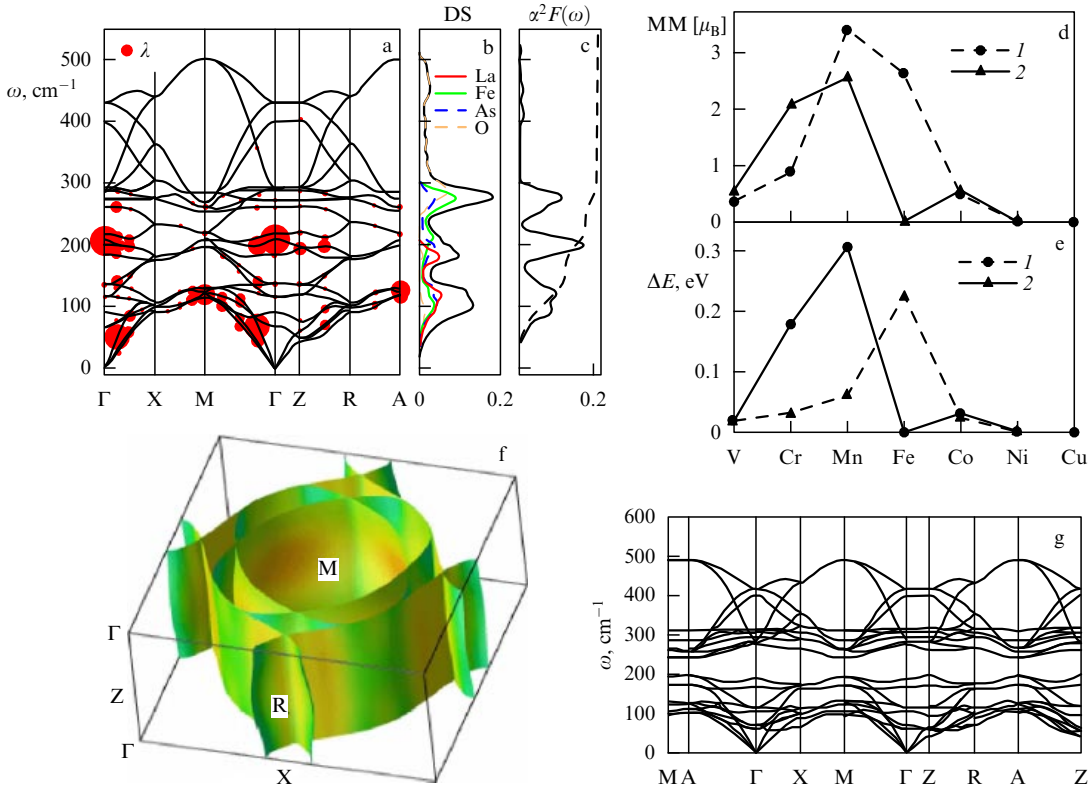

Figure 14. (a) Dispersion spectrum of phonon frequencies ω, (b) total and atomic densities of phonon states, and (c) Eliashberg function $\alpha^2F(\omega)$ for LaOFeAs [129]. The radii of distinguished regions in Fig. (a) are proportional to the partial electron–phonon coupling constants λ_{ep} for each phonon mode. (d) Magnetic moments on transition-metal atoms and (e) stabilization energies of the ferromagnetic state (relative to the magnetic state) $\Delta E = E^{tot}_{FM} - E^{tot}_{NM}$ for LaOMBi (curve *1*) [187] and LaOMAs (curve *2*) [177], where M = V, Cr, ..., Ni, Cu. (f) Fermi surface and (g) phonon spectrum of LaONiP.

calculated and the electron–phonon coupling constant λ_{ep} is evaluated. The main results are presented in Fig. 14. The spectrum of the phonon frequencies of the crystal is seen to cover the region up to $\omega \sim 500$ cm^{-1}, with the region of oxygen-atom vibrational frequencies (from 300 cm^{-1} to 500 cm^{-1}) being separated from the vibrational frequency range $\omega < 300$ cm^{-1} of the other lattice atoms, which overlap significantly (make a comparable contribution to the total density of phonon states) and, similarly to the bands of electron states (Fig. 12a), have small dispersion in the z direction, which allows clearly identifying the peaks of the Eliashberg function $\alpha^2F(\omega)$ (Fig. 14c). Figure 14a–c also shows that the phonon modes of individual atoms make comparable contributions to λ_{ep}, and the total value of this constant for LaOFeAs turns out to be very small: $\lambda_{ep} < 0.21$. Solving the Eliashberg equation for this λ_{ep} value gives the critical transition temperature $T_c \sim 0.8$ K, which is much lower than the experimental value $T_c \sim 26$ K. This clearly demonstrates the inapplicability of the standard Bardeen–Cooper–Schrieffer (BCS) theory for describing superconductivity in oxypnictides.

Attempts were made to describe the change in the band structure resulting from 1) electron doping of LaOFeAs, 2) changing the rare-earth metal type: LnOFeAs (Ln = Y, Ce, Pr, Nd, Sm) [30, 184], 3) changing the transition metal type: LaOMAs (M = V, Cr, ..., Ni, Cu) [177], 4) replacing arsenic by fluorine (oxyphosphides LaO(Fe, Ni)P [99, 100, 185, 186]) or bismuth (oxybismuthides LaOMBi (M = V, Cr, ..., Ni, Cu) [28, 187, 188]).

Model calculations of the change (due to hole or electron doping) in the electronic states [196] of the FeAs monolayer with the geometry corresponding to the geometry of these layers in LaOFeAs have shown that the DOS at the Fermi level decreases or increases monotonically; the monolayer ground state is antiferromagnetic. In the scenario proposed in [179], the leading part of LaOFeAs doping with fluorine amounts to suppressing ferromagnetic fluctuations in the original crystal.

The authors of paper [30], which bears the notable title "High-temperature superconductivity in oxypnictides of transition metals: a rare-earth puzzle?," systematically calculated a series of LnOFeAs (Ln = Y, Ce, Pr, Nd, Sm) phases and found no significant changes in the parameters of their band structure that could explain the large differences in the observed T_c values depending on the type of rare-earth metals. The role of the degree of localization of 4f electrons in the formation of the general band picture of LnOFeAs (Ln = Ce, Pr, Nd) was discussed in [184].

To clarify the role of 3d metals (M = V, Cr, ..., Ni, Cu) in the formation of the electronic and magnetic structure of oxyarsenides, a series of calculations was performed in [177]. LaOMAs crystals, except LaOFeAs, LaONiAs, and LaOCuAs, were found to be magnets (Fig. 14d, e); the LaOFeAs and LaONiAs phases, in which superconductivity was discovered, were noticed to lie at the magnetic stability boundary of the systems of this series.

A substantial difference was found between the oxyarsenide and oxyphosphide band structures. For instance, the FS

structure of the low-temperature ($T_c \sim 3.0-4.2$ K) superconductor LaONiP [101] (Fig. 14e) differs considerably from the LaOFeAs FS structure (Fig. 9f, g), which is associated with both the differences in the concentration of valence electrons in the cell of these phases and the stronger covalent Ni–P interactions compared to Fe–As interactions [101]. The phonon spectrum of LaONiP (Fig. 14f) consists of 12 phonon bands in the region $\omega < 200$ cm^{-1} that correspond to the acoustic modes and mixed-type modes mainly related to oscillations of metal atoms. This group of bands is separated by a gap from the group of higher bands with the maximum frequency about 500 cm^{-1}, reflecting the atomic oscillations of fluorine ($\omega < 300$ cm^{-1}) and oxygen ($\omega > 300$ cm^{-1}). According to [101], the electron–phonon coupling constant is $\lambda_{ep} = 0.58$, which is three times as large as λ_{ep} for LaOFeAs (~ 0.2 [129]). The critical temperature for LaONiP estimated in the Eliashberg model is $T_c \sim 26$ K, which agrees well with experiment. Hence, in contrast to the oxyarsenides considered above, LaONiP should be treated as conventional low-temperature BCS superconductors with the electron–phonon pairing mechanism.

Calculations for the series of LaO*M*Bi oxybismuthides (M = V, Cr, ..., Ni, Cu) [187, 188] allowed establishing that the LaONiBi phase is located at the magnetic instability boundary of this series, whereas LaOFeBi, unlike isoelectronic LaOFeAs, has notable local magnetic moments on iron atoms (Fig. 4d, e). This suggested [187] the presence of LaONiBi superconductivity, which was then successfully confirmed in experiment [30].

The action of external pressure on the LaOFeAs FS was analyzed theoretically in [181]. The topology of electron sheets of the FS was found to change under the action of external pressure owing to an increase in orbital degeneration, which appears to be similar to the effect observed upon oxyarsenide doping with fluorine. In turn, the increase in the orbital degeneration on the FS can lead to strong interorbital fluctuations and, consequently, to interorbital pairing, which is regarded as decisive in the mechanism of oxyarsenide superconductivity [181]. In the example of nonstoichiometric LnO$_{0.85}$FeAs (Ln = Sm and Nd) phases with negative compression factors $dT_c/dP = -1.8$ K GPa^{-1} (NdO$_{0.85}$FeAs) and $dT_c/dP = -1.4$ K GPa^{-1} (SmO$_{0.85}$FeAs), an analysis [197] was carried out of the external pressure effect on the $N(E_F)$ value, which, as follows from the computational results, decreases monotonically as the pressure increases from 0 to 12 GPa.

On the basis of calculations of the electron density distribution in an LaOFeAs crystal, the positron potential distribution V^+ was constructed in [198] as the inverted Coulomb potential V_{Coul} with the electron–positron correlation taken into account ($V^+ = -V_{Coul} + V_{corr}$); the wave functions of positrons were also calculated there. It was found that the positron density is maximum in interatomic pores of a La atom plane near As atoms and can be partially localized near Fe atoms. It was concluded that the positron annihilation method can be used in experimental studies of the FS topology in these metals.

4.1.2 Correlation effects. The effect of Coulomb correlations (see review [199]) on the electron states of 1111 oxypnictides was discussed in the example of LaO$_{1-x}$F$_x$FeAs [15, 200], SmO$_{1-x}$F$_x$FeAs [201], and LaOFeAs [130], with the application of the computational results in the framework of dynamic mean field theory (DMFT) using the LDA + DMFT method. According to [15, 202], normal-state oxypnictides belong to the family of strongly correlated metals; taking correlations into account must substantially affect the position of the 3d band of Fe, shifting its spectral maximum (relative to that obtained from LDA computations) by ~ 3.5 eV down from E_F [15]. On the other hand, the results in [130] testify to an insignificant effect of Coulomb correlations on the structure of LaOFeAs energy states: the Coulomb repulsion energy $U = 4.0$ eV does not exceed the bandwidth $W \sim 4$ eV. According to [130], the Hubbard subbands have low intensity and the main peak of the DOS of the Fe 3d band lies, according to LDA and LDA + DMFT estimates, in the energy range 1.2–0.8 eV lower than E_F, which agrees well with X-ray emission experiments [125]. It is still unclear why the conclusions in [15, 201] and [130] are contradictory, and the issue requires further research. In particular, it was noted in [202] that the theoretical estimates of U and J for 3d electrons of Fe depend greatly on the basis used. The calculations for LaOFeAs in the O 2p + As 4p + Fe 3d orbital bases and in the basis of only Fe 3d orbitals gave the respective values $U = 3-4$ eV and $U = 0.8$ eV.

Quite intriguing and attracting further attention are the results in [200], where (using the example of LaO$_{1-x}$F$_x$FeAs) a significant overestimation of the Fe atom magnetic moments calculated by both the standard LDA, LDA–GGA, and LDA + U methods was noted: $\sim 1-2\,\mu_B$ compared to the values of $0.2-0.35\,\mu_B$ obtained, for example, in the experimental studies of oxypnictides by the neutron diffraction method [20] or Mössbauer [144] or muon [145] spectroscopy. It is well-known that for a positive Coulomb potential U, the d-electron localization changes and the atomic magnetic moment increases. Model calculations [200] have been performed for negative U values, which may occur when $J > U$. The experimental Fe magnetic moment values were found to be reproduced for negative vales $U \sim -1$, which can be due to the magnetic nature of oxyarsenides, in particular, to the presence of charge density waves [200].

4.2 Simulation of oxypnictide properties

4.2.1 Magnetic properties. In band calculations, certain attention is given to the description of the magnetic structure of oxyarsenides and related phases.

In several standard band LDA calculations, LaOFeAs is interpreted [14, 15] as a nonmagnetic metal with possible ferromagnetic (FM) or antiferromagnetic (AFM) fluctuations. More detailed calculations have shown that the AFM state for LaOFeAs is more stable than the nonmagnetic state [126, 182], and the AFM state has a special stripe-like type of ordering (Fig. 15a, b) [107, 159, 178], which is confirmed by the neutron scattering data [20]. An analogous type of AFM ordering has recently been determined [203] in neutron experiments for NdOFeAs (Fig. 15a, b).

Comparative estimates of the energies of six possible LaOFeAs nonmagnetic and ferromagnetic states and four types of antiferromagnetic states, AFM-G, AFM-S, AFM-CE1, and AFM-CE2 (Fig. 15c–f), were obtained in [8]. Table 6 shows that the ground state of LaOFeAs is an S type (stripe-like) antiferromagnetic state in which the system is a bad metal with a very low DOS at the Fermi level. This agrees with the absence of superconductivity in undoped LaOFeAs. It was noted in [8] that the energy gain in stabilization of the AFM S state is rather small, and this system can assume a

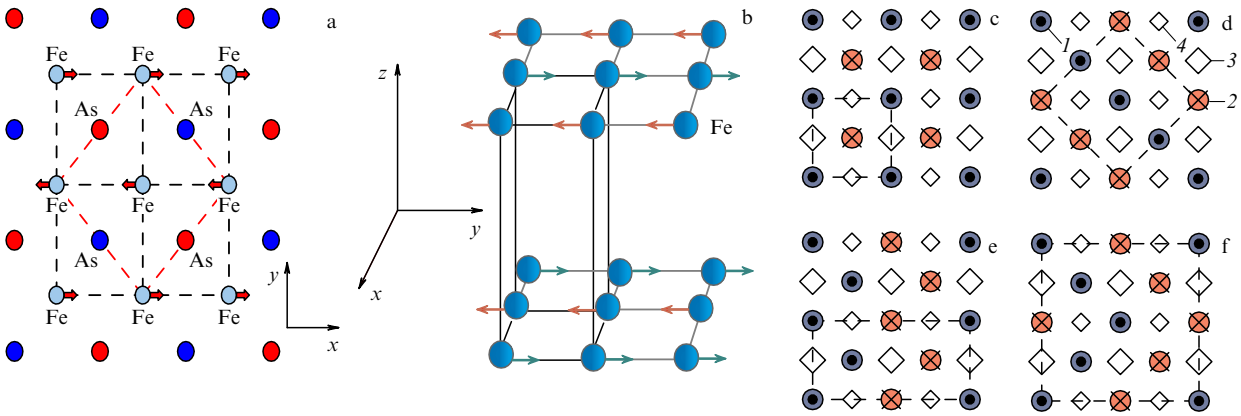

Figure 15. (a, b) Type of the AFM stripe-like Fe-atom spin ordering (in FeAs layers) for LaOFeAs [178] (a) and NdOFeAs [203] (b). (c – f) Types of AFM ordering in the FeAs layer for oxyarsenide LaOFeAs [8]: (c) AFM-G, (d) AFM-S, (e) AFM-CE1, and (f) AFM-CE2; *1* and *2* are Fe atoms with spin up (*1*) and spin down (*2*), *3* and *4* are As atoms in the arsenic atomic nets, upper (*3*) and lower (*4*) relative to the central net of Fe atoms.

large number of other metastable AFM configurations. Furthermore, the formation of an AFM structure can be accompanied by orbital ordering with a consequent structural transition of the oxyarsenide crystal from the tetragonal to the orthorhombic symmetry. But the calculation of LaOFeAs for the AFM-S state gives the value of the magnetic moment on Fe atoms about $2\,\mu_B$, which is much higher than the experimental value $0.26-0.36\,\mu_B$ [144, 145]. Table 6 demonstrates that the Fe magnetic moment closest to the experimental result was obtained for the FM state.

The authors of [204] noted an essential difference in the magnetic states of isostructural and isoelectronic oxyphosphide LaOFeP (which is a nonmagnetic metal) and antiferromagnetic LaOFeP and assumed that at $T = 0$, these systems are near the critical quantum point (CQP) of the AFM $\leftrightarrow$ paramagnet phase transition. To seek magnetic CQP in some superconducting oxyarsenides, magnetic phase diagrams of *Ln*OFeAs (*Ln* = Pr, Nd, Sm, Ce) compounds doped with electrons or holes were calculated [204] in the virtual crystal approximation. Undoped *Ln*OFeAs (*Ln* = Pr and Nd) is a paramagnet, whereas *Ln*OFeAs oxyarsenides, where *Ln* = La, Sm, and Ce, are antiferromagnets with the magnetic moment on the iron atoms respectively equal to $1.62\,\mu_B$, $1.08\,\mu_B$, and $0.66\,\mu_B$. The magnetic picture for doped *Ln*OFeAs crystals is shown in Fig. 16a. PrOFeAs and NdOFeAs pass into the AFM state at the critical hole concentration $x \sim 0.075$, while the AFM structure of CeOFeAs and SmOFeAs is destroyed when the respective electron dopant concentration reaches 0.25 and 0.60. Figure 16b presents the difference between the energies of the AFM state and the nonmagnetic state of doped CeOFeAs, and the experimental dependence of T_c on the electron dopant (fluorine) concentration. It can be seen that the AFM instability region and the superconducting region overlap, with the CQP lying in the latter region. The magnetic CQP of other oxypnictides also lies near these superconducting regions. Therefore, the occurrence of superconductivity in oxyarsenides in the vicinity of their magnetic CQP, i.e., near the magnetic instability boundary, may testify to an important role of magnetic fluctuations in the pairing mechanism for these superconductors. Such correlations between magnetism, CQP, and superconductivity were also noticed for a number of systems with heavy fermions, such as $CeRhIn_5$ [205], $CeCu_2Si_2$ [206, 207], or UPd_2Al_3 [208].

In the overwhelming majority of studies devoted to the oxypnictide magnetic structure, the greatest attention was given to the spin state of the iron atom nets. In this connection, we refer to recent paper [209], in which the role of the 4f sublattice of a metal (Nd) in the formation of the general magnetic structure of oxyarsenides was considered using the example of $NdO_{1-x}F_xFeAs$. The neutron diffraction method was used to determine that a long-range AFM order is formed in both the iron and neodymium sublattices at low temperatures (Fig. 16c); according to [209], the magnetic moments of Fe and Nd atoms are respectively given by approximately $0.9\,\mu_B$ and $1.55\,\mu_B$.

Table 6. Total energies ΔE_{tot} (relative to the energy of the nonmagnetic state) and magnetic moments (MM) [μ_B] of the Fe atom for ferromagnetic and possible types of AFM spin ordering in LaOFeAs [8].

Magnetic structure*	$-\Delta E_{tot}$, eV per formula unit **	Fe MM **
FM	0.004	0.40
AFM-G	0.080 (0.016)	1.89 (151)
AFM-S	0.174 (0.098)	2.12 (2.00)
AFM-CE1	0.064	1.88
AFM-CE2	0.116	2.12

* See Fig. 15.
** In parentheses are the values for relaxed structures.

4.2.2 Mechanical characteristics. The interest in the study of the elasticity parameters of the new oxypnictide superconductors is due to several reasons. First, the elastic constants C_{ij} of superconducting crystals can be related to important superconductivity parameters such as the Debye temperature Θ_D and the electron – phonon coupling constant λ [210]. Several empirical correlation relations between T_c and the mechanical characteristics of superconductors are known [211], according to which high T_c values are typically inherent in materials with a small bulk compression modulus B, i.e., with a high compressibility β. Indeed, for many systems with high T_c (YBCO, MgB_2, $MgCNi_3$, LnM_2B_2C, $Ln_2C_2X_2$, etc.), the compression moduli do not exceed $B \leqslant 200$ GPa ($\beta \geqslant 0.005$ GPa^{-1}) [210 – 216]. On the other hand, a superconducting transition (below $T_c \sim 11$ K) was

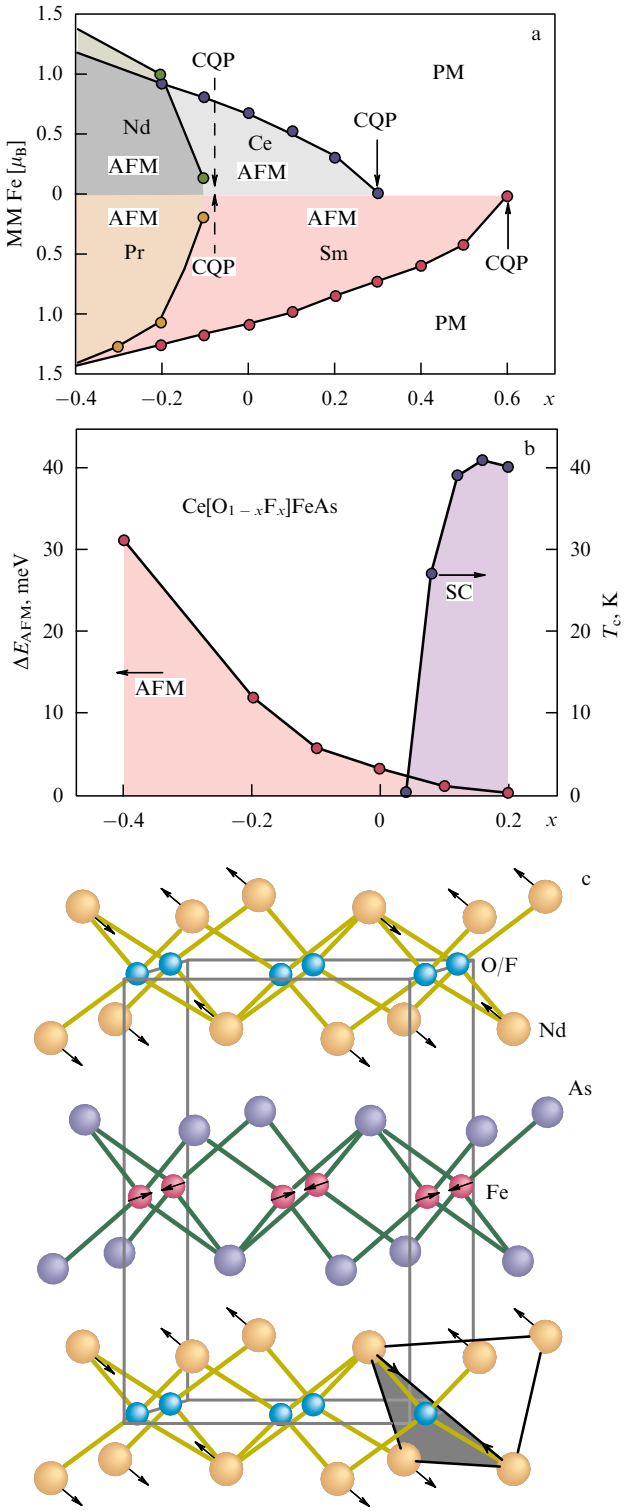

Figure 16. (a) Value of the magnetic moment (MM) of Fe atoms for hole-doped ($x < 0$) and electron-doped ($x > 0$) oxyarsenides *Ln*OFeAs (*Ln* = Pr, Nd, Sm, Ce), (b) the difference ΔE_{AFM} between the energies of the AFM state and the nonmagnetic state, and the superconducting transition temperature T_c for fluorine-doped CeOFeAs [203]. The regions of antiferromagnetic (AFM), paramagnetic (PM), and superconducting (SC) states of the systems and the critical quantum points (CQPs) are identified. (c) AFM structures of Ni and Fe sublattices according to the neutron diffraction data [209].

revealed for super-hard materials such as boron-doped diamond [217, 218].

Table 7. Elasticity parameters in the Voigt (V) and Reuss (R) approximations for a LaOFeAs single crystal and in the Voigt – Reuss – Hill (VRH) model for ceramics of LaOFeAs crystals.

Single crystal		
Elastic constants, GPa	C_{11}	191.9
	C_{12}	55.9
	C_{13}	61.6
	C_{33}	144.8
	C_{44}	44.1
	C_{66}	77.9
Compression modulus, GPa	B_V	98.5
	B_R	97.2
Shear modulus, GPa	G_V	56.5
	G_R	55.9
B_V/G_V		1.74
Ceramics		
Compression modulus B B_{VRH}, GPa		97.9
Compressibility β_{VRH}, GPa^{-1}		0.01022
Shear modulus G_{VRH}, GPa		56.2
Young modulus Y_{VRH}, GPa		141.5
Poisson ratio v		0.259

Owing to the possibility of using superconducting oxypnictides to generate high magnetic fields (see Section 4.2.1), a question arises as to the mechanical stability of magnets whose material is affected by high currents.

The mechanical parameters of single- and polycrystalline LaOFeAs, the basis phase of the new superconductors, were calculated in [193]. Six independent elasticity coefficients of this tetragonal crystal (C_{11}, C_{12}, C_{13}, C_{33}, C_{44}, and C_{66}) (Table 7) turned out to be positive, satisfying the well-known Born criterion of mechanical stability of the system: $C_{11} > 0$, $C_{33} > 0$, $C_{44} > 0$, $C_{66} > 0$, $C_{11} - C_{12} > 0$, $C_{11} + C_{33} - 2C_{13} > 0$, and $2(C_{11} + C_{12}) + C_{33} + 4C_{13} > 0$. The calculated mechanical anisotropy factor was $A = 2C_{44}/(C_{11} - C_{12}) = 0.65$. The elastic moduli of bulk compression B and shear G were calculated in two approximations, the Voigt (V) and Reuss (R) ones (see [219]):

$$B_V = \frac{1}{9}\left[2(C_{11} + C_{12}) + C_{33} + 4C_{13}\right],$$

$$G_V = \frac{1}{30}\left(M + 3C_{11} - 3C_{12} + 12C_{44} + 6C_{66}\right),$$

$$G_R = 15\left(18\,\frac{B_V}{C^2} + \frac{6}{C_{11} - C_{12}} + \frac{6}{C_{44}} + \frac{3}{C_{66}}\right)^{-1},$$

where $C^2 = (C_{11} + C_{12})\,C_{33} - 2C_{13}^2$ and $M = C_{11} + C_{12} + 2C_{33} - 4C_{13}$. The results are presented in Table 7. Because oxyarsenides are normally synthesized in the form of polycrystalline samples (see Table 1), the elasticity parameters for LaOFeAs ceramics were estimated. The ceramics — polycrystalline systems given by an aggregated mixture of microcrystallites with random mutual orientation — were calculated by averaging the values obtained by

the Voigt and Reuss schemes. For this, the Voigt – Reuss – Hill (VRH) approximation was used (see [219]) to obtain the averaged compression and shear moduli $B_{VRH} = 1/2\,(B_V + B_R)$ and $G_{VRH} = 1/2\,(G_V + G_R)$, and then the Young modulus Y_{VRH}, the Poisson ratio v, and the compressibility $\beta_{VRH} = 1/B_{VRH}$ for ceramics were determined (Table 7).

According to the results of calculations, $B_{VRH} > G_{VRH}$, and therefore the parameter limiting the LaOFeAs mechanical stability is the shear modulus G_{VRH}. The compression modulus B is rather small ($\sim$ 98 GPa), i.e., smaller than that for other superconducting materials, for example, MgB_2 ($B \sim 122-161$ GPa [220]), $MgCNi_3$ ($B \sim 172-210$ GPa [221]), YBCO ($B \sim 200$ GPa), and YNi_2B_2C ($B \sim 200$ GPa [212]). Therefore, compared to other superconductors, LaOFeAs is a soft material and has the high compressibility: $\beta \sim 0.0102$ GPa^{-1}.

Finally, according to the criterion in [222], the material is brittle if $B/G < 1.75$. For LaOFeAs, $B/G \sim 1.74$, i.e., the material is at the brittleness boundary. The Poisson ratio v is small for covalent systems ($v \sim 0.1$), whereas $v \sim 0.25$ for ion crystals [223]. Moreover, for covalent and ionic systems, we know the respective ratios $G \sim 1.1B$ and $G \sim 0.6B$. For LaOFeAs, $v \sim 0.26$ and $G_V/B_V \sim 0.58$, which confirms the ion type of interlayer interactions (see Fig. 13d).

4.3 Theoretical models of superconductivity in oxypnictides

The information on the band structure and properties of superconducting oxypnictides presented in Sections 4.1 and 4.2 was actively used in theoretical models investigating the superconductivity and magnetism mechanisms in these materials. We immediately note that the majority of such studies use rather well-known model representations of various 'nonstandard' pairing mechanisms (e.g., mechanisms due to the coupling to spin fluctuations, proposed earlier for the description of cuprate HTSC (see review [224])), which serve as a replacement of the traditional electron – phonon mechanism for FeAs superconductors. We briefly discuss the main such mechanisms in what follows.

The so-called minimal model proposed in [128] includes five 3d orbitals of Fe; the conclusion was drawn that spin fluctuations modes can determine a nonstandard mechanism of s-pairing. The possibility is considered of describing the superconducting state as a consequence of Coulomb interactions of d electrons of Fe atoms [225, 226]. It was assumed in [227] that the superconducting d-symmetry states in oxypnictides may occur after the destruction of a long-range magnetic order (spin density waves with variable magnetization direction) as a result of system doping.

A model of the structure of a superconducting FeAs layer was developed in [228], with the main focus on the degeneracy of d_{xz} and d_{yz} orbitals of Fe in a crystal field. The model allows the description of the antiferromagnetic state of basis phases and predicts the d type of superconducting states upon their doping. The authors of [13] showed that according to mean field theory, the most probable ground state of a superconductor is of the d_{xy} or $d_{xy} + id_{x^2-y^2}$ type, the second state being realized in doped systems as the temperature decreases. The predominant role of the d_{xy} type of superconducting state was also adopted in [229]. A number of other attempts to use model approaches to describe the type of pairing and the existence of magnetism and superconductivity were made in [18, 230 – 234]).

In the framework of the four-band model, the idea of a magnetic exciton and the behavior of spin and magnetic susceptibility in superconducting oxypnictides was developed in [235]. It was shown that the spin fluctuation spectrum is of the antiferromagnetic type due to both interband and intraband scattering; the features of magnetic exciton spectra in the superconducting state of the system were discussed.

A superconductivity mechanism relying on the occurrence of nonmagnetic bipolarons in doped oxypnictides was proposed in [236] based on the Bose condensation of the bipolarons (see also [237, 238]). The applicability of another, so-called hole mechanism of superconductivity (see [239]) to the description of oxypnictides is analyzed in [240]. A 'universal' superconductivity model proposed in [241] implies pairing of electrons with parallel spins and the existence of distinguished charge and magnetic bands (vortex lines) in oxyarsenides; this model was used to describe the effect of external pressure on the transition temperature. In [242], this model was used to calculate the optimum doping level of superconducting oxyarsenide. A possible superconductivity mechanism including the electron – electron and electron – hole pairings as the respective consequence of electron – phonon and Coulomb interactions is reported in [243].

Several effective Hamiltonians were proposed in [133, 244 – 247] and were used to consider the electron and hole behavior, the magnetic characteristics, the types of symmetry in paired states, and the pairing channels in Fe-containing oxypnictides. The superconducting states of tetragonal systems with two orbitals were classified in terms of group theory [248, 249].

In [106, 250 – 254], microscopic models of the magnetic characteristics of oxypnictides are developed, including spin wave interactions, pairing types and FS topologies [250, 251], types of superexchange interactions between Fe atoms and magnetic excitations [252], and magnetic states with different degrees of valence-electron delocalization [252]. A competitive role of two types of short-range superexchange interactions in the formation of coexisting collinear AFM systems in two sublattices and in the destruction of the magnetic order under hole and electron doping of oxypnictides were discussed in [106].

To summarize, we note that in spite of the variety of proposed microscopic models [13, 106, 133, 128 – 136, 240 – 254], the origin of the competition (or coexistence) of magnetic and superconducting phenomena, as well as the pairing mechanism in oxypnictide materials, remains a subject of discussion.

5. New superconductors based on ternary $A Fe_2As_2$ arsenides: the 122 phase

The discovery of superconductivity in materials based on quaternary layered *Ln*OFeAs oxyarsenides (1111 phase) [1 – 35] has stimulated an active search for new superconductors among other related compounds.

Particular attention has been attracted [255] by the arsenide $BaFe_2As_2$, a representative of the vast family of ternary 122 phases with the structural type of $ThCr_2Si_2$ [85, 256 – 261]. This arsenide, like the *Ln*OFeAs oxyarsenides, has a layered tetragonal structure formed by alternating FeAs layers and barium atomic nets; the same as in *Ln*OFeAs crystals, the molecular FeAs layers in $BaFe_2As_2$ consist of

conjugate $FeAs_4$ tetrahedrons (see Fig. 1). The study of the physical properties of $BaFe_2As_2$ [255] showed that this compound (a paramagnet) undergoes a phase transition at $T = 140$ K, as is clearly seen from temperature dependences of the thermal conductivity, conductance, and magnetic susceptibility. An similar anomaly of properties at close temperatures is exhibited by LaOFeAs, which has allowed concluding [255] that the arsenide $BaFe_2As_2$ is a promising matrix for obtaining new superconductors.

This assumption was soon perfectly confirmed: samples of potassium-doped arsenide $Ba_{1-x}K_xFe_2As_2$ showed a superconducting transition with the maximum temperature $T \sim 38$ K for the composition $Ba_{0.6}K_{0.4}Fe_2As_2$ [38]; a number of similar superconducting materials were then synthesized with close T_c values. We note that among the ideal (undoped) ternary $ThCr_2Si_2$-like phases, several low-temperature ($T_c < 5$ K) superconductors are known, specifically, $LaIr_2Ge_2$, $LaRu_2P_2$, $YIr_{2-x}Si_{2+x}$, and $BaNi_2P_2$ [39, 85, 258 – 262].

Presently, a number of superconducting materials based on ternary arsenide AFe_2As_2 phases (where A is an alkali-earth metal) have been synthesized and new information on their structural, conducting, magnetic, and electronic properties has been obtained. We note that in layered 122-phase AFe_2As_2 (as in the 1111-phase LnOFeAs), the conductivity has a sharply anisotropic character and is exclusively due to the states of FeAs layers, and the AFe_2As_2 arsenides pass into the superconducting state as a result of doping. At the same time, unlike LnOFeAs, the 122-phase AFe_2As_2 contains neither oxygen nor rare-earth elements.

5.1 Synthesis and crystal structure of 122 phases and superconducting materials based on them

As in the case of 1111 phases, one of the principal methods for obtaining samples of ternary AFe_2As_2 phases and superconducting materials based on them is solid-phase synthesis (SPS). Simple initial substances are typically used as reagents (see Table 2).

For example, polycrystalline $BaFe_2As_2$ samples were obtained in [255] from a mixture of pure Ba, Fe, and sublimated As (taken in the ratio 1.05:2:2) in an Al_2O_3 crucible, which was then sealed (in a pure argon atmosphere) inside a quartz tube. At the first stage the mixture was heated to $T = 1123$ K at the rate 50 K h^{-1}, kept at this temperature for ten hours, and then cooled to room temperature. After that, the product was homogenized (by grinding in an agate pounder) and again annealed at 1173 K for 25 h. When cooled, the product was again homogenized, pelleted by pressing, and heated to $T = 973$ K. As a result, black powder stable in air was obtained. Phase analysis has shown that the content of impurity phases in the $BaFe_2As_2$ samples thus prepared does not exceed 1%. Similar methods were used to synthesize other arsenides: ($SrFe_2As_2$, KFe_2As_2, $CsFe_2As_2$) (see Table 2). SPS of simple substances is frequently used to obtain superconducting (doped) materials based on these phases (see Table 2).

Another technique involves the use of a number of binary phases as precursors. The synthesis goes through several stages. For instance, to synthesize $Ba_{1-x}K_xFe_2As_2$ samples [41], first, simple substances were used to obtain arsenides of the corresponding metals: SrAs, KAs, and Fe_2As. Next, the powders of these arsenides were mixed and pelleted, the pellets were then wrapped into tantalum foil, sealed in a quartz tube in an Ar atmosphere, and annealed for 24 h at the temperature 750 – 900 °C. To obtain the superconducting $Ba_{1-x}K_xFe_2As_2$, the authors of [42] applied a 'mixed' method, taking metal arsenides (BaAs + FeAs) mixed with pure substances (Fe + K) as original reagents.

The most notable success was achieved in growing single-crystal arsenides (see Table 2). $SrFe_2As_2$ single crystals (lamellar, with the mean size $3 \times 3 \times 0.5$ mm) were grown [263] using crystallization in an Sn melt as follows. The Sr + Fe + As mixture was annealed at $T = 850$ °C for 12 h, ground, and then again annealed for 20 h at $T = 900$ °C. The obtained product (which mainly consisted of $BaFe_2As_2$ with a 5% impurity FeAs phase) was ground and immersed in a tin melt in the ratio $SrFe_2As_2 : Sn = 1 : 48$. The ampule was sealed, heated to $T = 1000$ °C, and then gradually cooled to $T = 500$ °C for 36 h. At the final stage (at $T = 500$ °C), the tin was filtered out of the $BaFe_2As_2$ crystals.

Superconducting $Sr_{1-x}K_xFe_2As_2$ and $A_{0.6}K_{0.4}Fe_2As_2$ (A = Sr, Ba) single crystals were grown by a similar method (in an Sn melt) [45] using simple starting substances. Synthesis of $EuFe_2As_2$ single crystals (from pure Eu + Fe + As) by the Bridgeman method was reported in [78]. High-quality $BaFe_2As_2$ single crystals were obtained by the spontaneous crystallization method [44]. Some other methods of synthesis are described in [264, 265].

Under normal conditions, AFe_2As_2 phases have a tetragonal structure ($ThCr_2Si_2$ type, space group $I4/mmm$) formed by alternating FeAs layers and atomic nets of alkali (alkali-earth) metals A (see Fig. 1). In a cell, the atoms occupy the following positions: Fe, 2d(0.5, 0, 0.25); As, 4e(0, 0, z_{As}); and A, 2a(0, 0, 0). The data available in the literature on the crystal structure parameters of these phases are presented in Table 8.

We note that the family of ternary $ThCr_2Si_2$-like phases is fairly large and includes more than 400 compounds. The information on the lattice parameters of many of them can be found in [266].

The features of the structural state of ternary arsenides in the low-temperature region were investigated. Well-pronounced anomalies in the temperature dependences of the electric resistance for polycrystalline ceramics $BaFe_2As_2$ at $T = 140$ K [38, 42, 255], $SrFe_2As_2$ at $T = 205$ K [37, 40, 41], and $CaFe_2As_2$ at $T = 170 - 150$ K [80, 81] and anomalies in the dependences of the thermal conductivity $C(T)$ and magnetic susceptibility $\chi(T)$ for $BaFe_2As_2$ single crystal [79, 52] correspond, according to X-ray diffraction data [79, 267], to a second-order structural phase transition. The results of experiments using neutron diffraction (on powder) [268] are indicative of a low-temperature transition of the $BaFe_2As_2$ crystal from the tetragonal structure (space group $I4/mmm$, $a = 0.395702$ nm, $c = 1.29685$ nm) to the orthorhombic one (space group $Fmmm$, $a = 0.561587$ nm, $b = 0.557125$ nm, $c = 1.29428$ nm), in which the atoms have the positions Fe 8f(1/4, 1/4, 1/4), As 8i(0, 0, z_{As}), and Ba 4a(0, 0, 0). According to neutronographic experiments, $SrFe_2As_2$ [269] undergoes a similar transition [269]. We note that no phase transition is observed in superconducting (doped by alkali metals) arsenides with decreasing the temperature.

No systematic data on the concentration changes in the lattice parameters of superconducting compositions $(Ca, Sr, Ba)_{1-x}(K, Na, Cs)_xFe_2As_2$ have yet been obtained. The measurements of individual samples only suggest that an anisotropic structure deformation may occur in the A sublattice upon a partial cation substitution. For instance, the $Ba_{0.6}K_{0.4}Fe_2As_2$ crystal, compared to the $BaFe_2As_2$

Table 8. Parameters of the crystal structure of the tetragonal ($ThCr_2Si_2$ structural type) ternary arsenides of rare-earth and transition metals and superconducting phases based on them.

Phase	T_c^{max}, K *	Cell parameters			Reference
		a, nm	c, nm	c/a	
KFe_2As_2	3.8	0.3841	1.3839	3.6026	[41]
$CsFe_2As_2$	2.7	0.3889	1.5006	3.8582	[41]
$CaFe_2As_2$	—	0.3912	1.1667	2.9824	[80]
$CaFe_2As_2$	—	0.3872	1.1730	3.0294	[81]
$SrFe_2As_2$	—	0.3924	1.238	3.1549	[37]
$SrFe_2As_2$	—	0.3961	1.2376	3.1245	[41]
$BaFe_2As_2$	—	0.3944	1.3115	3.3256	[79]
$EuFe_2As_2$	—	0.3910	1.2136	3.1036	[43]
$EuFe_2As_2$	—	0.3907	1.2114	3.1006	[78]
$Ca_{0.5}Na_{0.5}Fe_2As_2$	~ 20	0.3829	1.1862	3.0979	[81]
$Sr_{0.5}K_{0.5}Fe_2As_2$	37	0.3863	1.3554	3.5091	[79]
$Sr_{0.5}Cs_{0.5}Fe_2As_2$	37	0.3906	1.3701	3.5080	[41]
$Ba_{0.6}K_{0.4}Fe_2As_2$	38	0.3909	1.3212	3.3799	[38]
$Ba_{0.55}K_{0.45}Fe_2As_2$	~ 30	0.3919	1.3256	3.3825	[38]
$Ba_{0.85}La_{0.15}Fe_2As_2$	—	0.3957	1.2989	3.2825	[42]

* Maximum critical transition temperature for superconducting samples.

crystal, is compressed along the a-axis and extended along the c-axis [42]. The analysis of parameter variations in the $Sr_xK_{1-x}Fe_2As_2$ crystal structure for a series of samples with $x = 0$, 0.1, 0.3, 0.5, 0.6, 0.7, 0.8, 0.9, and 1.0 showed an increase in their cell volume with increasing the alkali-metal content [41]. But the parameters a and c change in an opposite manner: as the ratio K/Sr increases, the parameter a decreases (from 0.39156 nm for $Sr_{0.9}K_{0.1}Fe_2As_2$ to 0.38522 nm for $Sr_{0.1}K_{0.9}Fe_2As_2$), but c increases substantially. Accordingly, the ratio c/a increases from 3.1993 for $Sr_{0.9}K_{0.1}Fe_2As_2$ to 3.5740 for $Sr_{0.1}K_{0.9}Fe_2As_2$.

5.2 Superconductivity and magnetism

As was shown in the pioneering work [38], the transition to the superconducting state of the arsenide $BaFe_2As_2$ proceeds with a partial substitution of the univalent potassium K^{1+} for bivalent barium B^{2+} atoms, i.e., upon hole doping, and the critical temperature for $Ba_{0.6}K_{0.4}Fe_2As_2$ reaches $T_c \sim 38$ K. An analogous technique allowed obtaining $SrFe_2As_2$-based superconducting compositions by doping with potassium and cesium ($Sr_{1-x}(K, Cs)_xFe_2As_2$) with very close values $T_c \sim 37-38$ K [40, 41], and also $CaFe_2As_2$-based compositions by doping with sodium ($T_c \sim 20$ K) [81].

But the attempt to obtain a superconducting $BaFe_2As_2$ via its electron doping (partial substitution of trivalent La^{3+} for Ba^{2+}) failed. Some hopes were laid on $EuFe_2As_2$ as the basic phase of new arsenide superconductors, the physical properties of $EuFe_2As_2$ being similar to those of $BaFe_2As_2$ and $SrFe_2As_2$ [43, 270]. Measurements of the electric resistance and thermal conductivity of $EuFe_2As_2$ single crystals led the authors of [78] to the conclusion that this phase is a magnetic analogue of superconducting $Ba_{1-x}K_xFe_2As_2$.

The authors of [44] investigated the dependence of T_c on the concentration of hole dopants (potassium ions) in the composition of the $K_{1-x}Sr_xFe_2As_2$ phase. It was found that the maximum T_c value corresponds to $x \sim 0.5-0.6$ (Fig. 17a),

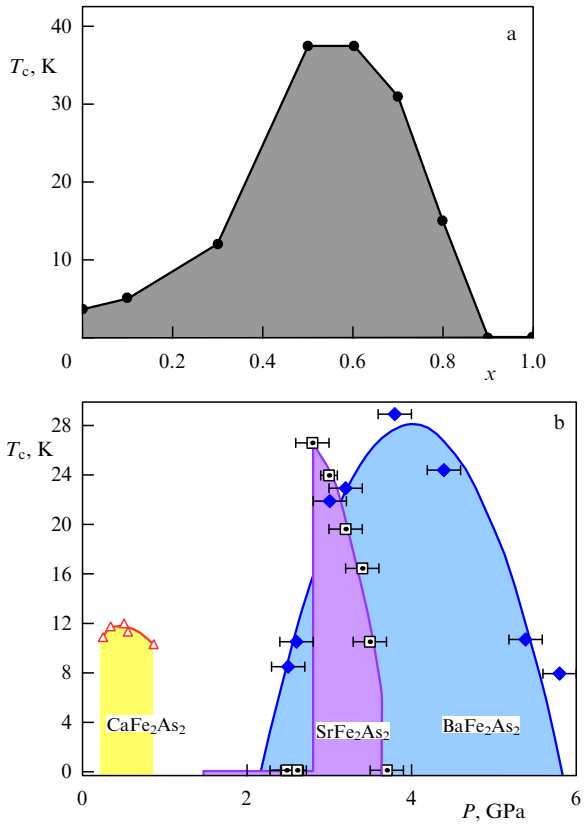

Figure 17. (a) Dependence of T_c on the $K_{1-x}Sr_xFe_2As_2$ composition [41]. (b) Dependence of T_c on the external pressure for undoped $CaFe_2As_2$, $SrFe_2As_2$, and $BaFe_2As_2$ phases [274].

whereas superconductivity disappeared from the system for $x \sim 0.9$. According to the measurements in [42], the Seebeck coefficient S has a rather large positive value for

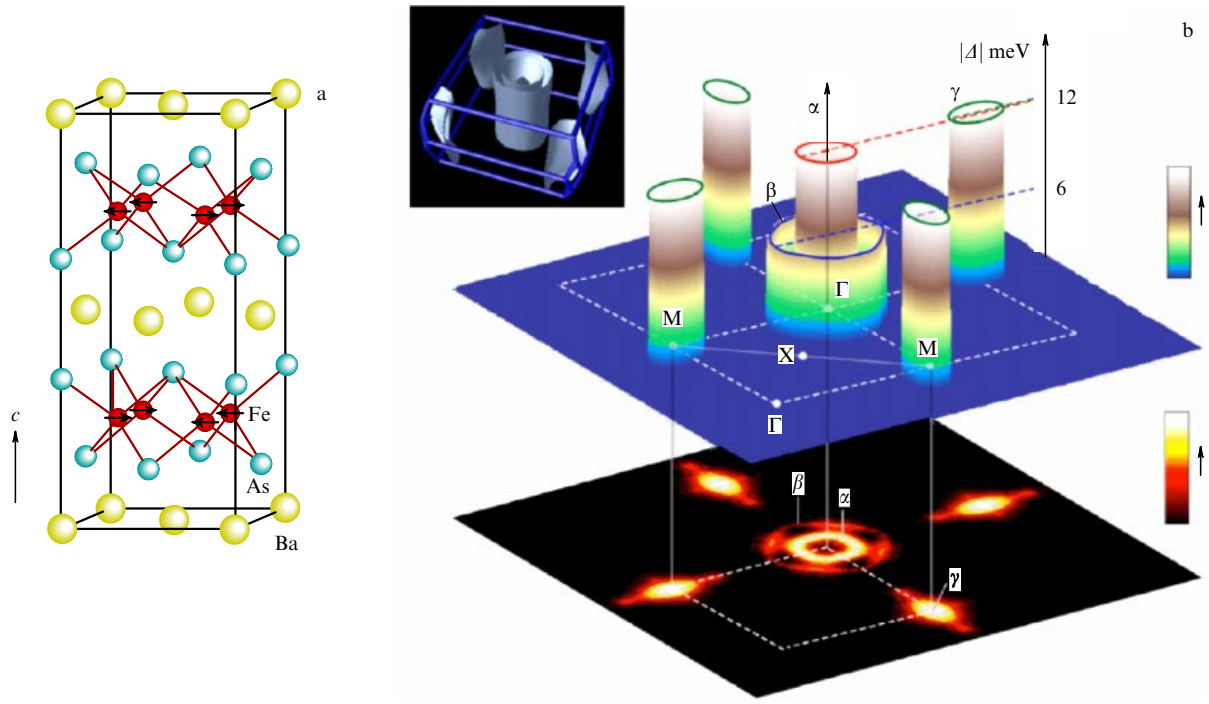

Figure 18. (a) $BaFe_2As_2$ magnetic structure according to neutron diffraction data [268]. (b) The view of a $Ba_{0.6}K_{0.4}Fe_2As_2$ FS according to the data of angle-resolved photoelectron spectroscopy [283]. Inset: the form of the FS according to the band calculation in [284]. Estimates of the superconducting gaps given in [283] are presented.

$K_{1-x}Sr_xFe_2As_2$. Consequently, the majority of carriers in such systems (as in HTSC cuprates) are holes, which distinguishes these systems from oxyarsenides, for which $S < 0$ [176]. The influence of the type of hole dopants (potassium or cesium) on the magnitude of the critical field in superconducting samples with similar compositions, $Sr_{0.6}K_{0.4}Fe_2As_2$ and $Sr_{0.6}Cs_{0.4}Fe_2As_2$, was considered in [41].

Interesting experiments [79] on single-crystal $BaFe_2As_2$ and $Ba_{0.55}K_{0.45}Fe_2As_2$ samples were carried out to study the anisotropy of the thermodynamic and electromagnetic properties of these layered phases. In particular, the room-temperature magnetic susceptibility χ turns out to be close to isotropic, but in the region of decreased temperatures ($T < 85$ K), its anisotropy was clearly pronounced: $\chi_{\|c} < \chi_{\perp c}$. For superconducting $Ba_{0.55}K_{0.45}Fe_2As_2$, the measured anisotropy coefficient of the upper critical field $\gamma = H_{\perp c}/H_{\|c}$, measured in [79], ranges from 2.5 to 3.5.

Studies of the effect of external pressure on the properties of 122 phases have begun [271–273]. For a superconducting single-crystal $Ba_{1-x}K_xFe_2As_2$ sample, it was found that T_c linearly decreases as the pressure increases [271]. Conversely, for nonsuperconducting $CaFe_2As_2$, a transition to the superconducting state (with the critical temperature below $T_c \sim 12$ K) was revealed [272, 273]. In recent paper [274], systematic studies of the pressure effect on the properties of undoped $CaFe_2As_2$, $SrFe_2As_2$, and $BaFe_2As_2$ have been performed and their superconducting transition (Fig. 17b) was found. In the series $CaFe_2As_2 \rightarrow SrFe_2As_2 \rightarrow BaFe_2As_2$, the superconducting transition region is shifted towards higher pressures, and the pressure-induced T_c value increases from ~ 12 K for $CaFe_2As_2$ to ~ 29 K for $BaFe_2As_2$. The latter value ($\Delta T_c \sim 29$ K) is the maximum ever obtained with the application of external pressure to superconductors [274].

The parameters of superconducting states of hole-doped 122 phases were discussed on the basis of optical spectroscopy data for $Ba_{0.6}K_{0.4}Fe_2As_2$ [275] and $Ba_{0.55}K_{0.45}Fe_2As_2$ [276] and scanning tunnel microscopy for $Sr_{1-x}K_xFe_2As_2$ [277].

Some experiments were conducted to study the relation between the structural and magnetic characteristics of AFe_2As_2 phases. From the optical spectroscopy data for $SrFe_2As_2$ and $EuFe_2As_2$ [270], a conclusion was drawn that these systems exhibit a spin instability and a pseudogap can be formed in their spectrum due to spin density waves. According to the data of NGR spectroscopy for ^{57}Fe nuclei, obtained for $BaFe_2As_2$ at $T = 298$, 77, and 4.2 K [38], a long-range magnetic order exists in this crystal at $T \leqslant 77$ K. The experimental results with the use of neutron diffraction on $BaFe_2As_2$ [268] and $CaFe_2As_2$ [278] have allowed assuming that their low-temperature (orthorhombic) phases involve a structure formed by magnetic moments of Fe atoms (Fig. 18a). Additional information on the magnetic characteristics of 122 phases was obtained using NMR [279, 280], μRS, and NGR spectroscopy [281].

In conclusion, we mention some interesting experimental studies of the electronic properties and topology of the FS of 122 phases using angle-resolved photoelectron spectroscopy. From these data, the authors of [282, 283] reconstructed the AFe_2As_2 FS reflecting the quasi-two-dimensional electronic structure of 122 phases and including hole cylinders in the center of the BZ and electron sheets at its edges, which agrees well with the band calculations [284] (Fig. 18b). The same method was used to analyze the FS evolution and to discuss the origin of the superconducting pseudogap under potassium doping of $BaFe_2As_2$ [285–287]. It was found in [285] that in $Ba_{1-x}K_xFe_2As_2$ (as compared to the original $BaFe_2As_2$), the radius of the hole cylinders (centered at the Γ point of

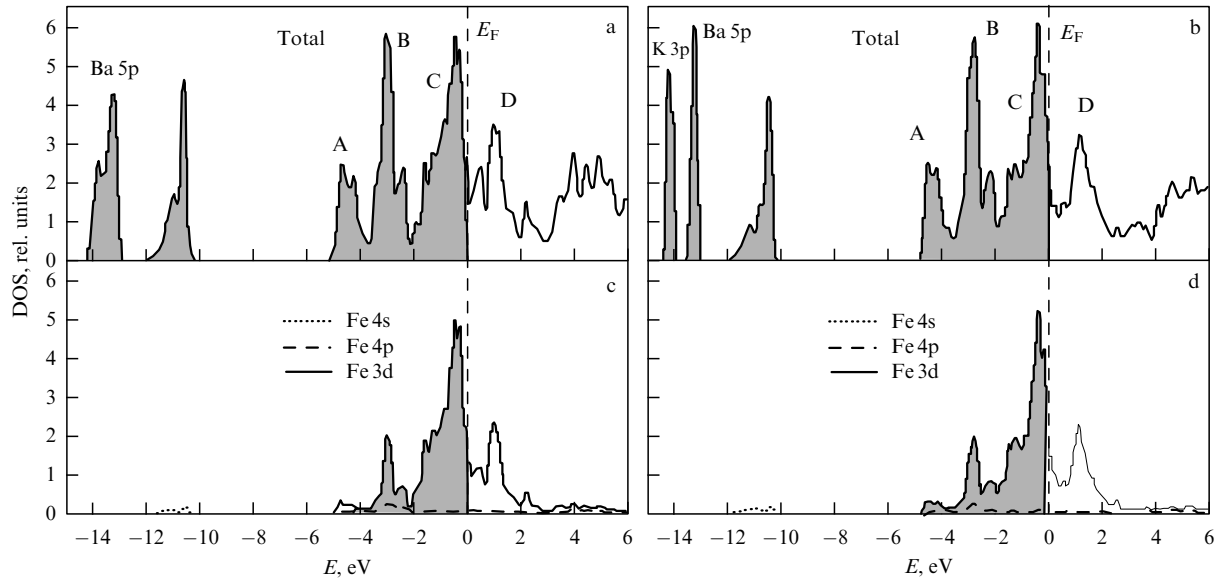

Figure 19. Total (a, b) and partial (c, d) (for iron atoms) densities of states of $BaFe_2As_2$ (a, c) and $Ba_{0.5}K_{0.5}Fe_2As_2$ (b, d) [288].

the BZ) increases and the electronic cylinders of the FS are compressed.

5.3 Band structure simulation and the properties of 122 phases

The computational methods of band theory were used to study the electronic and magnetic structure of ternary arsenide 122 phases $BaFe_2As_2$ [288–290], (Sr, Ba, La)Fe_2As_2 [37], and (Sr, Ba)Fe_2As_2 [284] and the doped phase $Ba_{0.5}K_{0.5}Fe_2As_2$ [288, 289].

The general idea of specific features of the electronic structure of the indicated phases is suggested in Fig. 19, which presents the DOS of $BaFe_2As_2$ and $Ba_{0.5}K_{0.5}Fe_2As_2$ [288]. We can see that in the region of high binding energies, the quasi-core Ba 5p states of $BaFe_2As_2$ lie in the energy range from −14.3 to −12.9 eV and As 4s states in the range from −12.0 to −10.2 eV, which are mixed with rather insignificant contributions of Fe 3d and Ba 5p states. The valence band largely consists of Fe 3d and As 4p states. Its structure [subbands A–C (Fig. 19)] includes the region of hybrid Fe 3d and As 4p states responsible for covalent Fe–As bonds (subbands A, B), while the pre-Fermi region (subbands C, D) mainly contains contributions from Fe 3d states. It is important that practically no impurities of barium valence states exist in the valence band region; in other words, in the arsenide lattice, these atoms are in an ionic state close to the Ba^{2+} state.

Therefore, conductivity in these phases is due to the FeAs layers; the intralayer Fe–As bonds have a significant covalent component, while the FeAs layers themselves interact in the crystal with neighboring Ba nets exclusively through ion bonds. Hence, these 122 phases, as the related 1111 phases, can be described as quasi-two-dimensional ion metals [195].

The question of the effect of Coulomb correlations on the fine distribution of energy bands in AFe_2As_2 phases remains open.

The $BaFe_2As_2$ magnetic structure was simulated in [290] under the assumption of nonmagnetic, FM, and collinear AFM states with spin stripe ordering (Fig. 5c), which is the most stable according to energy estimates. The magnetic moment per Fe atom was calculated for this state to be nearly 2.6 μ_B. For the AFM state, the Fermi level density ($N(E_F) \sim 2.4$ states per eV) notably decreases compared to that for the nonmagnetic state (~ 3.9 states per eV). Furthermore, the maximum contribution to $N(E_F)$ is made by the iron states with spin down, while the density of high-spin states is much lower, and therefore the authors of [290] refer $BaFe_2As_2$ to antiferromagnetic semimetals.

The main effect of barium sublattice doping by an alkali metal ($BaFe_2As_2 \rightarrow Ba_{0.5}K_{0.5}Fe_2As_2$) does not change the structure of pre-Fermi bands and reduces [288] to a partial depopulation of the Fe 3d-like subband. The DOS at the Fermi level, $N(E_F)$, increases by 20% owing exclusively to 3d states of Fe, whereas the contributions to $N(E_F)$ of As states remain at the level of 4%.

The change in the type of magnetic ordering depending on the degree of $BaFe_2As_2$ doping was analyzed in [289]. Two types of AFM ordering [in the FeAs layer, AFM-1 and AFM-2 (Fig. 20a)] under hole doping of $Ba_{1-x}K_xFe_2As_2$ were compared to the AFM ordering in electron-doped LaOFeAs. The main results are shown in Fig. 20b. First, in the entire range of the hole dopant concentration, the AFM state of $Ba_{1-x}K_xFe_2As_2$ is energetically more advantageous than the nonmagnetic (NM); in other words, doping does not suppress magnetism, unlike the electron doping of LaOFeAs. Second, the magnetic moment of Fe atoms in $Ba_{1-x}K_xFe_2As_2$ remains essentially constant irrespective of the Ba/K ratio, whereas with increasing the fluorine content in the LaOFeAs system, the magnetic moment sharply decreases to zero for $LaO_{1-x}F_xFeAs$ at $x = 0.2$. Finally, for $Ba_{1-x}K_xFe_2As_2$, the CQP exists between AFM-1 and AFM-2 states (it is reached for $J_2 = J_1/2$, where J_1 and J_2 are exchange integrals (Fig. 20a)), while in the $LaO_{1-x}F_xFeAs$ diagram, the CQP separates the AFM-2 state from the nonmagnetic states.

In conclusion, we briefly dwell on the first theoretical estimates of the mechanical characteristics of 122 phases, carried out in [291] in the example of $SrFe_2As_2$. The bulk compression modulus of this phase was found to be small (~ 67 GPa), much smaller than that for the 1111 phase LaOFeAs [~ 98 GPa (see Table 7)]. In addition, according to the estimates in [291], $SrFe_2As_2$ is brittle. It was shown

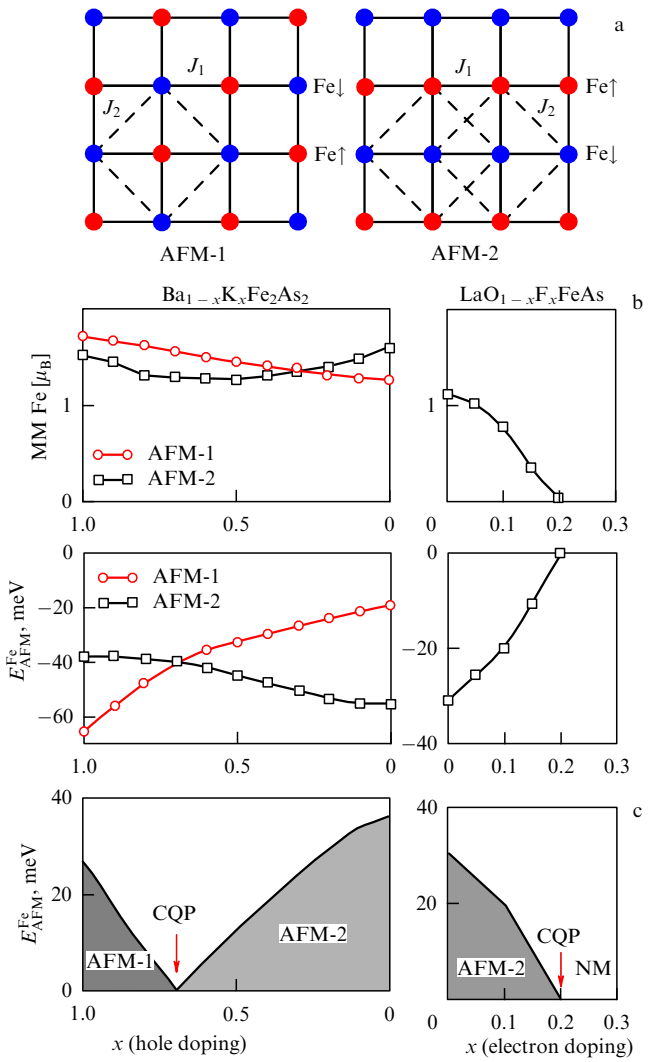

Figure 20. (a) Types of antiferromagnetic ordering in the FeAs layer: AFM-1 and AFM-2 for $Ba_{1-x}K_xFe_2As_2$ [289]. (b) Magnetic moments of Fe atoms and the stabilization energy of AFM states (relative to the nonmagnetic state energy $E_{NM} = 0$) per Fe atom for $Ba_{1-x}K_xFe_2As_2$ (hole doping) and $LaO_{1-x}F_xFeAs$ (electron doping) [289]. (c) Phase diagrams constructed on the basis of the calculation of the total energies of these 122 and 1111 phases. Critical quantum points and types of AFM structures (AFM-1 and AFM-2, stripe-like) are indicated.

in [291] that $SrFe_2As_2$ is mechanically much less stable and, obviously, much less strong than LaOFeAs. This can be qualitatively explained by referring to the specific features of the interatomic bonds in these phases. Indeed, for $SrFe_2As_2$, the system of chemical bonds involves covalent intralayer Fe – As bonds and ionic interactions between layers of the alkali-earth metal and FeAs layers, but for the oxyarsenide LaOFeAs, along with the above-mentioned components, an additional component of interlayer LaO – FeAs interactions (the covalent La – As bond) is realized.

6. Conclusion

In this review, an attempt is made to generalize the results of the first stage of the study of new FeAs superconductors that followed their discovery [1] in February 2008.

The main achievements of this stage can be described as follows. A new type of high-temperature ($T_c \sim 26-55$ K) superconductors based on two related families of layered compounds was discovered: quaternary oxyarsenides of transition and rare-earth *Ln*OFeAs metals of the 1111 phase and oxygen-free ternary AFe_2As_2 arsenides of 122 phases. Effective methods of synthesizing these superconducting materials in poly- and single-crystal states were elaborated. Numerous studies of their properties were conducted, including structural, superconducting, and magnetic properties. The computational methods of band theory were used to establish the features of the electronic structure and chemical bond, and the types of spin ordering and mechanical characteristics were estimated.

In particular, the structural (and magnetic) phase transition is observed for the majority of the initial (undoped) 1111 and 122 phases as the temperature decreases; this effect is suppressed under doping. The principal conditions for the superconducting transition of initial (undoped) 1111 and 122 phases were determined. For 1111 phases, the condition of such a transition is the electron or hole doping, which is realized as a result of atomic substitutions (or the formation of lattice vacancies) predominantly in the molecular rare-earth-metal – oxygen layers. On the other hand, the superconducting transition of 122 phases turns out to be possible either under their hole doping or under external pressure. In the latter case, a record high increase in the critical transition temperature ($\Delta T_c \sim 29$ K) was observed for 122 phases, reached when external pressure was applied. Another record-breaking result for this class of superconducting materials is an extremely high value of the upper critical field B_{c2} up to ~ 300 T found for some 1111 oxyarsenide superconductors, which can be important for the generation of strong magnetic fields.

New FeAs superconductors are exceedingly interesting subjects for revision and development of the existing model approximations of the origin of superconductivity because these materials are rich in iron, a metal having magnetic properties, and the superconducting transition occurs at the boundary of their magnetic instability.

At the same time, we can state that the studies of this new class of FeAs superconducting materials are at their early stages. Many problems are associated with further comprehensive investigation of their properties, for instance, those concerning the influence of baric treatment on the superconducting characteristics, grain-boundary and dimensional effects, comparison of the behavior of these systems in single-crystal, membrane, and nanocrystal states, and the role of impurity phases. It seems important to determine the features of the electronic and magnetic states of the FeAs superconductor surface.

Of undoubted interest are further studies aimed at widening the class of these superconducting systems, for example, setting up work to study the effects of the iron or arsenic (*Ln*OFeAs and AFe_2As_2) sublattice doping. The studies in this area have up to now been mainly limited to substitutions in *Ln*O layers or *A* atom nets. The first promising results have recently been obtained: cobalt-doped LaOFeAs exhibited a superconducting transition [292, 293] (with $T_c \sim 14$ K for the composition $LaOFe_{0.89}Co_{0.11}As$ [292]). Another important mark in the search for new superconducting materials may be the recently discovered LiFeAs superconductivity (with the maximum $T_c \sim 18$ K for the composition $Li_{0.6}FeAs$ [46]). This material may possibly start a new, third (after 1111 and 122 phases) family of so-called 111 superconductors.

In our opinion, such research work will be an important step in explaining the origin of superconductivity of systems near their magnetic instability boundary and the creation of adequate physical models for their description and, in addition, will be of paramount importance for the development of the physical science of materials of new superconductors.

In the manuscript prepress period, studies of new oxypnictide and pnictide superconductors were under way. We mention several most interesting results.

The search for new superconducting 1111 phases has been undertaken; $HoO_{1-\delta}FeAs$ ($T_c \sim 50.5$ K), $YO_{1-\delta}FeAs$ ($T_c \sim 46.5$ K), $DyO_{1-\delta}FeAs$ ($T_c \sim 52.2$ K), $TbO_{1-\delta}FeAs$ ($T_c \sim 48.5$ K) [294], GdONiBi ($T_c \sim 4.5$ K), and $Gd_{0.9}Sr_{0.1}ONiBi$ ($T_c \sim 4.7$ K) superconductors [295] have been synthesized. Cobalt- and nickel-doped 1111 phases in the iron sublattice [296–299] [300] were synthesized and the physical properties of oxypnictides were studied [301–312]. Interesting investigations were carried out in [313], where the growth dynamics of biological cells in their contact with $PrO_{1-\delta}FeAs$ was studied and the biological compatibility of this and related superconductors containing the toxic element arsenic was revealed.

A considerable number of works were devoted to 122 phases. New superconductors were synthesized, namely, $EuFe_2As_2$ ($T_c \sim 20$ K), $Eu_{0.5}K_{0.5}Fe_2As_2$ ($T_c \sim 32$ K) [314], $BaFe_{1.8}Co_{0.2}As_2$ ($T_c \sim 22$ K) [315], $SrNi_2As_2$ ($T_c \sim 0.6$ K) [316], $BaFe_{1.9}Ni_{0.1}As_2$ ($T_c \sim 21$ K) [317], and $BaNi_2As_2$ ($T_c \sim 0.7$ K) [318]. Studies of the various physical properties of 122 phases were continued [319–335].

Stoichiometric 111 phase LiFeAs (space group $P4/nmm$, PFCl structural type, lattice parameters $a = 0.3792$ nm and $c = 0.364$ nm) with the superconducting transition temperature 18 K was synthesized [336] (see also [337]). Pioneering studies of specific features of the band structure of LiFeAs [338–340] and $Li_{0.5}FeAs$ and LiCoAs phases were performed [338].

Among the most important recent results is also the discovery of superconductivity ($T_c \sim 8$ K) [341] in the α phase of iron monoselenide $FeSe_{1-x}$ ($x \sim 0.12$). This phase has a layered tetragonal structure (PbO type, space group $P4/nmm$) in which each layer is formed by conjugate $FeSe_4$ tetrahedrons, the same as conducting FeAs layers of the above-discussed 1111, 122, and 111 phases. In subsequent experiments, varying the degree of $FeSe_{1-x}$ nonstoichiometry has allowed the authors of [342–344] to obtain polycrystalline samples with $T_c \sim 14$ K and then to reach the critical temperature $T_c \sim 27$ K by applying external pressure to these samples. $FeSe_{1-x}$ single crystals were grown [345] and NMR experiments (on ^{77}Se nuclei) were carried out [346]. The band structure, the FS topology, and FeSe magnetic interaction parameters were investigated. Finally, it was found that upon substitution of tellurium atoms for part of the selenium atoms in the FeSe composition, the obtained $Fe(Se_{1-x}Te_x)_{0.82}$ samples are also superconductors with $T_c \sim 14$ K [349]. In our opinion, further detailed studies of the physical properties of superconducting FeSe (as the chemically simplest prototype of the above-discussed family of oxypnictide and pnictide superconductors) are of considerable interest and will provide deeper insight into the origin of these interesting materials.

References

1. Kamihara Y et al. *J. Am. Chem. Soc.* **130** 3296 (2008)
2. Bednorz J G, Müller K A *Z. Phys. B* **64** 189 (1986)
3. Hebard A F et al. *Nature* **350** 600 (1991)
4. Nagamatsu J et al. *Nature* **410** 63 (2001)
5. Hand E *Nature* **452** 922 (2008)
6. Takahashi H et al. *Nature* **453** 376 (2008)
7. Day C *Phys. Today* **61** (5) 11 (2008)
8. Ishibashi S, Terakura K, Hosono H *J. Phys. Soc. Jpn.* **77** 053709 (2008)
9. Chen X H et al. *Nature* **453** 761 (2008)
10. Hunte F et al. *Nature* **453** 903 (2008)
11. Cho A *Science* **320** 432 (2008)
12. Chen G F et al. *Phys. Rev. Lett.* **100** 247002 (2008)
13. Li J, Wang Y-P *Chinese Phys. Lett.* **25** 2232 (2008)
14. Singh D J, Du M-H *Phys. Rev. Lett.* **100** 237003 (2008)
15. Haule K, Shim J H, Kotliar G *Phys. Rev. Lett.* **100** 226402 (2008)
16. Cho A *Science* **320** 870 (2008)
17. Wen H-H et al. *Europhys. Lett.* **82** 17009 (2008)
18. Han Q, Chen Y, Wang Z D *Europhys. Lett.* **82** 37007 (2008)
19. Ren Z-A et al. *Europhys. Lett.* **82** 57002 (2008)
20. de la Cruz C et al. *Nature* **453** 899 (2008)
21. Wu D et al. *Sci. China G* **51** 715 (2008)
22. Cheng P et al. *Sci. China G* **51** 719 (2008)
23. Sun Y, Guidry M, Wu C L *Chinese Sci. Bull.* **53** 1617 (2008)
24. Grant P M *Nature* **453** 1000 (2008)
25. Chen G-F et al. *Chinese Phys. Lett.* **25** 2235 (2008)
26. Ren Z-A et al. *Chinese Phys. Lett.* **25** 2215 (2008)
27. Yang J et al. *Supercond. Sci. Technol.* **21** 082001 (2008)
28. Kozhevnikov V L et al. *Pis'ma Zh. Eksp. Teor. Fiz.* **87** 747 (2008) [*JETP Lett.* **87** 649 (2008)]
29. Fratini M et al. *Supercond. Sci. Technol.* **21** 092002 (2008)
30. Nekrasov I A, Pchelkina Z V, Sadovskii M V *Pis'ma Zh. Eksp. Teor. Fiz.* **87** 647 (2008) [*JETP Lett.* **87** 560 (2008)]
31. Hadjiev V G et al. *Phys. Rev. B* **77** 220505(R) (2008)
32. Mu G et al. *Chinese Phys. Lett.* **25** 2221 (2008)
33. Ou H-W et al. *Chinese Phys. Lett.* **25** 2225 (2008)
34. Chen T Y et al. *Nature* **453** 1224 (2008)
35. Ding L et al. *Phys. Rev. B* **77** 180510(R) (2008)
36. Ren Z-A et al. *Europhys. Lett.* **83** 17002 (2008); arXiv:0804.2582
37. Krellner C et al. *Phys. Rev. B* **78** 100504(R) (2008); arXiv:0806.1043
38. Rotter M, Tegel M, Johrendt D *Phys. Rev. Lett.* **101** 107006 (2008); arXiv:0805.4630
39. Mine T et al. *Solid State Commun.* **147** 111 (2008)
40. Chen G-F et al. *Chinese Phys. Lett.* **25** 3403 (2008)
41. Sasmal K et al. *Phys. Rev. Lett.* **101** 107007 (2008); arXiv:0806.1301
42. Wu G et al. *Europhys. Lett.* **84** 27010 (2008); arXiv:0806.1459
43. Ren Z et al. *Phys. Rev. B* **78** 052501 (2008)
44. Wang X F et al., arXiv:0806.2452
45. Chen G F et al., arXiv:0806.2648
46. Wang X C et al., arXiv:0806.4688
47. Hiroi Z, arXiv:0805.4668
48. Connelly N G et al. (Eds) *Nomenclature of Inorganic Chemistry, IUPAC Recommendations 2005* (Cambridge: Royal Society of Chemistry Publ., 2005)
49. Ding Q et al., arXiv:0806.0976
50. Lu W et al. *New J. Phys.* **10** 063026 (2008)
51. Chen G F et al. *Phys. Rev. Lett.* **100** 247002 (2008); arXiv:0803.3790
52. Cheng P et al., arXiv:0804.0835
53. Wang C et al. *Europhys. Lett.* **83** 67006 (2008); arXiv:0804.4290
54. Prozorov R et al., arXiv:0805.2783
55. Jia Y et al. *Appl. Phys. Lett.* **93** 032503 (2008); arXiv:0806.0532
56. Ren Z-A et al., arXiv:0803.4283
57. Fuchs G et al., arXiv:0806.0781
58. Awana V P S et al. *J. Supercond. Novel Magn.* **21** 167 (2008)
59. Bos J-W G et al. *Chem. Commun.* **31** 3634 (2008)
60. Li Z et al. *Phys. Rev. B* **78** 060504(R) (2008); arXiv:0803.2572
61. Yanagi U et al. *Phys. Rev. B* **77** 224431 (2008); arXiv:0806.0123
62. Li L-J et al. *Phys. Rev. B* **78** 132506 (2008); arXiv:0806.1675
63. Wu G et al. *Phys. Rev. B* **78** 092503 (2008); arXiv:0806.1687
64. Martinelli A et al. *Supercond. Sci. Technol.* **21** 095017 (2008)
65. Liu C et al., arXiv:0806.2274

66. Ma Y et al., arXiv:0806.2839
67. Gao Z et al. *Supercond. Sci. Technol.* **21** 112001 (2008)
68. Gao Z et al. *Supercond. Sci. Technol.* **21** 105024 (2008)
69. Hashimoto K et al., arXiv:0806.3149
70. Singh S et al., arXiv:0806.3571
71. Zimmer B I et al. *J. Alloys Comp.* **229** 238 (1995)
72. Nientiedt A T, Jeitschko W *Inorg. Chem.* **37** 386 (1998)
73. Kayanuma K et al. *Thin Solid Films* **516** 5800 (2008)
74. Kamihara Y et al. *J. Am. Chem. Soc.* **128** 10012 (2006)
75. Watanabe T et al. *Inorg. Chem.* **46** 7719 (2007)
76. McQueen T M et al. *Phys. Rev. B* **78** 024521 (2008)
77. Hamlin J J et al. *J. Phys. Condens. Matter* **20** 365220 (2008)
78. Jeevan H S et al. *Phys. Rev. B* **78** 052502 (2008)
79. Ni N et al. *Phys. Rev. B* **78** 014507 (2008)
80. Ni N et al. *Phys. Rev. B* **78** 014523 (2008)
81. Wu G et al. *J. Phys. Condens. Matter* **20** 422201 (2008); arXiv:0806.4279
82. Ronning F et al. *J. Phys. Condens. Matter* **20** 322201 (2008)
83. Nientiedt A T et al. *Chem. Sci.* **52** 560 (1997)
84. Brylak M, Möller M H, Jeitschko W *J. Solid State Chem.* **115** 305 (1995)
85. Quebe P, Terbüchte L J, Jeitschko W *J. Alloys Comp.* **302** 70 (2000)
86. Lincke H et al. *Z. Anorg. Allg. Chem.* **632** 1804 (2006)
87. Ma C et al., arXiv:0806.3159
88. Lee C-H et al. *J. Phys. Soc. Jpn.* **77** 083704 (2008)
89. Nomura T et al. *Supercond. Sci. Technol.* **21** 125028 (2008); arXiv:0804.3569
90. Margadonna S et al., arXiv:0806.3962
91. Yildirim T, arXiv:0805.2888
92. McGuire M A et al. *Phys. Rev. B* **78** 094517 (2008); arXiv:0806.3878
93. Luetkens H et al., arXiv:0806.3533
94. Takeshita S et al. *J. Phys. Soc. Jpn.* **77** 103703 (2008); arXiv:0806.4798
95. Shekhar˚ et al., arXiv:0806.1661
96. Hicks C W et al., arXiv:0807.0467
97. Yamamoto A et al. *Appl. Phys. Lett.* **92** 252501 (2008)
98. Kamihara Y et al. *Phys. Rev. B* **77** 214515 (2008)
99. Lebègue S *Phys. Rev. B* **75** 35110 (2007)
100. Zhang W-B et al. *Phys. Rev. B* **77** 214513 (2008)
101. Subedi A, Singh D J, Du M-H *Phys. Rev. B* **78** 060506(R) (2008); arXiv:0806.3785
102. Kohama Y et al. *J. Phys. Soc. Jpn.* **77** 094715 (2008); arXiv:0806.3139
103. Meisner G P *Physica B + C* **108** 763 (1981)
104. Chen G F et al., arXiv:0803.4384
105. Zhao J et al. *Nature Mater.* **7** 953 (2008); arXiv:0806.2528
106. Si Q, Abrahams E *Phys. Rev. Lett.* **101** 076401 (2008)
107. Yildirim T *Phys. Rev. Lett.* **101** 057010 (2008)
108. Mu G et al., arXiv:0806.2104
109. Lu W et al. *Solid State Commun.* **148** 168 (2008); arXiv:0804.3725
110. Ding Q et al., arXiv:0806.2379
111. Zocco D A et al. *Physica C* **468** 2229 (2008); arXiv:0805.4372
112. Lorenz B et al. *Phys. Rev. B* **78** 012505 (2008)
113. Wang X L et al., arXiv:0806.0063
114. Narduzzo A et al. *Phys. Rev. B* **78** 012507 (2008)
115. Senatore C et al. *Phys. Rev. B* **78** 054514 (2008)
116. Yang H et al. *Phys. Rev. B* **78** 092504 (2008); arXiv:0806.0980
117. Ren C et al., arXiv:0804.1726
118. Weyeneth S et al., arXiv:0806.1024
119. Dubroka A et al., arXiv:0805.2415
120. Jia Y et al. *Appl. Phys. Lett.* **93** 032503 (2008)
121. Shan L et al., arXiv:0803.2405
122. Zhu X et al. *Supercond. Sci. Technol.* **21** 105001 (2008)
123. Malone L et al., arXiv:0806.3908
124. Khasanov R et al. *Phys. Rev. B* **78** 092506 (2008); arXiv:0805.1923
125. Kurmaev E Z et al., arXiv:0805.0668
126. Cao C, Hirschfeld P J, Cheng H-P *Phys. Rev. B* **77** 220506(R) (2008)
127. Eschrig H, arXiv:0804.0186
128. Kuroki K et al. *Phys. Rev. Lett.* **101** 087004 (2008)
129. Boeri L, Dolgov O V, Golubov A A *Phys. Rev. Lett.* **101** 026403 (2008)
130. Shorikov A O et al., arXiv:0804.3283
131. Sushko P V et al., arXiv:0807.2213
132. Si Q, Abrahams E, arXiv:0804.2480
133. Daghofer M et al., arXiv:0805.0148
134. Kroll T et al., arXiv:0806.2625
135. Liu Y et al. *Chinese Phys. Lett.* **25** 3761 (2008); arXiv:0805.3821
136. Ou H W et al. *Solid State Commun.* **148** 504 (2008); arXiv:0806.0078
137. Ishida Y et al., arXiv:0805.2647
138. Malaeb W et al. *J. Phys. Soc. Jpn.* **77** 093714 (2008); arXiv:0806.3860
139. Koitzsch A et al., arXiv:0806.0833
140. Sato T et al. *J. Phys. Soc. Jpn.* **77** 063708 (2008)
141. Yanagi H et al. *Phys. Rev. B* **77** 224431 (2008)
142. Sato T et al. *Phys. Rev. Lett.* **83** 2254 (1999)
143. Jia X et al. *Chinese Phys. Lett.* **25** 3765 (2008); arXiv:0806.0291
144. Kitao S et al. *J. Phys. Soc. Jpn.* **77** 103706 (2008); arXiv:0805.0041
145. Klauss H-H et al. *Phys. Rev. Lett.* **101** 077005 (2008)
146. Nowik I et al. *J. Phys. Condens. Matter* **20** 292201 (2008)
147. Felner I et al., arXiv:0805.2794
148. Tegel M et al., arXiv:0805.1208
149. Nowik I, Felner I *J. Supercond. Novel Magn.* **21** 297 (2008)
150. Nakai Y et al. *J. Phys. Soc. Jpn.* **77** 073701 (2008)
151. Grafe H-J et al. *Phys. Rev. Lett.* **101** 047003 (2008)
152. Matano K et al. *Europhys. Lett.* **83** 57001 (2008); arXiv:0806.0249
153. Mukuda H et al., arXiv:0806.3238
154. Ahilan K et al. *Phys. Rev B* **78** 100501(R) (2008)
155. Braford W, Gunn J M F *Physica C* **156** 515 (1988)
156. Sonier J E, Brewer J, Kiefl R F *Rev. Mod. Phys.* **72** 769 (2000)
157. Atanassova Y K et al. *Phys. Rev. B* **50** 586 (1994)
158. Zhao S C et al., arXiv:0806.0885
159. Dong J et al. *Europhys. Lett.* **83** 27006 (2008)
160. Drew A J et al., arXiv:0805.1042
161. Carlo J P et al., arXiv:0805.2186
162. Klauss H-H et al. *Phys. Rev. Lett.* **101** 077005 (2008); arXiv:0805.0264
163. Luetkens H et al. *Phys. Rev. Lett.* **101** 097009 (2008); arXiv:0804.3115
164. Yates K A et al. *Supercond. Sci. Technol.* **21** 092003 (2008)
165. Chen T Y et al. *Nature* **453** 1224 (2008); arXiv:0805.4616
166. Shan L et al. *Europhys. Lett.* **83** 57004 (2008)
167. Samuely P et al., arXiv:0806.1672
168. Wang Y et al., arXiv:0806.1986
169. Boris A V et al., arXiv:0806.1732
170. Drechsler S L et al., arXiv:0805.1321
171. Millo O et al. *Phys. Rev. B* **78** 092505 (2008); arXiv:0807.0359
172. Dubroka A et al. *Phys. Rev. Lett.* **101** 097011 (2008)
173. Zhu Z W et al. *New J. Phys.* **10** 063021 (2008)
174. Cheng P et al. *Phys. Rev. B* **78** 134508 (2008); arXiv:0806.1668
175. Kohama Y et al. *Europhys. Lett.* **84** 37005 (2008); arXiv:0806.4215
176. Pinsard-Gaudart L et al. *Phys. Status Solidi* (*RRL*) **2** 185 (2008)
177. Xu G et al. *Europhys. Lett.* **82** 67002 (2008)
178. Ma F, Lu Z-Y, Xiang T, arXiv:0804.3370
179. Mazin I I et al. *Phys. Rev. Lett.* **101** 057003 (2008)
180. Mazin I I et al., arXiv:0806.1869
181. Zhang H-J et al., arXiv:0803.4487
182. Ma F, Lu Z-Y *Phys. Rev. B* **78** 033111 (2008)
183. Yin Z P et al. *Phys. Rev. Lett.* **101** 047001 (2008)
184. Pourovskii L et al. *Europhys. Lett.* **84** 37006 (2008); arXiv:0807.1037
185. Che R et al., arXiv:0805.0397
186. Kamihara Y et al. *Phys. Rev. B* **77** 214515 (2008); arXiv:0805.2983
187. Shein I R, Kozhevnikov V L, Ivanovskii A L *Phys. Lett. A* **372** 5838 (2008)
188. Shein I R, Kozhevnikov V L, Ivanovskii A L *Phys. Rev. B* **78** 104519 (2008)
189. Chen B et al. *Science* **291** 1021 (2001)
190. Yaghi O M et al. *Nature* **423** 705 (2003)
191. Mellot-Draznieks C, Férey G *Curr. Opin. Solid State Mater. Sci.* **7** 13 (2003)
192. Bader R F W *Atoms in Molecules: A Quantum Theory* (Oxford: Clarendon Press, 1990)
193. Shein I R, Ivanovskii A L *Scripta Mater.* **59** 1099 (2008)
194. Vildosola V et al. *Phys. Rev. B* **78** 064518 (2008); arXiv:0806.3285
195. Shein I R, Ivanovskii A L *Pis'ma Zh. Eksp. Teor. Fiz.* **88** 115 (2008) [*JETP Lett.* **88** 107 (2008)]
196. Dai J, Li Z, Yang J, arXiv:0806.3865
197. Yi W et al., arXiv:0807.0675

198. Takenaka H, Singh D J *Phys. Rev. B* **78** 052503 (2008)
199. Izyumov Yu A, Kurmaev E Z *Usp. Fiz. Nauk* **178** 25 (2008) [*Phys. Usp.* **51** 23 (2008)]
200. Nakamura H et al., arXiv:0806.4804
201. Craco L et al. *Phys. Rev. B* **78** 134511 (2008); arXiv:0805.3636
202. Anisimov V I et al., arXiv:0807.0547
203. Chen Y et al., arXiv:0807.0622
204. Giovannetti G, Kumar S, van den Brink J *Physica B* **403** 3653 (2008); arXiv:0804.0866
205. Park T et al. *Nature* **440** 65 (2006)
206. Gegenwart P et al. *Phys. Rev. Lett.* **81** 1501 (1998)
207. Stockert O et al. *Phys. Rev. Lett.* **92** 136401 (2004)
208. Sato N K et al. *Nature* **410** 340 (2001)
209. Qiu Y et al., arXiv:0806.2195
210. Lei M et al. *Phys. Rev. B* **47** 6154 (1993)
211. Hirsch J E *Phys. Rev. B* **55** 9007 (1997)
212. Meenakshi S et al. *Phys. Rev. B* **58** 3377 (1998)
213. Jaenicke-Rössler U et al. *Physica C* **305** 209 (1998)
214. Wang H-Y et al. *Phys. Rev. B* **72** 172502 (2005)
215. Shein I R, Bannikov V V, Ivanovskii A L *Physica C* **468** 1 (2008)
216. Güçlü N et al. *Physica C* **433** 115 (2005)
217. Ekimov E A et al. *Nature* **428** 542 (2004)
218. Takano T et al. *Diamond Relat. Mater.* **16** 911 (2007)
219. Shein I R et al. *Fiz. Tverd. Tela* **49** 1015 (2007) [*Phys. Solid State* **49** 1067 (2007)]
220. Islam A K M A et al. *Solid State Commun.* **139** 315 (2006)
221. Vaitheeswaran G et al. *J. Phys. Condens. Matter* **19** 326214 (2007)
222. Pugh S F *Philos. Mag.* **45** 833 (1954)
223. Haines J, Léger J M, Bocquillon G *Annu. Rev. Mater. Res.* **31** 1 (2001)
224. Maksimov E G *Usp. Fiz. Nauk* **170** 1033 (2000) [*Phys. Usp.* **43** 965 (2000)]
225. Lee P A, Wen X-G, arXiv:0804.1739
226. Weng Z-Y, arXiv:0804.3228
227. Huang X, arXiv:0806.3125
228. Li T, arXiv:0804.0536
229. Yao Z-J, Li J-X, Wang Z D, arXiv:0804.4166
230. Qi X-L et al., arXiv:0804.4332
231. Seo K, Bernevig B A, Hu J *Phys. Rev. Lett.* **101** 206404 (2008); arXiv:0805.2958
232. Wan Y, Wang Q-H, arXiv:0805.0923
233. Barzykin V, Gor'kov L P *Pis'ma Zh. Eksp. Teor. Fiz.* **88** 142 (2008) [*JETP Lett.* **88** 131 (2008)]
234. Yang S et al., arXiv:0807.0587
235. Korshunov M M, Eremin I *Phys. Rev. B* **78** 140509(R) (2008); arXiv:0804.1793
236. Wachter P, arXiv:0806.0900
237. Alexandrov A S, Ranninger J, Robaszkiewicz S *Phys. Rev. B* **33** 4526 (1986)
238. Mott N F *Physica C* **205** 191 (1993)
239. Hirsch J E, Marsiglio F *Phys. Rev. B* **39** 11515 (1989)
240. Marsiglio F, Hirsch J E *Physica C* **468** 1047 (2008); arXiv:0804.0002
241. Huang X, arXiv:0805.0355
242. Huang X, arXiv:0807.0899
243. Mazov L S, arXiv:0805.4097
244. Shi J, arXiv:0806.0259
245. CvetkovicV, Tesanovic Z, arXiv:0804.4678
246. Manousakis K et al. *Phys. Rev. B* **78** 205112 (2008); arXiv:0806.3432
247. Nakamura K, Arita R, Imada M *J. Phys. Soc. Jpn.* **77** 093711 (2008); arXiv:0806.4750
248. Zhou Y, Chen W-Q, Zhang F-C *Phys. Rev. B* **78** 064514 (2008); arXiv:0806.0712
249. Wang Z-H et al., arXiv:0805.0736
250. Ran Y et al., arXiv:0805.3535
251. You W-L et al., arXiv:0807.1493
252. Yao D-X, Carlson E W *Phys. Rev. B* **78** 052507 (2008); arXiv:0804.4115
253. Wu J, Phillips P, Castro Neto A H *Phys. Rev. Lett.* **101** 126401 (2008); arXiv:0805.2167
254. Haule K, Kotliar G, arXiv:0805.0722
255. Rotter M et al. *Phys. Rev. B* **78** 020503(R) (2008)
256. Johnson V, Jeitschko W *J. Solid State Chem.* **11** 161 (1974)
257. Pfisterer M, Nagorsen G *Z. Naturforsch. B* **35** 703 (1980)
258. Shelton R N, Braun H F, Musick E *Solid State Commun.* **52** 797 (1984)
259. Francois M et al. *J. Less-Common. Met.* **113** 231 (1985)
260. Jeitschko W, Glaum R, Boonk L *J. Solid State Chem.* **69** 93 (1987)
261. Hirjak M et al. *J. Less-Comm. Met.* **105** 139 (1985)
262. Jeitschko W, Reehuis M *J. Phys. Chem. Solids* **48** 667 (1987)
263. Yan J-Q et al. *Phys. Rev. B* **78** 024516 (2008)
264. Luo H et al. *Supercond. Sci. Technol.* **21** 125014 (2008); arXiv:0807.0759
265. Tegel M et al., arXiv:0806.4782
266. Hoffmann R, Zheng C *J. Phys. Chem.* **89** 4175 (1985)
267. Dong J K et al., arXiv:0806.3573
268. Huang Q et al., arXiv:0806.2776
269. Zhao J et al. *Phys. Rev. B* **78** 140504(R) (2008); arXiv:0807.1077
270. Hu W Z et al., arXiv:0806.2652
271. Torikachvili M S et al., arXiv:0807.1089
272. Torikachvili M S et al. *Phys. Rev. Lett.* **101** 057006 (2008); arXiv:0807.0616
273. Park T et al. *J. Phys. Condens. Matter* **20** 322204 (2008)
274. Alireza P L et al., arXiv:0807.1896
275. Li G et al. *Phys. Rev. Lett.* **101** 107004 (2008); arXiv:0807.1094
276. Yang J et al., arXiv:0807.1040
277. Boyer M C et al., arXiv:0806.4400
278. Goldman A I et al. *Phys. Rev. B* **78** 100506(R) (2008); arXiv:0807.1525
279. Fukazawa H et al., arXiv:0806.4514
280. Baek S-H et al., arXiv:0807.1084
281. Jesche A et al. *Phys. Rev. B* **78** 180504(R) (2008); arXiv:0807.0632
282. Yang L X et al., arXiv:0806.2627
283. Ding H et al. *Europhys. Lett.* **83** 47001 (2008); arXiv:0807.0419
284. Nekrasov I A, Pchelkina Z V, Sadovskii M V *Pis'ma Zh. Eksp. Teor. Fiz.* **88** 155 (2008) [*JETP Lett.* **88** 144 (2008)]
285. Liu C et al., arXiv:0806.3453
286. Zhao L et al., arXiv:0807.0389
287. Liu H et al. *Phys. Rev. B* **78** 184514 (2008); arXiv:0806.4806
288. Shein I R, Ivanovskii A L *Pis'ma Zh. Eksp. Teor. Fiz.* **88** 115 (2008) [*JETP Lett.* **88** 107 (2008)]
289. Xu G et al., arXiv:0807.1401
290. Ma F, Lu Z-Y, Xiang T, arXiv:0806.3526
291. Shein I R, Ivanovskii A L, arXiv:0807.0984
292. Sefat A S et al., arXiv:0807.0823
293. Cao G et al., arXiv:0807.1304
294. Yang J et al., arXiv:0809.3285
295. Ge J, Cao S, Zhang J, arXiv:0807.5045
296. Sefat A S et al. *Phys. Rev. B* **78** 104505 (2008)
297. Li H et al., arXiv:0807.3153
298. Kawabata A et al., arXiv:0808.2912
299. Kawabata A et al., arXiv:0807.3480
300. Cao G et al., arXiv:0807.4328
301. Kimber S A J et al., arXiv:0807.4441
302. Zhao J et al. *Phys. Rev. B* **78** 132504 (2008); arXiv:0807.4872
303. Aczel A A et al., arXiv:0807.1044
304. Chang B C et al., arXiv:0807.2833
305. Tropeano M et al. *Phys. Rev. B* **78** 094518 (2008); arXiv:0807.0719
306. Ignatov A et al., arXiv:0808.2134
307. Christianson A D et al. *Phys. Rev. Lett.* **101** 157004 (2008); arXiv:0807.3370
308. Le Tacon M et al., arXiv:0809.2898
309. Coldea A I et al., arXiv:0807.4890
310. Lu D H et al., arXiv:0807.2009
311. Drew A J et al., arXiv:0807.4876
312. Kametani F et al., arXiv:0809.3393
313. Yang S et al., arXiv:0809.2169
314. Jeevan H S et al. *Phys. Rev. B* **78** 092406 (2008); arXiv:0807.2530
315. Sefat A S et al. *Phys. Rev. Lett.* **101** 117004 (2008); arXiv:0807.2237
316. Bauer E D et al., arXiv:0808.1694
317. Li L J et al., arXiv:0809.2009
318. Ronning F et al. *J. Phys. Condens. Matter* **20** 342203 (2008); arXiv:0807.3788
319. Yildrim T, arXiv:0807.3936
320. Kumar M et al., arXiv:0807.4283
321. Kaneko K et al., arXiv:0807.2608
322. Miclea C F et al., arXiv:0808.2026

323. Altarawneh M et al., arXiv:0807.4488
324. Dai J et al., arXiv:0808.0065
325. Kitagawa K et al. *J. Phys. Soc. Jpn.* **77** 114709 (2008); arXiv:0807.4613
326. Goko T et al., arXiv:0808.1425
327. Gooch M et al. *Phys. Rev. B* **78** 180508(R) (2008); arXiv:0809.2054
328. Chia E E M et al., arXiv:0809.4097
329. Zbiri M et al., arXiv:0807.4429
330. Su Y et al., arXiv:0807.1743
331. Mittal R et al. *Phys. Rev. B* **78** 104514 (2008); arXiv:0807.3172
332. Alireza P L et al., arXiv:0807.1896
333. Kreyssig A et al. *Phys. Rev. B* **78** 184517 (2008); arXiv:0807.3032
334. Leithe-Jasper A et al., arXiv:0807.2223
335. Lee H et al., arXiv:0809.3550
336. Tapp J H et al. *Phys. Rev. B* **78** 060505(R) (2008); arXiv:0807.2274
337. Pitcher M J et al. *Chem. Commun.* 5918 (2008); arXiv:0807.2228
338. Shein I R, Ivanovskii A L *Pis'ma Zh. Eksp. Teor. Fiz.* **88** 377 (2008) [*JETP Lett.* **88** (5) (2008)]
339. Nekrasov I A, Pchelkina Z V, Sadovskii M V *Pis'ma Zh. Eksp. Teor. Fiz.* **88** 621 (2008) [*JETP Lett.* **88** 543 (2008)]; arXiv:0807.1010
340. Belashchenko K D, Antropov V P, cond-mat/arXiv:0809.2586
341. Hsu F-C et al. *Proc. Natl. Acad. Sci. USA* **105** 14262 (2008)
342. Margadonna S et al. *Chem. Commun.* 5607 (2008); arXiv:0807.4610
343. Mizuguchi Y et al. *Appl. Phys. Lett.* **93** 152505 (2008); arXiv:0807.4315
344. Li L et al., arXiv:0809.0128
345. Zhang S B et al., arXiv:0809.1905
346. Kotegawa H et al., arXiv:0808.0040
347. Pulikkotil J J, van Schilfgaarde M, Antropov V P, arXiv:0809.0283
348. Subedi A et al. *Phys. Rev. B* **78** 134514 (2008); arXiv:0807.4312
349. Fang M H et al., arXiv:0807.4775